TAILORING HYDROGEL MICROSTRUCTURE VIA PHASE SEPARATION AND KINETIC TRAPPING

by

Simon Vieth

Bachelor of Engineering - Chemical Engineering
Ryerson University
Toronto, Ontario, Canada, 2004

A thesis
presented to Ryerson University in fulfillment of the
thesis requirement for the degree of
Master of Applied Science
in
Chemical Engineering

Toronto, Ontario, Canada, 2007

I hereby declare that I am the sole author of this thesis.

I authorize Ryerson University to lend this thesis to other institutions or individuals for the purpose of scholarly research.

Simon Vieth

I further authorize Ryerson University to reproduce this thesis by photocopying or by other means, in total or in part, at the request of other institutions or individuals for the purpose of scholarly research.

Simon Vieth

Abstract

TAILORING HYDROGEL MICROSTRUCTURE VIA PHASE SEPARATION AND KINETIC TRAPPING

Simon Vieth, Bachelor of Engineering (2004)
Master of Applied Science in Chemical Engineering (2007)
Department of Chemical Engineering
Ryerson University, Toronto, Ontario, Canada

Control of the microstructure of a biopolymeric phase-separated system is presented as part of an effort to develop a novel platform for controlled drug release. Under certain conditions, aqueous mixtures of biopolymers exhibit thermodynamic incompatibility and separate into distinct phases, each concentrated in one component and poor in the other. Upon initiation of phase separation (PS), droplets of one phase, the included phase, appear and ripen over time such that shared surface area with the continuous phase is minimized. Gelation is a means of halting droplet growth prior to bulk PS (BPS). The purpose of this research is to establish the means to dictate the microstructure of a PS system by: (i) understanding the effects of biopolymer concentration on PS temperature, TPS; (ii) modeling the growth of droplets within the included-phase; (iii) examining the efficacy of gelation as a means of trapping microstructure and (iv) investigating the characteristic microstructures of biopolymer systems undergoing a two-step temperature quench.

Acknowledgements

A heartfelt thanks is due to Dr. Dérick Rousseau for his supervision, unending support and insight throughout the course of this research. The efforts of the committee charged with examining this research are acknowledged (Dr. Ramdhane Dhib, Dr. Ginette Turcotte and Dr. Phillip Chan of the Department of Chemical Engineering, Ryerson University and Dr. Allan Paulson of the Food Science Program, Department of Process Engineering and Applied Science, Dalhousie University). The Advanced Food and Materials Network and Ryerson University are recognized for their financial support of the work herein. Finally, Dr. Christopher Yip of the University of Toronto and Alireza Abbasi of Ryerson University are acknowledged for their technical support in the areas light scattering experimentation and theoretical modeling, respectively.

For my Tetyanka.

Table of Contents

List of Figures

List of Tables

List of Appendices

Chapter 1

Introduction

Prepared foods often contain mixtures of two or more biopolymers to control viscosity and texture. In this context, the importance of phase behavior and network formation in complex food systems is reflected in a number of recent publications, where phase separation between incompatible biopolymers is viewed as both a desirable or undesirable process, depending on the application[1-4]. This thesis aims to elucidate the unique roles of a series of competing processes (aqueous mixed biopolymer phase-separation, separated system microstructural evolution and mixed biopolymer gelation) in the context of influencing the microstructure of a separated aqueous biopolymer mixture.

A biopolymer is defined as a polymeric macromolecule that has biological origin and functionality[5]. Examples of such food-related biopolymers include proteins (*e.g.*, gelatin and whey) and polysaccharides (*e.g.*, dextran and guar gum). The structural diversity of biopolymers is in stark contrast to the regular molecular nature of synthetic polymers. Despite this, the behavior exhibited by synthetic polymer mixtures, and their governing theories, are readily applied in the study of biopolymers, enabling their use in describing the compatibility of biopolymers in aqueous solution[6].

The temperature-dependent nature of the compatibility of synthetic polymer mixtures has been used for a wide range of industrial applications, including liquid crystal films[7] and plastics with unique rheological properties[8]. Phase separation of aqueous mixtures of two different biopolymers is a similar phenomenon that may have applications in the food industry[9]. An example is the use of aqueous biopolymer composites with unique fracture behavior in mimicking the texture of fat removed from low-fat foods[10]. As such, significant theoretical and experimental research has been conducted to elucidate the processes that bring an aqueous mixture of two biopolymers from a miscible, homogeneous solution to a bulk-separated, two-phase system.

1.1 Phase Separation Fundamentals

A biopolymeric system is defined, and made unique, by the concentration of its constituent biopolymers within a typically aqueous solvent environment[11]. It has been shown that even though the biopolymeric components of most aqueous biopolymer mixtures are hydrophilic in nature, this fact does not always ensure that such a mixture will homogeneously combine at all temperatures. Phase behavior for such a mixed system is characterized by a critical temperature above which its components remain a miscible, intimately mixed homogeneous solution. When the system temperature is decreased below the characteristic critical temperature, the constituent biopolymers become incompatible and separate into distinct phases. Each of these phases is rich in one biopolymer and poor in the other. For a period of time following the initial quench, the new phases will compositionally

enrich until they have reached their thermodynamically-governed equilibrium concentrations.

Soon after the initiation of phase separation, a system at compositional equilibrium, with an included phase dispersed throughout a continuous phase, behaves much like a destabilizing water-in-water emulsion. Such a system will undergo a microstructural coarsening in an effort to minimize the area of surface contact between the phases[12]. If the system is allowed to coarsen indefinitely, it will eventually reach a state of bulk phase separation. In this state, the system is no longer composed of one phase dispersed throughout another, but is characterized by a homogeneous, single phase layer atop another with a single, common interface (Figure 1.1).

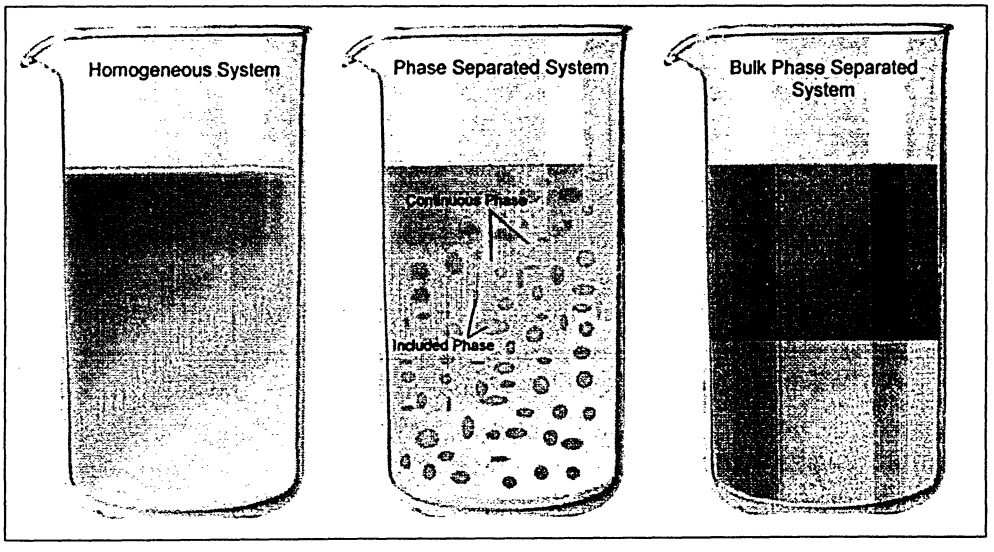

Figure 1.1: A diagrammatic representation of the three regimes of a phase-separating aqueous mixture of biopolymers.

The separation of a mixed system into two compositionally-distinct phases and subsequent microstructural coarsening are kinetic processes. Their rates are influenced by factors such as temperature, the level of biopolymer

incompatibility, the degree of favourable interaction between the biopolymers, phase viscosity and interfacial tension between the two separated, coexisting phases. As well, the relative rates of the separation and coarsening processes are the main factors in determining the system's microstructure. A system's microstructure will be made unique by the average size distribution and spatial orientation of the structures characterizing its included phase.

The absence of phase separation in food systems is unusual given the elevated concentrations of biopolymers typically found. For example, the concentration of gelatin typically required to form a self-supporting gelled network may also induce phase separation in an aqueous mixture with certain polysaccharides. Furthermore, separative behavior is amplified in foods that undergo molecular ordering or gelling. Non-separating systems do exist, however, and are generally characterized by a low drive for phase separation that is inhibited by rapid gelation of its components[12;13]. Such systems are considered mixed gels since they form an interpenetrating network at a molecular level. The novel industrial application of such systems remains limited, however, and designed textural applications have been focused on separating biopolymers[14;15;15].

1.2 Phase Separation Mechanisms from Phase Diagrams

For practical purposes, it can be assumed that most food systems are made of mixtures of biopolymers in water[16]. These ternary systems are often made up of water in excess of 90% (by weight). As such, the most common way to predict phase behavior in these systems is to use a phase diagram representing the concentrations of the two constituent biopolymers. These two-dimensional phase diagrams can be compiled from experimental data or from theoretical models that take into account the physical and chemical properties of the biopolymers and the solvent. Phase diagrams typically take the form of a temperature-composition diagram (Figure 1.2A) or a composition-composition diagram (Figure 1.2B).

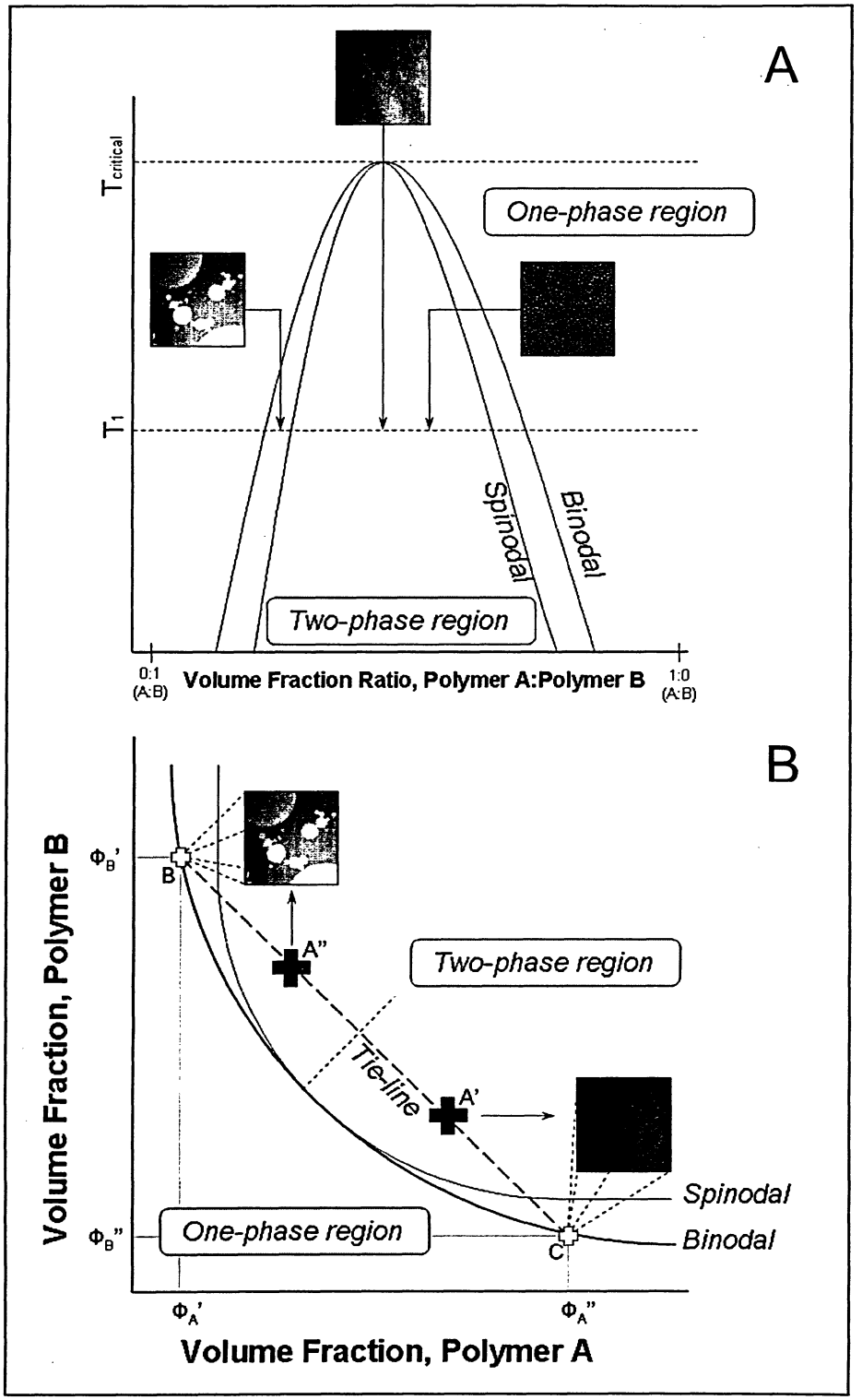

Figure 1.2: (A) Upper critical separation temperature (UCST) phase diagram. (B) Composition-composition phase diagram. Both phase diagrams serve to describe the phase compatibility behavior of their characteristic polymers in mixtures. Images shown are experimentally-obtained phase-separated gelatin-maltodextrin composites. Adapted from Tran *et al.*[6].

Both phase diagrams show the position of the binodal curve with respect to system temperature and system composition. The binodal, or phase compatibility curve, divides the miscible region, at lower biopolymer concentrations from the immiscible region, at higher concentrations. Mixed systems defined by points lying outside of the binodal (*i.e.*, above the phase separation temperature in Figure 1.2A and closer to the origin in Figure 1.2B) are miscible and remain homogeneous mixtures indefinitely.

Phase diagrams also indicate the compositions of the coexisting phases that result from separation. In Figure 1.2B, a system above the binodal will separate into two phases whose compositions are dictated by the characteristic tie-line slope of the aqueous biopolymer-biopolymer mixed system. Both samples A' and A'' are diagrammatically shown to separate into two coexisting phases whose compositions are denoted as B and C. Sample A' is shown to separate into a system with a continuous (dark) phase and an included (light) phase, whereas sample A'' is the opposite. The position of the original sample on the tie-line will determine the relative volumes of the coexisting phases after separation, and furthermore will determine which phase is continuous. The general rule for biopolymers is that phase continuity is governed by the phase with the highest volume fraction[12]. The unique situation of equivalent volume fractions leads to a bi-continuous system where neither system is continuous in nature. Such a system is shown in the micrograph inset of Figure 1.2A, at the apex of the phase diagram.

Phase diagrams serve not only to distinguish the region of biopolymer compatibility from that of the phase separative region, but also to indicate which phase separation mechanism(s) occur at specific points within the diagram. In both types of phase diagrams (Figure 1.2A & 1.2B), the monophasic region is distinguished from the separative region by the binodal (equilibrium) curve. Phase separation of systems brought into the two-phase region proceeds because of a Gibbs free energy change that leads to a thermodynamically-unfavourable mixed state. This phase separation may proceed by one of two types of known mechanisms, each exhibiting different changes in the Gibbs free energy. The specific location of the biopolymeric system on the phase diagram serves to indicate which mechanism predominates. Within the binodal curve lays the spinodal curve, which serves to separate the unstable from the metastable phase separating regions (Figure 1.2A and 1.2B).

Systems lying within the unstable region will separate *via* spinodal decomposition (SD), whereas metastable systems separate *via* the nucleation and growth (NG) mechanism. The two mechanisms are also differentiated by the way in which their constituent phases manifest themselves following the onset of phase separation[17]. The primary distinction between the two mechanisms lies in how the separated systems evolve immediately following separation onset. NG-separated systems exhibit a continuous increase in the volume of the included phase up until equilibrium volume fractions are attained. During this time, all inclusions exhibit unchanging equilibrium concentrations. Conversely, SD-separated systems exhibit an evolution in phase concentrations

following the immediate establishment of inclusion volume fraction. In biopolymer systems, the growth rates during these two initial processes are high, having been observed to occur within tens of seconds[10;18;19].

The different evolutionary behaviors of NG and SD mean the resultant morphologies resulting from the two separation mechanisms differ noticeably. The characteristic microstructures resulting from NG and SD separation are shown in the insets of Figure 1.2A. The NG-separated system (on the left) results from a quench below the binodal but not below the spinodal. The characteristic SD-microstructure (on the right) is shown to occur when the system is deeply quenched below the spinodal curve. At the initiation of phase separation, SD will yield a large population of inclusions with a narrow size distribution, whereas NG systems will exhibit a wide range of droplet sizes as nuclei appear over time[6]. The unique case of a critical-quench occurs with systems located at or immediately above the apex of the phase diagram (Figure 1.2A). The resultant microstructure will have a bicontinuous nature where one phase is not dominant over the other. Such a system will exhibit an intertwined morphology that is noticeably different from the droplet morphology mentioned previously. An important property of the critical point on the temperature-composition phase diagram (Figure 1.2A) is that no system, regardless of composition, will phase separate when the system temperature is greater than $T_{critical}$.

1.3 Microstructural Tailoring *via* Phase Separation

One of the most distinctive properties of a phase-separated aqueous biopolymer system is the diverse range of microstructures that can be attained by controlling the biopolymeric composition of the mixture, temperature quench rate and gelation. Each of these parameters has a strong influence on final system microstructure. Following the onset of phase separation, the included phase may exhibit changes in its size, shape, biopolymeric concentration and distribution. During this stage, the system behaves as a water-in-water emulsion, during which coarsening of the included phase may result from droplet coalescence, Ostwald ripening, creaming or sedimentation. The comparative rates of these processes are influenced by the relative rheologies, interfacial tensions and densities of the phases[12;20;21].

This microstructural evolution will continue until an equilibrium state is reached in the form of a bulk phase-separated system. However, the coarsening process may be arrested through the kinetic trapping of the system microstructure[10;22]. Kinetic trapping is the gelation-induced "freezing" of one or more components in a separating system. This process severely restricts the kinetics of coarsening by inhibiting the movement of the inclusions and impeding the redistribution of water between the coexisting phases[11;23]. As such, the microstructural morphology of a system is greatly dictated by the length of the period it resides between a state of active phase separation and the onset of coarsening-inhibiting kinetic trapping. From an industrial application standpoint, the most important task in controlling microstructure is the ability to

slow down or stop coarsening when the desired morphology is obtained. In biopolymer systems, the microstructural evolution described above is most commonly halted by gelation of one or both components following a period of phase separation[24].

1.4 Strategies for Modeling Phase-Separated System Behavior

It has been shown that compositional and thermal factors affect the phase separation process and microstructural evolution of biopolymer mixtures. Though there exists a complex set of factors that influence these behaviors (pH, ionic strength, temperature, concentration) it is possible to develop an insight into this behavior using physical models, such as the Flory-Huggins theory of polymer mixing[25;26]. The modeling of phase separative behavior typically falls into one of two groups: determination of miscibility behavior of biopolymers in aqueous mixtures[14;27]; and representations of phase separation kinetics and coarsening rates[3;20;28].

Calculation of the binodal curves of aqueous mixed biopolymer systems is based on two criteria, namely the minimization of Gibbs free energy and the equality of chemical potentials between coexisting phases. This calculation is most commonly performed using the polymer mixing theories established by Flory and Huggins[29]. The extension of this analysis to biopolymer systems has been previously reported, indicating the applicability of polymer theories in describing biopolymer behavior[14;14;27]. Application of the Flory-Huggins theory to biopolymer systems has yielded qualitative descriptions of phase behavior, and as such has been seen as the model of choice to model these systems[14].

Much theoretical work has been done on the kinetics of separation in synthetic polymer systems separating in an unstable or metastable manner[30-33]. Models presented have addressed this behavior from both a molecular dynamics approach and from a mean-field standpoint. More complex models have examined the transient nature of polymer network formation (and the resulting elastic energy term) and its effect on coarsening[34]. Investigation of the concurrent gelling and phase separation of synthetic polymer systems has primarily focused on the arresting nature of gelled network formation. This research stopped short of looking at the effect of gelation as a driving force for demixing[24]. Recent work has demonstrated that the physical and kinetic behavior of separating synthetic polymer systems is the same as in aqueous biopolymer systems[19;35-37]. This claim was verified by the observations of the universal phase separation mechanisms (SD and ND) and expected growth exponents in biopolymer demixing polymer composites. These observations indicate that the phase separation process well characterized for polymer mixtures is the very same phenomena observed in biopolymer systems and may be modeled as such.

1.5 Thesis Proposals and Objectives

The following is a list of the proposals and objectives for this thesis, where phase separation in aqueous gelatin-maltodextrin mixtures is experimentally investigated:

1. To characterize the compatibility behavior of aqueous mixtures of gelatin and maltodextrin and translate this

behavior onto phase diagrams. The theoretically predicted co-solubility of gelatin and maltodextrin will be modeled with the Flory-Huggins theory of polymer miscibility using experimentally determined physical parameters.

2. To investigate the period of microstructural evolution following phase separation. The coarsening mechanism(s) observed to dominate during phase separation will be modeled. This model will elucidate the general coarsening behavior of the gelatin-maltodextrin system.

3. To test the efficiency of kinetic trapping of a phase-separated and coarsening system through gelatin gelation by physical (molecular entanglement) and chemical (covalent crosslinking) means.

1.6 Methodology and Approach

It is proposed that the wide array of microstructures attainable through biopolymer phase separation may be predictably controlled once the stages of phase separation are well characterized. With an understanding of biopolymer compatibility, the characteristic phase separation temperature of uniquely composed systems will be determined. This result will indicate when phase separation will begin during a thermal quench. Translation of the global biopolymer compatibility behavior will yield a phase diagram, from which the

compositions of the coexisting phases will be determined. Separation of the two-phase region of the phase diagram into unstable and metastable regions will help in determining the resultant microstructure of phase-separated systems.

An understanding of the evolution of the morphology of phase-separated systems will add another element in the precise tailoring of microstructure. Empirical observation of the route a separated system takes on its way to becoming a fully bulk-separated system will uncover the dominating mechanisms of emulsion destabilization. Theoretical modeling of this process will allow for the description of coarsening in a wide range of systems.

Microstructural tailoring is partly contingent on obtaining a desired average droplet size within the separated system. During coarsening-driven microstructure evolution, a number of average droplet sizes will be generated. An equally important criterion in tailoring is being able to stop the evolution of the microstructure when the desired average droplet size is attained. The rapid gelation (relative to coarsening) of one or both components has been presented previously as a method of fixing microstructure in separated biopolymer applications[38]. Immobilization of the solvent (water) by gelation of the gelatin mixture component will prevent microstructural evolution to the extent that the system will be trapped from further coarsening.

1.7 Thesis Organization

The thesis presented here is divided into nine chapters organized in the following fashion:

Chapter 1 briefly introduced the phase separation process, specifically in relation to biopolymer systems. Phase diagrams were introduced as tools that elucidate mixture compatibility behavior, and the subsequent growth of phase-separated structures was presented. Kinetic trapping was mentioned as a proposed final step in the tailoring of the microstructure of phase-separated systems.

Chapter 2 presents phase separation of biopolymers and synthetic polymers in the context of a review of recent literature. Experimental and theoretical analyses of phase-separated systems are presented in two parts, phase separation and morphological growth, and physical properties of separated systems.

Chapter 3 presents a theoretical background of the long-standing governing theories of polymer phase compatibility (Flory-Huggins theory) and phase separation (Cahn-Hilliard theory).

Chapter 4 presents the biopolymers used throughout this study of phase separative behavior, gelatin and maltodextrin. A novel, non-cytotoxic chemical crosslinker, genipin, is also presented as a potential additive yielding enhanced structural and stability properties in the gelatin-maltodextrin system. The experimental techniques used throughout the course of this study are also discussed.

Chapter 5 covers the experimental determination of phase behavior of aqueous mixed gelatin-maltodextrin solutions. Flory-Huggins theory is applied in an effort to characterize the general trends of gelatin-maltodextrin mixed behavior and also provide a series of phase diagrams depicting system compatibility over a range of temperature and compositional conditions.

Chapter 6 breaks down the process of included phase maturation (coarsening) following phase separation. An existing model describing coarsening in polymer systems is applied in an effort to simulate microstructural coarsening in aqueous biopolymer mixtures.

Chapter 7 investigates the feasibility of kinetically trapping microstructural growth *via* physical and chemical crosslinking.

Chapter 8 discusses the rarely reported phenomenon of secondary phase separation in gelatin-maltodextrin systems.

Chapter 9 summarizes the results presented in the thesis and discusses their potential applications in the context of proposed future studies in the area of biopolymeric phase separation.

Chapter 2

Literature Review: Phase Separation in Mixed Biopolymers

This literature review is broken down into two parts. The first part serves as an introduction to gelatin (GL) and maltodextrin (MD), components of the most commonly investigated biopolymer composites. Part 2 looks at published work in the area of phase separation as observed in biopolymer systems.

Aqueous mixed biopolymer (e.g., protein-polysaccharide) solutions regularly exhibit thermodynamic incompatibility, which initiates phase separation. The cause of this incompatibility is usually related to the attractive or repulsive molecular nature of the components. Biopolymers exhibiting opposite charges will tend to attract, leading to segregated insoluble complexes. Conversely, neutral or similarly-charged polymers will segregate into distinct phases when the mixing of the different species is less thermodynamically-favoured than intimate mixing of the same type of molecules. Such behavior forms the basis of a significant amount of research into the behavior of mixed biopolymer/colloid systems[3;14;16;18;19;39-41].

2.1 Biopolymer Mixture Constituents and Gelling Behavior

A large number of phase behavior investigations of biopolymer mixed systems have focused on GL-MD in aqueous solution[1;14;35;37;42]. The charge neutrality of MD leads to a segregative mechanism of separation when mixed with GL. This separation mode produces mixed composite systems that are able to impart a wide range of textural properties in food and pharmaceutical applications[12]. Furthermore, separation of GL and MD occurs at temperatures slightly above that of GL gelation, meaning it is possible to allow microstructural coarsening to proceed to a desired extent then quickly kinetically trap this evolution. Finally, the concentration of strongly gelling GL in both resultant phases allows for the formation of self-supporting gels in one or both of the separated phases.

The thermoreversible nature of physical GL gels has been overcome by the use of chemical crosslinkers[3]. Of these, genipin has shown the most promise in food and pharmaceutical applications due to its low cytotoxicity and high rate and extent of crosslinking[43;44].

The following section covers GL and MD structure, properties and gelling behavior. Subsequently, genipin is discussed and its crosslinking mechanism is presented. Finally, gelling behavior and criteria of defining a gelled network are discussed.

2.1.1 Gelatin

GL is one of the most prominent biopolymers used industrially. Its widespread use includes applications in photography, adhesive manufacture, pharmaceutical preparation and food formulations[45]. The desirable qualities of an aqueous gelled GL networks include its stability, reversibility, transparency and its ability to form self-supporting gels. The most industrially useful property of GL is gel formation, which exhibits a strong dependence on average molecular weight. The molecular weight of GL is highly dependent on its processing conditions and its origin. As such, there can be functional variability amongst GL grades and origins.

GL is a product of the irreversible hydrolytic degradation of collagen[41]. Collagen is the primary protein of white fibrous connective tissues (i.e. bone, skin, and tendon) in animals and is the most abundant mammalian protein[46;47]. High in nonessential amino acids, collagen is made up of three strands of tropocollagen intertwined to form a triple helix of polypeptide chains in a rod-like shape[48]. These polypeptide chains can exceed 1000 residues in length, or 100000 kDa in molecular weight. *In vivo*, collagen is the result of the further assemblage of these rods into small fibrils, which are stabilized by covalent crosslinks[49]. During the production of GL from collagen, the triple helices are broken down by hydrolysis into the random globular coils that are characteristic of GL[50]. Because of the non-specific nature of the hydrolysis, GL is not a homogeneous product, exhibiting a wide range of molecular sizes[46].

In the food industry, GL is typically produced from bovine and porcine collagen, with equine collagen being used in adhesive production and fish GL being used as a mammalian GL substitute. The differences between GLs from varying sources have been the focus of much research[48;49]. The primary finding of this work was that GL properties (gel strength, critical gelation concentration) were highly dependent on animal origin. Porcine and bovine GLs were found to behave similarly, whereas fish GL was observed to have significantly reduced gel strength.

The most commonly used industrial descriptor of GL is the bloom value, which is a measure of the firmness and strength of a set gel. The relationship between the bloom value of a GL and average molecular weight has been indirectly touched upon in phase separation research. In comparing the effects of bloom value on standardized phase separative behavior, it has been found that GL samples with higher bloom values (greater set gel strength) promote phase separation in GL-MD solutions[46].

GL possesses the primary subunit of collagen in triple helix form. GL helices dissolve in water typically above 40°C and form transparent rigid gels upon cooling at concentrations > 0.5% (w/w)[45]. Upon heating in aqueous solution, the triple helices unravel and GL is in the form of dissolved, flexible random coils[45;51]. Cooling leads to the formation of junction zones between small segments of multiple GL molecules as they revert to their triple helix configuration. Evolution of the gelled structure can occur over a long period of time as the network continues to reorganize and form links of increasing

stability[5]. Atomic force microscopy of this evolution has shown that initial gelation is characterized by the formation of interwoven triple helix aggregates. Over longer periods of time, the network develops as the aggregates reform as fibrous structures extending throughout the gel[52].

2.1.2 Maltodextrin

MD is a starch hydrolysis product typically formed *via* the breakdown of corn or potato starches by means of acid, enzymatic or heat treatment[48]. The hydrolysis process yields a wide range of oligosaccharides and polysaccharides, the distribution of which is dependent on the extent and origin (*e.g.*, heat, acid or enzymatic hydrolysis) of reaction[53]. The broad range of products is generally classified by the dextrose equivalency number (DE), which is a relative measure of the reducing power of the specific fraction. Dextrose is a commonly used synonym for D-glucose, the biologically functional form of glucose ($C_6H_{12}O_6$). The maximum DE number is that of glucose, which has a value of 100. As such, it is apparent that a hydrolysis fraction exhibiting a high DE value will have undergone a great degree of breakdown. MDs are classified as hydrolysis products having DE values of 20 or lower, with numbers in the range of 1-10 being quite common[53].

MDs contain both linear amylose (molecular mass range 105-106 g/mol) and branched amylopectin (molecular mass range 107-109 g/mol, with branching points every 25 to 30 glucose units) (Figure 2.1)[53]. Though DE value is inversely related to the number of glucose units, MDs with the same DE value can have very different molecular configurations of these constituent

subunits. The ratio of linear (amylose) to branched (amylopectin) varies according to starch source, though generally amylase content is in the range of 15-35%[12]. The specific ratio is important because it is the interplay between amylose and amylopectin that leads to MD network gelation, which gels in a similar mechanism to starch gelation[51].

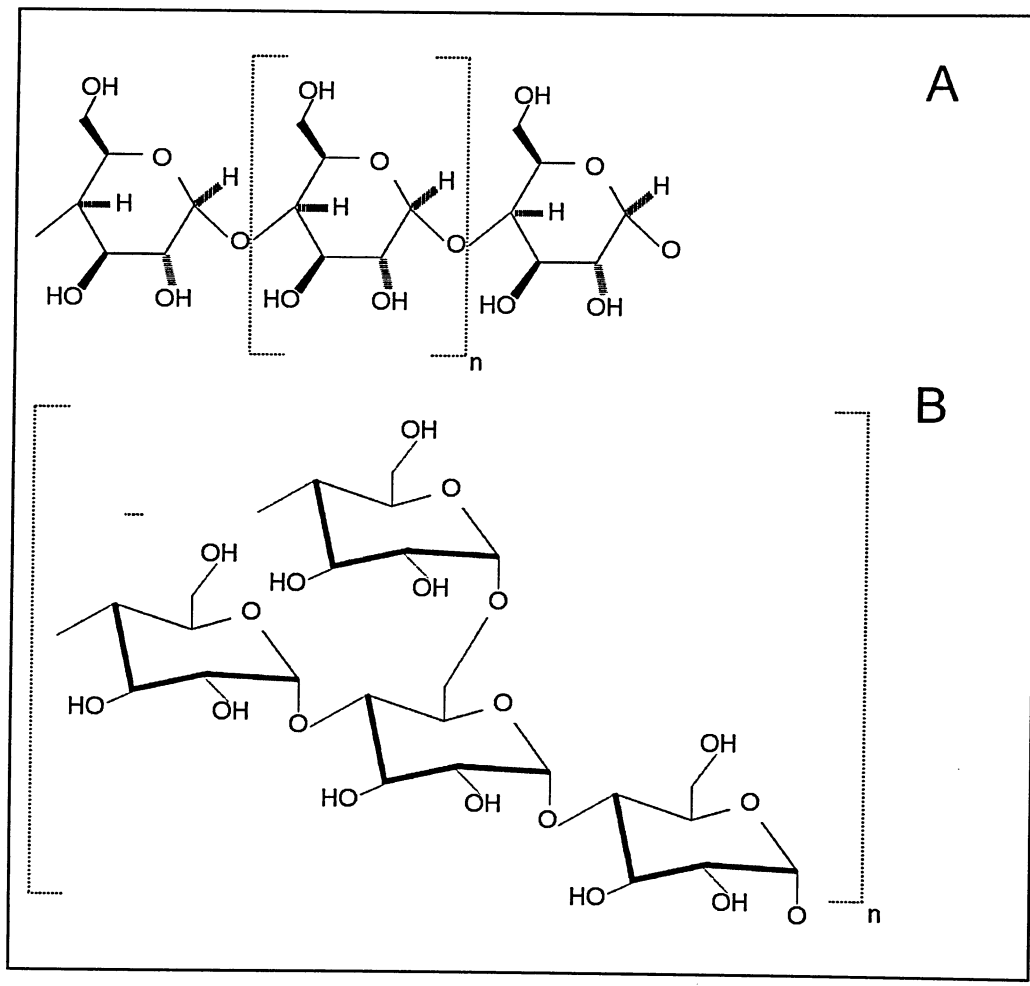

Figure 2.1: Diagrammatic structures of (A) amylose (exhibiting α(1→4) linkages) and (B) amylopectin (exhibiting linear α(1→4) linkages and branched α(1→6) linkages). Adapted from Chronakis[53].

In food applications, MD use has increased in the last few decades[54]. Low DE MDs display similar textural characteristics to fats, and as such have received a great deal of attention in the development of calorie-reduced food

products[53]. The industrially-important properties of MD include dry bulking, dispersion promotion and aqueous gelling behavior, which is most applicable to phase separation. MD gelation results from the coupling of soluble amylose molecules with the branched and linear components of amylopectin[23]. A handful of linear amylose molecules have extended helical regions disrupted by short disordered regions. Entanglement of these fractions is the initiating and accelerating step in MD gelation. Conformational ordering follows with the formation of helical-junctions of amylose chains. Interaction of the linear segments of amylopectin components with helical amylose forms secondary helical species which aggregate and form crystalline domains. These domains are intermingled in solution with the disordered amylose chain segments. Because portions of the amylopectin molecule are long, they can be involved in formation of numerous crystalline domains. At sufficient concentration, the aggregated network of these domains corresponds to network formation in the MD sample[53;53]. Overall, the synergistic intertwining of different biopolymer fractions characterizes MD gelling. This process emphasizes the need for high molecular weight helices (capable of forming ordered domains) and shorter aggregate structures (which cooperatively associate oligomers) in the formation of the gelled network[53]. This result confirms findings of differing gelling behaviors for MDs having different DE values[46]. Specifically, lower MDs with lower DE values will generally yield stronger gels more rapidly. Schierbaum *et al.* showed the time-dependent nature of MD ordering using a number of

techniques (DSC, X-ray scattering, rheology) and found a plateau in shear modulus occurred in the range of 1-3 days[47].

2.1.3 Genipin

Genipin (Figure 2.2) is a natural plant extract that has recently been used as a natural chemical crosslinking agent[37;43]. It has been shown to have a low cytotoxicity, especially relative to other chemical crosslinkers, such as glutaraldehyde. As well, numerous studies have shown it to be a highly effective crosslinker, both in terms of extent and rate[55-57]. It is derived from the fruits of the *Genipa americana* and *Gardenia jasminoides*, fruit-bearing plants common to South America and Asia, respectively. Enzymatic hydrolysis of the compound geniposide, extracted from the fruit of these plants with β-glucosidase yields genipin. Reaction of genipin with primary amines in the presence of oxygen can yield a vibrant blue color, and as such it has seen much use as a food dye. Other applications include its use in the treatment of a wide array of ailments in Chinese medicine.

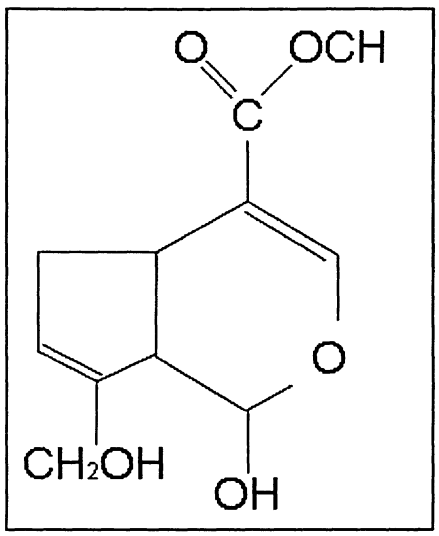

Figure 2.2: Diagrammatic representation of the molecular structure of genipin. Adapted from Butler *et al.*[61].

The crosslinking of GL by genipin has been demonstrated to occur because of its covalent reaction with primary amine groups[58]. Butler proposed a mechanism for the formation of crosslinks and described two reactions involving different sites on the genipin molecule[59]. Genipin fixation with amino group-containing molecules is thought to begin with the formation of the Genipin-amino complex resulting from a Genipin-mediated nucleophilic attack[59;60]. Subsequently, an aldehyde group is formed upon opening of the genipin ring. Crosslinking is completed when this complex attacks a second amino group. An inherent phenomenon of genipin fixation is self-polymerization, which occurs by radical reaction of two amino-attached open genipin rings[55;60]. Genipin fixation is considered a more reactive mechanism relative to other chemical crosslinkers because of this phenomenon[43]. Genipin self-polymerization has been shown to yield an increase in genipin molecular weight from 226 (monomer) to ~ 3900-7900[57]. Assuming sufficient amino-

bearing substrate is present, the self-polymerization enables the formation of both short-range and long-range crosslinks within the gelled network.

2.1.4 Gels and Gelling Behavior

As mentioned, one of the most important properties of GL is its ability to form physical gels. Flory defined a gel as being made up of crosslinked polymeric molecules linked together to form an interconnected network[12;29]. Gels have been further classified as molecular networks having stress-resisting bulk properties, which result from the interconnected network extending throughout the gel phase[61]. In food systems, physical gels are formed by weak thermoreversible interactions between molecules, such as hydrogen bonds or hydrophobic interactions[12]. In biopolymeric gel formation, GL serves to entrap water molecules in a three-dimensional network. GL's ability to form self-supporting gels at low concentrations in aqueous solution enables the network to imbibe a great deal of water. Though this behavior is exhibited by all gelling biopolymers, the specific properties of their resultant gels are dependent the type, structure and interactions of the gelling molecular species.

The gelling of GL is a two-step process, with the initial phase lasting a few hours, and the slower second phase that may proceed for days. The time-variant nature of gelling indicates that GL gels are normally not at an equilibrium state[62]. From cursory perspective, these processes result from an attempt by individual biopolymer chains to return to their triple helix form[45;48;61]. It is the formation of these helical structures that characterize GL gel behavior and network formation[49]. When the temperature is raised above

gelation temperature (typically in the range of 30°C), the reverse process occurs as helices transition to coils and the gel becomes liquid. Gelation requires a critical minimum protein concentration to occur. Lundin has reported this to be approximately 0.5% for GL in aqueous solution[12].

Before gelation, intermolecular connectivity is small and the material relaxes rapidly when stressed. When the gel point is approached, the rate of relaxation rises sharply, eventually diverging to infinity at gelation. Dynamic rheological tests are used to monitor this behavior throughout the gelation process because the small strain magnitude imparted during testing minimally modifies the forming structure. Numerous criteria for the gel point exist, though each has its inherent drawbacks[61]. A selection of the more common definitions follows:

- G'-G'' crossover
  - Gelling behavior in thermosetting resins is typically defined by the point of crossover between the storage, G', and loss, G'', moduli determined *via* dynamic oscillatory rheometry[61]. This method has been used often in the determination of gelling behavior in biopolymers[45]. The main drawback of this method is that some polymers exhibit an oscillation frequency dependence of gel time. Despite this, researchers have hypothesized that the G'-G'' crossover is likely very close to the gelation phase transition[51;61].

- Relaxation modulus
  - The onset of a power law behavior of the relaxation modulus at gel point has been observed, and taken to be a satisfactory indicator of gelation[20]. However, the power law behavior in a wide range of polymer systems has been shown to exhibit an equally wide range of power law exponents, which are dependent on the thermal history and concentration of the sample.
- Threshold G'
  - Initiation of gelled network formation has been observed to begin over a period of time while the sample is still in its liquid state[48;53]. In the liquid region, system viscosity is found to be very low. Taking this behavior into account, the gel point may be defined as the point where the transient system storage modulus, G', begins to increase above experimental noise. This method is not rigorous and is highly likely to vary amongst experimental equipment used.

2.2 Biopolymeric Phase Separation

Phase separation in GL - starch mixture was first observed by Beijerinck in 1894, where it was found that the co-miscibility of GL and soluble starch in aqueous solution was temperature-dependent[9]. When mixed below this temperature, the system would yield two phases. Since then, research in this area has grown exponentially. It is somewhat ironic, then, that many of the early papers in this research cohort observed phase separation serendipitously.

Most notably, in examining the effect of sugar concentration on GL gel strength, Mars remarked that beyond a critical sugar concentration, systems would exhibit severe turbidity and a noticeable decrease in storage modulus[12]. The observation, of course, was that of phase separation of the system into distinct GL-rich and sugar-rich phases.

2.2.1 Phase Behavior in Biopolymer Mixtures

The phase behavior of biopolymers is important in food processing operations as most foods are multicomponent (*e.g.*, dairy products, thickened soups, etc.). Understanding how the various biopolymers added to a processed food interact (or not) is vital to control microstructure, ensure optimal product functionality and minimize production costs[63]. For example, the sensory perception of texture, mouthfeel and flavor perception of a fat-free ice cream requires that the biopolymers added (*e.g.*, guar gum, starch and GL) generate the desired microstructure. Tailored design of such a product will be aimed at creating a dispersed phase of droplets or air bubbles throughout a soft solid continuous phase[63] while maintaining desirable sensory attributes and keeping processing expenditures at a minimum. This approach, which is now quite common in the development of value-added novel foods, may be broken into two research loci - i. phase compatibility behavior and mechanisms of phase separation, and; ii. physical properties of phase-separated systems. The former is covered in depth in this chapter as it provides the foundation for the research presented later. The latter is briefly touched upon insofar as it gives insight into the utility of the tailoring of the microstructure of phase-separated biopolymeric

systems. Phase separation in biopolymer mixtures has been typically investigated in protein-polysaccharide[3;5;24;34;64;65] or polysaccharide-polysaccharide[3;12;66] aqueous mixed systems.

2.2.2 Experimental Descriptions of Biopolymer Phase Behavior

Like many other biopolymer mixtures, the GL-MD system exhibits a limited miscibility at a molecular level and, when thermodynamic conditions dictate, the formation of multicomponent, non-equilibrium dispersed systems results[1].

In studies of biopolymer phase-separating systems, numerous factors influencing the occurrence and progression of phase separation have been identified[67]. These include temperature, mixture composition, pH, ionic content and the molecular weight of mixture components. Of these, none are more readily investigated than the effects of temperature and biopolymer concentration/ratio[10;66]. Early studies by Khomutov described the phase behavior of GL-starch in aqueous solution in form of a phase diagram (Chapter 1, Section 1.2.1) demarcating the soluble, insoluble and gelling regions[64]. Khomutov made two fundamental observations: firstly, a strong dependence of microstructure on residence time in the two-phase liquid region was noted; secondly, a relationship between biopolymer ratio and phase separation temperature was seen. Loren *et al.* reported similar observations, noting an increase in phase separation temperature accompanying an increase in GL or MD content and that the relative rates of phase separation and gelation determined morphology[4;16]. This effect was seen to be more dramatic for

increases in GL content, indicating an underlying effect of molecular weight, configuration or charge on the phase separation temperature.

Semenova *et al.* further elucidated the roles of molecular factors (molecular weight, size, conformation) on the intensity of interactions of a wide range of biopolymer mixtures which exhibited strong differences in molecular nature, as is the case with GL and MD[68]. They concluded that the strength of unfavourable interactions between biopolymers in solution was correlated with the contribution of the excluded volumes of the uncharged biopolymer molecules. Furthermore, critical conditions for phase separation were essentially determined by the strength of the interactions and not necessarily the nature of the factors controlling such interactions, including volume contributions or electrostatic interactions. Various factors influencing molecular interactions were reported by Schmitt, including temperature, pH, ionic strength, protein-polysaccharide ratio, molecular charge, and molecular weight[67]. These factors will influence complexation of like components and stability of this segregation, though not all factors are equal in effect. For example, ionic content only influences the rate of phase separation, but will not determine whether or not it occurs[27;69]. Lowering pH, however, acts to increase the electrostatic charge on Type A GL (*i.e.*, acid treated porcine tissue), thereby slightly enhancing compatibility with oligosaccharides[27;70].

A number of strategies have been employed in the experimental characterization of biopolymer phase separation behavior (producing phase diagrams like those shown in Figure 1.2). One is the determination of phase

separation temperature for a given system. This has been done by iteratively diluting a separated system at constant temperature until turbidity has just disappeared[15;66]. The new concentrations of the components in the mixture are determined by factoring in the dilution volume. It is these concentrations that make up a single point on the binodal (or compatibility) curve in Figure 1.2.

Another approach examines the phase compositions for a system demixing at a given temperature. Two phases will coexist following bulk phase separation of a system at temperatures below that of separation onset. At this temperature, the coexisting phases are themselves homogeneous, and as such are at equilibrium. Determination of the compositions of these phases (for biopolymers, typically by spectrophometric assay) yields two points on the phase diagram, connected by a tie-line[14].

Another method has been to observe the time-dependent increase in turbidity of a separating system for various temperatures. As the system temperature decreases below separation temperature, the rate at which turbidity forms will increase. A successive decrease in temperature will yield a relationship between onset of turbidity and temperature. The phase separation temperature is determined by extrapolating this relationship to the point where turbidity onset is zero[64].

Construction of phase diagrams that incorporate tie-line information extends the functionality of the diagram. Such a phase diagram is a tool for elucidating phase separation behavior and not simply an indicator of phase compatibility. Phase separation of a given system is described not only by its

characteristic temperature, but also by the concentrations of the resulting phases. Determination of biopolymer phase compositions has been performed using Raman microscopy, fluorimetry (with fluorescently-labeled polysaccharides) and spectrophotometry[13;27;71].

Phase behavior may also be controlled by altering the molecular weight of the components in a mixture[23], where it was observed that GL-MD systems having identical compositions but differing component molecular weights had differing phase separation temperatures, specifically that higher weight fractions increased the phase separation temperature. Characteristic phase continuity was also manipulated by decreasing the chain length of one component (protein) and/or increasing the length of the other (polysaccharide). Molecular weights also affected the physical properties of the phase-separated GL-MD gel whereby the addition of a high molecular weight fraction of GL induced transformation from a weakened deswelled gel to a reinforced composite gel[23]. Vinches *et al.* reported a high sensitivity to GL molecular weight on the placement of the cloud-point curve, and a radical reduction in compatibility upon the addition of a small amount of a long-chain oligosaccharide to an otherwise short-chain sample[27]. It was reported that a significant increase in the phase separation temperature (in the order of 3°C) resulted from the substitution of only 2% of the originally short oligosaccharide.

The effect of component molecular weight on phase separation has been investigated by examining the behavior of systems phase separating slightly above and below the GL gelation temperature[16;59;72]. When phase separation

occurred below gelation temperature, a noticeable time delay was observed prior to phase separation. The observed delay was found to correspond with the time for GL to reach a certain degree of ordering[4]. Formation of GL physical crosslinks serves to effectively increase the average molecular weight of the component in solution. This increase is sufficient to alter the thermodynamic parameters governing the miscibility of GL in mixed solution. Loren stated that it was this ordering that drove polymer incompatibility and subsequent phase separation. Butler *et al.* observed a similar effect in quenches into the gelling region, specifically a time-delay related to the time required for GL ordering[3].

2.2.3 Theoretical Descriptions of Biopolymer Phase Behavior

The basis for the thermodynamic drive towards separation is in the interactions of the mixture's constituent biopolymers with one another as well as with the solvent[11]. These interactions are broken down into the enthalpic and entropic contributions associated with the mixing of these molecules[5]. Enthalpy-driven interactions are typical for biopolymer incompatibility and are adequately described by the Flory-Huggins theory (Chapter 3, Section 3.1) of polymer mixing[5]. Entropic considerations are more prevalent in systems where excluded volume or depletion interactions play an important role, such as in mixtures of random coiled polysaccharides and covered protein particles like micelles[73].

Gibbs tangent analysis is crucial for the description of the global phase stability and theoretical equilibrium of mixed systems[74]. Determination of global phase diagrams using this fact has been extensively conducted

theoretically and experimentally for synthetic polymers and biopolymers using a variety of equations of state or governing equations. The second virial coefficient equation of state was used by Simonet *et al.* in modeling guar-dextran phase behavior, demonstrating the use of equation of state modeling in biopolymer systems[75]. Despite this, it is the Flory-Huggins theory of polymer mixing that has been most frequently used to describe the miscibility behavior observed in biopolymeric mixtures[33;69].

Flory-Huggins theory is a statistical thermodynamic approach to Gibbs free energy calculation that relates the stability/miscibility of a biopolymeric mixture to three main sets of parameters, namely component molecular weights, interaction parameters (χ) and mixture component concentration terms[27;27;29]. The χ parameters are often interpreted as empirical quantities that are used to bridge the gap between the simple theories of Flory-Huggins and the diverse range of phase behaviors observed in polymer mixtures[1]. While phase compositions and molecular weights are easily determined experimentally and from previous research, χ values are less readily available in literature. As such, the χ parameters are often used as fitting parameters in the modeling of experimentally-determined tie-lines[14]. Having said this, the χ parameters are physically obtainable as they are directly related to the second virial coefficients of the biopolymers in solution, which are obtainable by light scattering, vapor sorption, osmotic pressure and swelling equilibrium, among other means[26;75].

Given the relative temperature-independent nature of biopolymer molecular weight in the absence of gelled network formation, it has been stated

that the driving force for phase separation is solely governed by the temperature dependence of the Flory-Huggins interaction parameters[76]. The published work of Mumby and Sher is unique in being one of the few descriptions of binary polymer solution phase behavior found by the author to acknowledge the temperature and composition dependence of the χ parameters[26]. Such an acknowledgement remains absent for biopolymeric mixtures, possibly because of the relative infancy of theoretical thermodynamic research in this area. One of the more current, robust models of biopolymeric compatibility behavior was conducted by Clark, who used existing tie-line data to fit the Flory-Huggins theory[14]. He calculated three model parameters (one molecular weight term and two χ values) and their uncertainties by using them as fitting parameters. Due to the irreducible parameter correlation (degrees of freedom of the governing equations), the remaining molecular weight and χ were experimentally determined. The phase diagrams calculated generally provided a good fit, though the procedure was discounted by the author due to discrepancies between calculated and experimental molecular weights and χ values. Clark described the Flory-Huggins approach as an inaccurate quantitative predictor of phase behavior. The semi-quantitative utility of the model was noted, however, based on the ability to exhibit influences of molecular factors on the binodal, tie lines, critical points and tie-line slope. Clark's critiques of the Flory-Huggins approach are tempered by noting his disregard of dependence of χ on temperature and concentration, the improved utility of the model when using

fewer fitting parameters and the assumption of polymer monodispersity throughout his work.

Simonet *et al.* are unique in having compared the utility of the Flory-Huggins theory to virial coefficient expansion equation of state in modeling the phase behavior of the guar-dextran system[75]. Second virial coefficients and molecular weights were first determined using light scattering. It was found that both models yielded quite similar results and both satisfactorily fit with experimental results. The author attributed slight discrepancies to polydispersity of one of the components. The closeness of the two models was hardly unexpected, however, given that both are based on excluded volume interactions and have similar expressions for chemical potentials.

2.2.4 Phase-separated Structure Evolution

A further consequence of concurrent phase separation and gelling was the retardation of the development of microstructure. Gelation has been observed to 'kinetically'-trap systems in a non-equilibrium state[23]. In general, higher temperatures allow coarsening to occur for a period prior to trapping of the microstructure. Gelation in competition with phase separation will severely reduce the coarsening (*i.e.* droplet growth) rate as the hydrodynamic flow required is suppressed[36]. Despite this, Butler also reported a noticeable evolution in microstructure days after trapping[72]. This observation agrees with that of Loren *et al.*, who stated that the elasticity required to trap the system is not related to that found immediately at the gel point. The 'viscofying' of the

solution required to hinder structural development occurs over an extended period of time[16].

Following the onset of phase separation, two processes will lead to equilibrium in the system. Depending on the temperature quench, two phases will result from a counter-directional diffusion of dissimilar polymers to phases that are rich in one polymer and depleted in the other. This process is said to occur relatively rapidly (Table 2.1) in the GL-MD system as phase separation quickly evolves into the later stage of coarsening.

Table 2.1: Relative rates of phase-separated composition and structure evolution for the mechanisms of phase separation in biopolymers.

	Time scale		
	0-10s seconds	hours	days
	Phase separation	Ripening	Bulk phase separation
Nucleation and Growth (NG)			
Phase volume	3	1	1
Concentration of phases	1	1	1
Structural evolution	2	2	1
Spinodal Decomposition (SD)			
Phase volume	1	1	1
Concentration of phases	3	1	1
Structural evolution	2	2	1

1=slow rate; 2=moderate rate; 3=high rate
Adapted from Lundin[12].

Coarsening onset is characterized by a well-defined morphology, sharp interfaces between phases and equilibrium phase compositions[3]. When equilibrium compositions are attained, the system continues to evolve in an effort to minimize the total contact area between the two phases. With the

exception of rapid, deep quenches below the gelation temperature or for systems whose phase separation temperature is below that of gelation, kinetically-trapped systems generally exhibit equilibrium phase compositions in the absence of phase stability (the driving force for coarsening)[3].

At the onset of thermodynamic incompatibility, a biopolymeric mixture will separate into two new phases. The mechanism by which this process proceeds is dependent on where the temperature quench lands the system on the phase diagram, or more specifically, whether the separating system is unstable or metastable. In GL-MD mixed systems, both unstable and metastable systems have been observed in the form of separation *via* the spinodal decomposition (SD) and nucleation and growth (NG) mechanisms, respectively[69]. Keller has described the metastable state as one possessing a local free energy minimum, but not a global stable equilibrium[77]. Such behavior has been observed in polymer blends in phase transitions that are impeded by kinetic limitations, or energy barriers, along the pathway to thermodynamic equilibrium[77]. Though both mechanisms occur in the GL-MD system, numerous studies have observed only SD[24;36;69]. This occurrence, coupled with the sharp transition from NG to SD observed by Butler, points to a small metastable region in the GL-MD system[72].

The evolution of GL-MD phase-separated microstructure has been well characterized in both the NG mechanism and in the three unique stages of SD, characterized as the early, intermediate and late stages of phase separation[3;16;24;37;65;72]. The most common technique in observing

microstructural mechanisms during phase separation is to measure changes in the peak of the scattering function of a sample examined by static light scattering (SLS), where the behavior of the peak is correlated to changes in the structure function[3;34;35]. The most significant difference between NG and SD in the GL-MD was confirmed by Butler when it was seen that dynamic scaling occurred during SD but not NG, which was seen as a difference in the behavior of the structure function[72]. In this study, Butler observed a coarsening exponent of 1/3 for SD growth, that is, an increase in average inclusion size as a function of time to the power of 1/3. Loren *et al.* substantiated this finding by also reporting an initial growth that was independent of temperature and had a coarsening exponent of 1/3[24]. After a period of growth, a crossover was observed when the characteristic growth exponent changed to a value in the range of 0.75-1.58. The actual value of the growth exponent following crossover was found to be inversely related to the end temperature of the system. A crossover from 1/3 to 1 was observed in slowly gelling systems[10]. Loren further explained that the crossover was the point of transition from intermediate SD, where growth was governed by diffusion, to the late stage of SD and beyond, where hydrodynamic flow began to have an increasing role in coarsening. The growth behavior in synthetic polymers was characterized by Tokuyama, where the diffusion controlled regime was found to occur slightly more rapidly with an exponent of 1/2, while later stages were slightly slower at 1/3[78]. It is conceivable that the growth differences are attributed to the relative disparate molecular sizes of synthetic polymers and biopolymers. A small

molecule would likely encourage diffusion, but would not initiate hydrodynamic flow with the same intensity as a larger molecule given its lower density. The evolution from early/intermediate growth to late stage growth has been shown be occur quite rapidly (Table 2.1) in the GL-MD system, indicating rapid attainment of equilibrium phase compositions[3].

Rheological measurements and microscopy by Foster *et al.* established that biopolymer separating systems are governed by the same stability principles as for oil-water emulsions, and as such may taken to follow the same physical and theoretical behaviors[12;79]. Independent of this finding, the water-in-water emulsion resulting from aqueous biopolymer phase separation has been proposed to undergo a number of emulsion destabilizing processes[39]. Late stage coarsening behavior has been proposed to be driven by a coalescence mechanism, which accelerates when droplets reach a critical size and z-direction hydrodynamic flows are initiated[59]. This finding, coupled with percolation observations of Loren *et al.*, indicates beyond the coalescence driven regime lies an area of a number of confounding coarsening mechanisms that remain undiscussed in the context of biopolymeric systems, such as coalescence, Ostwald ripening and sedimentation. Loren does, however, present an attempt at clarifying the events characteristic in a SD phase separation mechanism and subsequent microstructural coarsening, namely SD followed by self-similar growth, diffusion of inclusions, percolation-to-cluster transition and finally coalescence[16].

2.2.5 Concurrent Phase Separation and Gelation

The temperature quench depth strongly affects size, volume fraction and number of inclusions in phase-separated systems. In the GL-MD system, the behavior of GL-continuous systems was observed as a function of quench depth and it was found that a deeper quench favoured larger MD inclusions, a higher population of MD inclusions and a greater volume fraction of the included phase[16]. The implication of these results, as they pertain to the progression of a coalescing system, is explored later in this thesis in more detail. The result of an increased quench depth is that eventually phase separation is found to proceed concurrently with gelation. Loren *et al.* observed an increased size of MD inclusions as phase separation temperature increased and as quench rate decreased[16]. These finding are logical, given that a higher phase separation temperature effectively increases the size of the two-phase liquid region, allowing for more coalescence time. The effect of decreased rate of cooling serves to increase coalescence opportunity.

When phase separation and gelation occur in close temperature proximity, unique microstructures have been reported. When phase separation occurs during gelation, a varied microstructure results and is attributed to the competition between the two processes[4;32]. When phase separation occurs below the gelation temperature, the thermodynamic properties of the components are altered. An effective increase in GL molecular weight, resulting from physical entanglement of GL chains, drives phase separation.

Small inclusions in a diffuse microstructure result and are evidence of incomplete phase separation aborted by rapid gelation.

A number of researchers have reported the phenomenon of secondary phase separation in GL-MD systems, especially deep quenches. Following an initial deep quench, primary phase separation is initiated and subsequent phase enrichment and droplet growth follow. For sufficiently deep and slow quenches into the gelling region, the effective molecular weight increase of GL acts to alter the equilibrium conditions of the system and induce a second phase separation[3;65]. This has been reported as a second MD phase within the GL regions of the composite[65]. However, as will be examined later in this thesis, secondary phase separation is prevalent in both phases, which enables the creation of a four-phased system.

Chapter 3

Theoretical Background

The goal of this chapter is to develop the theoretical background of the enthalpic and entropic contributions involved in biopolymer phase separation. Focus is on the Flory-Huggins theory, which describes the free energy of mixing in a polymer mixture, and on the Cahn-Hilliard theory, which explains the mechanisms of phase separation based on the different changes in free energy that result from polymer mixing.

Depending on the desired application, phase separation may be a favourable or undesirable process. For example, the manufacturing of confectionary jellies is a process that requires intimate mixing of components whereas creation of textured fat-substitutes may benefit from phase separation. In either scenario, an *a priori* understanding of the compatibility of the mixture components is required.

The two thermodynamic parameters which determine the miscibility of biopolymers in mixed solution are entropy and enthalpy. Both terms combine to give a value of the system's Gibbs free energy change upon mixing of its components. Gibbs free energy is the thermodynamic potential of a system and gives an indication of the amount of work obtainable from it. A system at equilibrium exhibits a minimization of Gibbs free energy, or, no remaining

potential to do work[80;81]. Entropy and enthalpy contribute to the Gibbs free energy in opposite directions. An increase in enthalpy upon mixing will result if heat is required to solubilize mixture components and will lead to an increase in Gibbs free energy. Conversely, an increase in entropy, resulting when systems become more disordered on a molecular level, will serve to decrease Gibbs free energy. A system will reach a state of equilibrium when its change in Gibbs free energy resulting from some process has reached a minimum value.

In mixtures of neutral biopolymers, there is typically an enthalpic advantage for molecules in the mixed system to be surrounded by other molecules of the same type. The basis for this behavior is seen in the analogy of a mixture of equal numbers of two different dipolar molecules. As the difference in dipole strengthens, so too increases the enthalpic advantage of segregation of the two types of molecules. In the case of small molecules, the enthalpic drive for segregation is outweighed by the entropic benefit of mixing (*e.g.*, a mixture of ethanol and water follows this trend, whereas a mixture of oil and water does not behave this way due to their differences in polarity). This behavior is contrasted by that of polymers which exhibit less entropy of mixing because of the reduced number of molecules that are free to move independently in solution. This promotes the separation of components into two co-existing phases, each enriched in one polymer and depleted in the other, when thermodynamically favourable.

Food systems exhibit a number of behaviors that are characterized by changes in entropy and enthalpy. The solubilization of high concentrations of

table sugar (sucrose) in water often requires the addition of heat. This process is a classic example of positive enthalpy of mixing, one that moves a system away from equilibrium. Conversely, entropy is increased when ice is dissolved in water, as the energy gradient between these two phases is dispersed. This gradient is indicative of the system's ability to do work that shows its change in Gibbs free energy is not at a minimum value.

Miscible behavior in biopolymer mixtures is a result of a greater change in entropy of mixing than that of enthalpy of mixing. This results when the entropic advantage of random molecular mixing outweighs the enthalpic advantage of biopolymer molecules being segregated. When the multi-component biopolymer system is brought within the biphasic region (normally *via* a temperature quench), enthalpy will dominate and segregation will occur until a free energy minimum is attained. The phases born during phase separation will exist as equilibrium solutions of a dominant polymer saturated with a small equilibrium concentration of the other polymer[12]. In summary, the theoretical description of the phase behavior of a system is based in the description of the enthalpic and entropic contributions of components upon mixing.

3.1 Flory-Huggins Theory and the Thermodynamics of Polymer Mixtures

3.1.1 Thermodynamic Considerations of Polymer Mixing

The stability of a mixture of polymers will tend towards a state of minimal Gibbs free energy upon mixing. If such a state favours miscibility, the

polymer mixture will be homogeneous. Conversely, immiscibility will result if mixing is not thermodynamically favoured.

Most mixed systems are characterized by a critical temperature above which miscibility is favoured and below which immiscibility reigns. If two polymers are mixed at a temperature where the Gibbs free energy of the mixed system is lower than that of the individual components, a stable, homogeneous mixture will form. Furthermore, if the stable system is brought below its critical temperature, the polymer mixture will separate in an effort to minimize its Gibbs free energy. From this, it can be seen that a miscibility condition for two polymers in solution is a net decrease in Gibbs free energy upon mixing

$$\Delta G_M = \Delta H_{mix} - T\Delta S_{mix} < 0 \qquad (3.1)$$

where ΔH_{mix} and ΔS_{mix} are the changes in enthalpy and entropy, respectively, accompanying the mixing process and T is the absolute temperature.

The statistical-thermodynamic theory of Flory and Huggins was developed to describe the free energy of mixing in a polymer mixture[29;29]. The Flory-Huggins theory expresses the individual terms of the change in Gibbs free energy equation in terms of thermodynamic models based on physical and measurable parameters of the constituent components of the mixture, namely molecular weights, volume fractions and a parameter expressing the degree of interaction between components.

The entropic contribution of polymers in mixture is associated with the theoretical number of molecular arrangements that the polymers can occupy whilst in mixed state. The enthalpic contribution deals with the interactions

between similar and dissimilar polymer segments. In contrast to the mixing of small molecules, polymer mixtures are non-ideal. Non-ideal mixing behavior is defined as having an enthalpy of mixing term that cannot be neglected[77]. Generally, the enthalpy of polymer mixing is positive[67;82]. Thus, if mixing is to occur, the resultant entropy change must be sufficiently high. When the entropic term outweighs the enthalpic term the resultant Gibbs free energy term favours solubility, but does not guarantee it. Mixing of components below their miscibility temperature will result in a separated system of coexisting phases.

Before discussing the conditions for mixture stability and the governing equations of this behavior, a few terms should be defined. A partial molar quantity is the derivative of any quantity, *M*, with respect to the number of moles of one of the components when all other parameters are fixed

$$\overline{M}_i = \left(\frac{\partial M}{\partial n_i}\right)_{T,P,n_j} \tag{3.2}$$

Mathematical manipulation of this equation for a system at constant temperature and pressure yields the Gibbs-Duhem equation

$$\sum_i n_i d\overline{M}_i = 0 \tag{3.3}$$

Gibbs free energy, *G* may be substituted into Equation 3.3 in place of *M*.

Before mixing n_1 moles of polymer *1* with n_2 moles of polymer *2*, the sum of the free energies of both components is based on

$$G_{component} = \sum_{i=1}^{2} g_i n_i \tag{3.4}$$

Here, g_i is then the molar free energy of the each type of polymer. After mixing, the free energy of the mixture is expressed as

$$G_{mixture} = \sum_{i=1}^{2} \overline{G}_i n_i \tag{3.5}$$

Combining equations (3.4) and (3.5) yields the change in Gibbs free energy resulting from mixing of the two polymers

$$\Delta G_M = G_{mixture} - G_{component} = \sum_{i=1}^{2} \left(\overline{G_i} - g_i\right) n_i \tag{3.6}$$

Taking the total number of moles in the mixture to be n_1+n_2, and dividing both sides of equation (5.6) by this term gives the generalized result for change in Gibbs free energy of mixing for a single mole of the polymer mixture

$$\Delta g_m = \sum_{i=1}^{2} \left(\overline{G}_i - g_i\right) x_i \tag{3.7}$$

It is convention to refer to the partial molar Gibbs free energy, $\overline{G}_i$, as the chemical potential, which is symbolized as μ_i. Also, g_i is the partial molar Gibbs free energy for the pure, unmixed component, which is a property characteristic of each polymer, and is typically denoted by $[\mu_i{}^0]$ [62].

Upon mathematical rearrangement and application of these definitions to Equation (3.7), equations for the chemical potential as a function of change in Gibbs free energy of mixing of a binary polymer mixture result

$$\Delta\mu_1 = \Delta g_m - x_2 \frac{d\Delta g_m}{dx_2} \tag{3.8a}$$

$$\Delta\mu_2 = \Delta g_m + x_1 \frac{d\Delta g_m}{dx_2} \tag{3.8b}$$

where x_i is the mole fraction of polymer i in the mixture.

The Flory-Huggins theory provides a platform for relating the change in Gibbs free energy of mixing to composition and chemical potentials, thus enabling the solution of equations (3.8a) and (3.8b) and the calculation of phase equilibria for a given system.

3.1.2 Thermodynamically Stable and Unstable Phase Behavior

As was previously mentioned, a negative change in Gibbs free energy upon mixing is not a sufficient condition to guarantee miscibility. A negative ΔG_M may yield either a single-phase or phase-separated system. The chemical potentials of components at any possible composition are calculated from the tangent to the Δg_m curve (Figure 3.1).

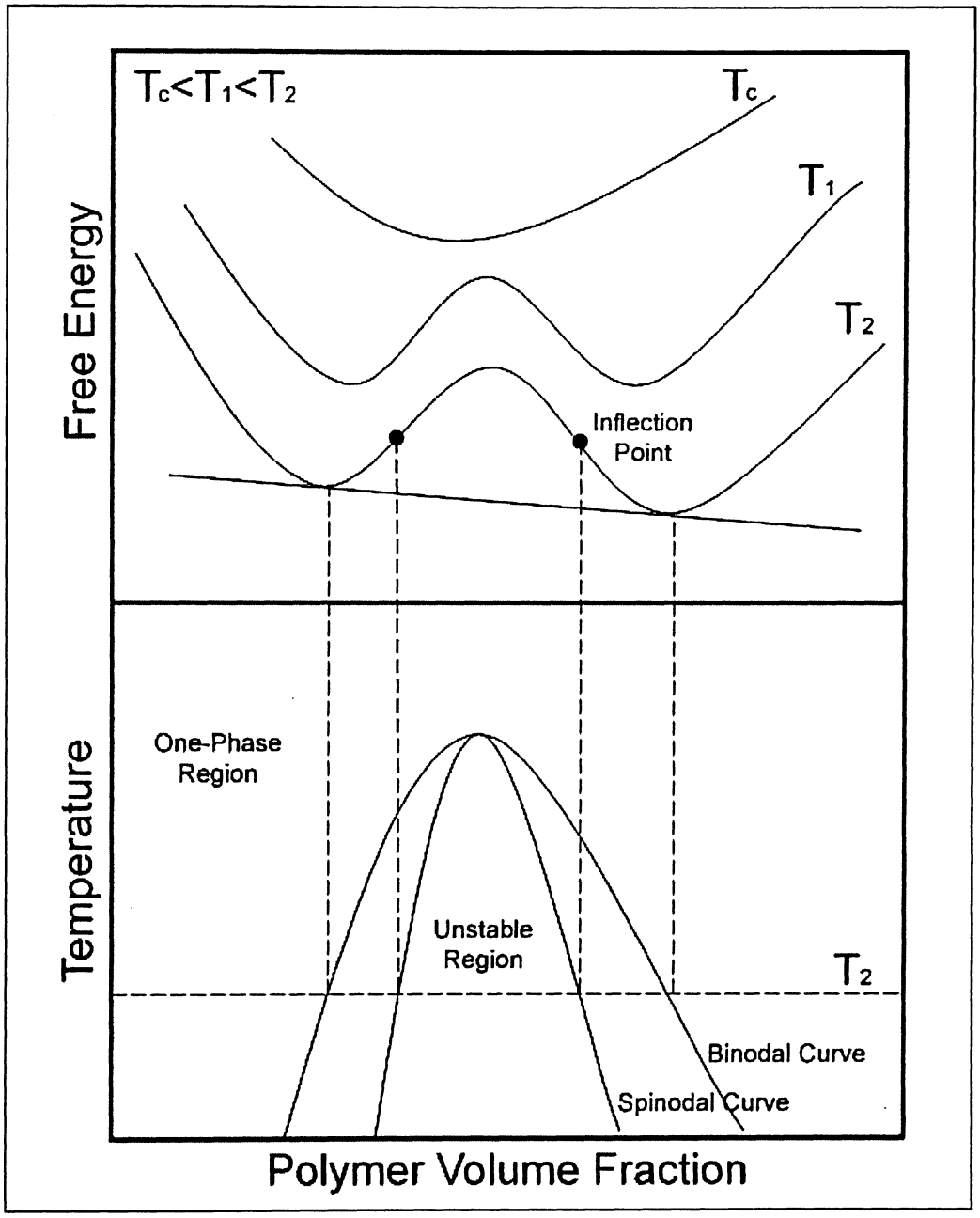

Figure 3.1: Plot of the free energy of a polymer mixture as a function of volume fraction. The characteristic shape of the curve differs depending on whether the system is miscible (T_c) or immiscible (T_1 and T_2). Translation of the free energy plot to a temperature-composition phase diagram is done by extending the tangent points ($\frac{\partial G}{\partial x_i} = 0$) and inflection points ($\frac{\partial^2 G}{\partial x_i^2} = 0$) for a series of curves (Adapted from Tran *et al.*[6]).

For single-phase solutions the entire curve describing the change in Gibbs free energy of the system is concave upwards and as such it is impossible to have two compositions with the same chemical potentials. Below the critical temperature of the system, the Δg_m curve takes on a bimodal shape where it is now possible for two x_i values to exhibit equal chemical potentials. These two, compatible x_i conditions are indicative of two phases coexisting in equilibrium and are binodal points. Any phase composed so that it resides on the curve between these two points may eventually separate into these two phases. Separation is generally favoured under these circumstances as the free energy of the two-phase system is lower than that of the single, mixed system.

Inflection points on this curve are the spinodal points of the system, which are determined based on the stability criteria, $\frac{\partial^2 G_M}{\partial x_i^{\,2}} = 0$. Between these points, the curve is concave downwards and systems residing in this region are unstable to all concentration fluctuations and will phase separate spontaneously into two coexisting phases. Between the binodal and the spinodal points lies the region of metastability where the system may exist as a one phase system for a finite period of time before phase separating. From this, it is apparent that a negative ΔG_M is, on its own, not a sufficient condition for phase separation given the existence of multiple points on the curve, where $\frac{\partial G}{\partial x_i} = 0$. More important is the shape of the curve which will determine the mechanism, time scale and likelihood of phase separation.

3.1.3 Flory-Huggins Theory of Free Energy Changes in Polymer Mixtures

Flory-Huggins theory is a statistical thermodynamic tool that enables the determination of the free energy change of mixing of a polymer in a solvent. Derivation of the working equations of this theory is based on the assumption that there is no change in volume upon mixing. From this, the calculation of free energy change upon isothermal mixing of the polymers is reduced to a calculation of the entropy of mixing.

To accomplish this calculation, a statistical approach based on a lattice model of molecules in solution is taken. A two-dimensional lattice is envisioned, with each lattice site having z neighbors, where z is known as the coordination number of the lattice. Each lattice site is capable of accommodating a single solvent molecule or polymer segment, defined as a polymer fraction having an equivalent volume as a solvent molecule. Each polymer molecule is assumed to be initially disordered, monodisperse, flexible and composed of m segments. Here, m is not the degree of polymerization of the polymer, but is related to the ratio of molar volumes of the polymer and solvent.

The lattice is taken to be initially empty and the number of ways (Ω) n_1 solvent molecules can be arranged with n_2 polymer molecules in $n_0=n_1+mn_2$ lattice sites is calculated. Based on the primary assumption that the enthalpy of mixing is zero, each lattice-filling polymer arrangement has the same energy and is equally likely to occur. Filling the lattice with polymer molecules is governed by the condition that two consecutive segments of a polymer chain

must reside in neighboring lattice sites. When the value of Ω is determined, the entropy of mixing is given by

$$S_{mixture} = k \ln \Omega \tag{3.9}$$

where k is Boltzmann's constant. Flory-Huggins theory uses the lattice analogy to formulate expressions for the entropy and enthalpy change upon mixing of two polymer species. The derivations of these expressions, and their combination into an expression for change in Gibbs free energy, follow.

3.1.3.1 Entropy Change on Mixing

Calculation of the entropy change upon mixing is based on the analysis of the arrangements of polymer molecules in the lattice. Once all polymer molecules are placed, solvent molecules are placed in any remaining unoccupied lattice sites.

Placement rules dictate that when j polymer molecules have been placed, the number of free lattice sites remaining will be n_0-jm. The first segment of the (j+1)st molecule can be arranged in n_0-jm different ways. Since the second segment of the molecule is adjacent, its placement is restricted to being placed in one of the z neighboring sites, all of which may not be vacant. If the polymer is concentrated, the average fraction of neighboring sites occupied, f, will be equal to the fraction of occupied sites for the entire lattice. As such, the second segment of the (j+1)st molecule can be placed in $z(1-f)$ different ways. It follows that the third segment will have $(z-1)(1-f)$ available placement options, and so on.

After mathematical manipulation, the simplified equation for entropy of mixing is given by

$$\Delta S = -R[n_1 \ln \phi_1 + n_2 \ln \phi_2] \tag{3.10}$$

This equation represents the Flory-Huggins entropy change resulting from the mixing of a polymer in solvent and is independent of the coordination number.

3.1.3.2 Enthalpy Change on Mixing

If the Flory-Huggins assumption of athermal mixing of polymers was true, the negativity of the $T\Delta S_M$ would always be equal to zero and miscibility would almost always be favoured. Since polymer dissociation is generally an endothermic process, this result is not adequate[29]. If the assumption of no change in volume upon mixing holds, the change in enthalpy will equal the change in internal energy, $\Delta H=\Delta U$ [82]. The internal energy term, ΔU, is an expression of the polymer and solvent molecular interactions. These intermolecular forces decrease as intermolecular distance grows. This result indicates that the lattice model presented is a sufficient platform to describe entropy change upon mixing since one need only consider interactions of neighboring molecules.

In a lattice filled with polymer chains and solvent molecules, any randomly-chosen polymer segment will be surrounded by z neighboring molecules. Of these, $z\phi_2$ are polymeric and $z\phi_1$ are solvent (where ϕ_i is the fraction of polymers of species i). Defining all possible energies of interaction: i) solvent-solvent as e_{11}; ii) polymer-polymer as e_{22}; and iii) polymer-solvent as e_{12}, the total energy of interaction for a single polymer chain is

$$z\phi_2 e_{22} + z\phi_1 e_{12} \tag{3.11}$$

Since the total number of polymer segments in the lattice is $n_0\phi_2$, the net energy of interaction for all of the polymer segments is

$$\frac{z}{2} n_0 \phi_2 (\phi_2 e_{22} + \phi_1 e_{12}) \tag{3.12}$$

In a similar fashion, the total interaction energy for a single, random solvent molecule defined as

$$z\phi_1 e_{11} + z\phi_2 e_{12} \tag{3.13}$$

and for all $n_0\phi_1$ solvent molecules as

$$\frac{zn_0\phi_1}{2}(\phi_1 e_{11} + \phi_2 e_{12}) \tag{3.14}$$

Prior to mixing, the energy of interaction between like segments of the polymer is

$$\frac{n_0\phi_2 z e_{22}}{2} \tag{3.15}$$

The similar quantity for the pure solvent is

$$\frac{n_0\phi_1 z e_{11}}{2} \tag{3.16}$$

The change in internal energy upon mixing, ΔU, will be the sum of the energies of all pure components subtracted from the energies of the components in solution

$$\Delta U = \Delta e z n_o \phi_1 \phi_2 \tag{3.17}$$

where

$$\Delta e = \frac{1}{2}(2e_{12} - e_{11} - e_{22}) \tag{3.18}$$

This value is dependent on the coordination number of the lattice which is not physically known. To remedy this, the value e is lumped with the parameter z to yield the "interaction parameter", χ. This parameter, which may be obtained from experiments or as a fitting parameter of phase behavior data, is positive for endothermic mixing and negative for exothermic mixing. The resulting expression for the enthalpy of mixing is

$$\Delta H_M = \Delta U_M = kT\chi_1 n_0 \phi_1 \phi_2 = kT\chi_1 n_1 \phi_2 \tag{3.19}$$

3.1.3.3 Free Energy Change, Chemical Potentials and Implications of the Flory-Huggins Theory

Having derived expressions for the changes in entropy (Equation 3.10) and enthalpy (Equation 3.19) upon mixing of a polymer in solvent, the free energy balance is now given by

$$\Delta G_M = kT\left(n_1 \ln \phi_1 + n_2 \ln \phi_2 + \chi_1 n_1 \phi_2\right) \tag{3.20}$$

It is interesting to note that, since volume fractions are always less than unity, the first two bracketed terms in this equation will be negative. The sign of the third term will depend on the interaction parameter, which will usually be positive. The interaction parameter varies inversely with temperature, so that for all systems, a high enough temperature will yield a change in Gibbs free energy of mixing < 0. This is evidence of the oft-mentioned fact that polymer dissolution generally requires a sufficient level of heating.

By increasing the polymer weight (and fixing all other parameters), the value of n_2 decreases proportionally because the unit volume of the polymer segment increases. The result is that the change in Gibbs free energy of mixing becomes less negative, with the implication being that a high molecular weight

polymer is less likely to be solubilized than the low molecular weight fraction of the same polymer. The utility of this is seen in separation processes such as fractionation, where the quench of a saturated polymer solution will first result in precipitation of the highest molecular weight fraction.

The Flory-Huggins theory may be coupled with the thermodynamic phase equilibrium criterion, $\mu_i^A = \mu_i^B$, to yield phase composition equations. Since the chemical potential is the partial molar Gibbs free energy (as discussed in Section 3.1.1), differentiation of the expression for Gibbs free energy of the mixture yields

$$G_{mixture} = n_1 g_1 + n_2 g_2 + RT(n_1 \ln \phi_1 + n_2 \ln \phi_2 + \chi_1 n_1 \phi_2) \tag{3.21}$$

with respect to number of moles of polymer and solvent, n_2 and n_1, respectively it follows that

$$\mu_1 = \frac{\partial G_{mixture}}{\partial n_1} = g_1 + RT\left(\ln \phi_1 + \frac{n_1}{\phi_1}\frac{\partial \phi_1}{\partial n_1} + \frac{n_2}{\phi_2}\frac{\partial \phi_2}{\partial n_1} + \chi_1 \phi_2 + \chi_1 n_1 \frac{\partial \phi_2}{\partial n_1} \right) \tag{3.22a}$$

$$\mu_2 = \frac{\partial G_{mixture}}{\partial n_2} = g_2 + RT\left(\ln \phi_2 + \frac{n_1}{\phi_1}\frac{\partial \phi_1}{\partial n_2} + \frac{n_2}{\phi_2}\frac{\partial \phi_2}{\partial n_2} + \chi_1 n_1 \frac{\partial \phi_2}{\partial n_2} \right) \tag{3.22b}$$

Simplifying these equations (Equations 3.22a and 3.22b) yields the Flory-Huggins equations for the chemical potential of the polymer (*1*) – polymer (*2*) solution:

$$\frac{\mu_1 - \mu_1^0}{RT} = \ln(1-\phi_2) + \phi_2\left(1 - \frac{1}{m}\right) + \chi_1 \phi_2^2 \tag{3.23a}$$

$$\frac{\mu_2 - \mu_2^0}{RT} = \ln(1-\phi_2)(1-m) + \ln \phi_2 + \chi_1 m(1-\phi_2)^2 \tag{3.23b}$$

By equating the chemical potential balances (Equations 3.23a and 3.23b) developed for each of the phases in existence in the separated mixture, a system of two equations with four unknowns (ϕ_1 and ϕ_2 for phase A, and ϕ_1 and ϕ_2 for phase B) results. By arbitrarily choosing the composition of one of the phases, the set of equations is reduced to a system of two equations with two unknowns (the remaining ϕ_1 and ϕ_2 values for the other, undefined phase). Solution of the system of equations yields the composition of the phase in coexistence with the initial, arbitrarily-defined phase. The compositions of the two coexistent phases are represented by two points on the binodal/compatibility curve of the system. The coexistent nature of the two points is indicated by their connection with a common, unique tie-line. Extension of this method of coexistent-phase-composition determination to a three component system (*i.e.* aqueous mixtures of two different biopolymers) forms the basis of the theoretical component of Chapter 6.

3.2 Cahn-Hilliard Theory and Mechanisms of Phase Separation

At the onset of thermodynamic incompatibility in a polymer mixture, phase separation will proceed by one of two mechanisms depending on whether the system is unstable or metastable. The sufficient and necessary conditions for the stability of a mixture are based on the entropy-enthalpy balance derived by Gibbs and previously described (Section 3.1.1). The criterion for mixture miscibility is given by

$$\left(\frac{\partial^2 G}{\partial n^2}\right)_{T,P} > 0 \qquad (3.24)$$

If this condition is not met, the solution may be subjected to concentration fluctuations. Metastability will result if the left-hand term in equation (Equation 3.24) is equal to zero. In this case, a stable single phase will exist for a finite period of time until critical concentration fluctuations occur, forming nuclei, enriched in the minority polymer, that begin to grow in size while maintaining their enriched composition. The work required to form the nuclei is a direct measure of the metastability of the system. Theoretical calculations show that this work term approaches zero as the system approaches the spinodal curve (demarcating the unstable region). Metastable droplet growth will proceed as long as a difference in chemical potentials between phases exists.

Of the two phase separation mechanisms, unstable spinodal decomposition (SD) is more complex than nucleation and growth (NG). Publications to date have tended to observe a SD with a far greater regularity in GL-MD systems[3;4]. This result may indicate that, at the very least, SD is far more prominent in the GL-MD system than NG, possibly because of the negligible difference between the binodal and spinodal curves (and, hence, the metastable and unstable regions)[83]. The SD process is characterized by three unique stages and is best visualized as a series of sine waves each describing a unique spatial change in concentration. Early stage SD is typified by an increasing amplitude of concentration fluctuation from t_i to t_1 while maintaining a constant wavelength. During this stage, "uphill diffusion" proceeds as the

minority polymer depletes in the continuous phase and migrates to the enriching inclusions[6]. Diffusion continues in intermediate SD, which exhibits an increase in the amplitude of the concentration fluctuation from time t_1 to t_2, coupled with an increase in the wavelength. Finally, during late stage SD, concentration fluctuations finally reach their critical values. These values are the equilibrium phase compositions of the separated system. It is also during this stage that the wavelength lengthens, due to coarsening of the microstructure.

The most prominent theoretical explanation of SD was laid forth by Cahn [84]. This theory was based on the unique method of free energy calculation previously developed by Cahn and Hilliard[85]. The theory considers an inhomogeneous solution whose composition throughout differs slightly from the average composition of the entire system. The free energy of such a system is made up of a homogeneous free energy term and a term accounting for the increase in free energy accompanying these concentration fluctuations. The free energy for such a solution is given by

$$G = \int \left(g(\phi) + \kappa (\nabla \phi)^2 \right) dV \tag{3.25}$$

where $g(\phi)$ is the free energy of the homogeneous mixture, which can be obtained from Flory-Huggins theory (Equation 3.20). $\kappa(\nabla\phi)$ is an expression of the free energy consequence of the concentration gradient, where κ is related to the interfacial constant.

It is seen from this relationship that the solution is stable for all infinitesimal concentration fluctuations if $\frac{\partial^2 g}{\partial \phi_1^{\,2}} > 0$. If $\frac{\partial^2 g}{\partial \phi_1^{\,2}} < 0$ the solution is

unstable to such a fluctuation where the first term of Equation 3.25 dominates. By choosing a large enough distance scale, fluctuations satisfying this criterion can always be found. In other words, in an unstable system, there always exists a compositional fluctuation gradient long enough to initiate separation.

CH theory describes the flux of the different polymers in a mixture as they diffuse away from their depleted phases to phases where they are enriched. The net polymer flux in the system is related to the free energy expression (Equation 3.25) as follows

$$J = \frac{\partial G}{\partial \phi} = -M\nabla\left(\frac{\partial g(\phi)}{\partial \phi} - 2\kappa\nabla^2\phi\right) \tag{3.26}$$

where M is an expression of the polymer mobility and is always positive. Relating this flux to the rate of change of polymer concentration with time to yields the non-linear CH equation

$$\frac{\partial \phi}{\partial t} = \nabla\left[M\nabla\left(\frac{\partial g(\phi)}{\partial \phi} - 2\kappa\nabla^2\phi\right)\right] \tag{3.27}$$

which describes separative growth of the intermediate and late stages of SD.

In early stage SD, the initial concentration fluctuations are quite small, and as such the CH equation may be approximated to be linear about the average concentration, ϕ_0

$$\frac{\partial \phi}{\partial t} = M\left(\left.\frac{\partial^2 g(\phi)}{\partial \phi^2}\right|_{\phi_0} \nabla^2\phi - 2\kappa\nabla^4\phi\right) \tag{3.28}$$

Solution of the non-linear CH equation is obtained *via* a Fourier series, which yields the general solution

$$\phi(r,t)-\phi_0=\sum_k A(k,t)e^{ikr} \tag{3.29}$$

where

$$A(k,t)e^{ikr}=A(k,0)e^{R(k)t} \tag{3.30}$$

$$R(k)=-Mk^2\left(\left.\frac{\partial^2 g}{\partial\phi^2}\right|_{\phi_0}+2\kappa k^2\right) \tag{3.31}$$

$$k=\frac{2\pi}{\lambda} \tag{3.32}$$

The fluctuation wavelength is denoted as λ. *R(k)* is known as the fluctuation amplification factor and must be greater than 0 for concentration fluctuations to occur. This value will result for wavenumbers, k, in the range $0<k<k_{critical}$, where the critical wavenumber is given by

$$k_{critical}=\left[-\left(\frac{1}{2\kappa}\right)\left.\frac{\partial^2 g(\phi)}{\partial\phi^2}\right|_{\phi_0}\right]^{1/2} \tag{3.33}$$

The single, characteristic fluctuation wavelength that will propagate fastest upon separation is given by

$$k_m=\frac{1}{\sqrt{2}}k_{critical} \tag{3.34}$$

The result of the CH theory of SD is that phase separation and enrichment is described as an evolution of concentration fluctuation waves. The manifestation of these waves in the microstructural evolution of phase-separated systems helps explain the primary difference between SD and NG. The two-phase structures resulting from separation are influenced by the relative volume fraction of the two constituent phases. When equal volume fractions exist, an

interconnected system unique to SD was predicted by Cahn. In systems where one volume fraction dominates, a separated system will exhibit one phase enclosed by the next similar to that of NG. Cahn further characterized SD growth behavior as it contrasts with NG. In an NG separating system, the new phase will initiate from a small regions (nuclei) which proceed to grow in extent over time. At any time during this process, the structure is clearly two-phase and compositions at points throughout the system are those of either one phase or the other. SD composition changes gradually in both directions from the average and, at least in early stages, the entire composition range between the concentration extremes exist within the system. Over time, the spread in composition increases as the two phases become more concentrated in either polymer. The key difference between SD and NG described here is that SD growth is not in the extent (characteristic wavelength) of the fluctuations but in the amplitude (concentration). This type of growth is only possible in the unstable region where such a change leads to a decrease in free energy (Equation 3.26). This implies that in the unstable region, not only will fluctuations occur, but when they do they will not spontaneously disappear. Observation of such fluctuations is evidence that the spinodal curve has been crossed.

Chapter 4

Experimental Methods

The following chapter introduces each of the experimental methods used in the analysis of phase separating aqueous mixtures of gelatin (GL) and maltodextrin (MD). Specific measurements associated with each experiment are addressed within the experimental sections of subsequent chapters. Unless otherwise indicated, all experiments within this thesis were performed in triplicate, as were their respective measurements.

4.1 Biopolymer Sample Preparation

The chemical and physical properties of GL and MD have been thoroughly described in the literature[2;45;53]. A summary of these findings was presented in Chapter 2, Section 2.1. What follows is a description of the experimental techniques used to prepare aqueous solutions of these biopolymers.

The GL used for all experiments herein was a Type A GL, acid-treated porcine tissue extract, 275 Bloom (Sigma-Aldrich, Mississauga, Ontario, Canada). The MD used was a Paselli-starch extract having a dextrose equivalency (DE) value of 5 (Tate and Lyle, Decatur, Illinois, USA).

Aqueous GL and MD stock solutions were prepared, and later combined, to produce the mixed systems analyzed throughout this thesis. In preparation of the GL stock solution, double-distilled (DD) H_2O was heated to 60°C in a 500 mL Erlenmyer flask on a stirring hot plate. GL powder was weighed and added gradually with stirring. Once all of the GL was added, the flask was capped with a rubber stopper to prevent moisture loss. The aqueous solution was left to stir for a period of 30 minutes during which time the GL dissolved. Following solubilization, the pH of the aqueous GL solution was determined with a pre-calibrated bench-top pH meter (Fisher Scientific, Ottawa, Ontario, Canada). Stock solutions were generally observed to have a pH in the range of 6.5-6.8. Concentrated NaOH solution (2 M) was added drop-wise to increase pH to 7. Finally, GL content was again analyzed (by dry-weight analysis) in order to confirm the concentration of the stock solution as 15%. Samples were transferred in vials and refrigerated until use for a period no longer than one week.

Preparation of MD stock solutions followed an almost identical method. DDH_2O was heated to 90°C and MD powder was solubilized, with stirring, over a period of 30 minutes. The elevated temperature of solubilization, relative to that of GL preparation, was a result of the thermal instability of GL at such temperatures (generally, above 80°C). pH was raised to 7 *via* the addition of a few drops of concentrated NaOH. The MD stock solution was prepared to a concentration of 30% (w/w) and was stored in sealed vials and refrigerated until use for a period no longer than one week.

Mixed biopolymer sample preparations were made in test-tubes through the addition of GL and MD stock solutions to yield the samples having desired concentrations. Samples were often diluted with a volume of DDH_2O during this process. A short period (~ 1 minute) of test tube vortexing ensured mixing of the stock solution volumes and was followed by short-term sample storage at 80°C to avoid undesired phase separation. Mixed samples were generally used within 6 hours of preparation and were discarded after 24 hours at the 80°C resting temperature.

4.2 Biuret Assay of Total Protein Content

The Biuret assay is one of the longest serving and most effective means of measuring the total protein content of a sample. Gornall *et al.* successfully applied its use to the determination of proteins in serum, a complicated matrix of proteins, polysaccharides and salts[86]. It was used in this thesis to determine GL content. The assay yields a protein concentration-dependent color change upon reaction of a sample with the Biuret reagent. The intensity of this color is monitored spectrophotometrically and is related to protein concentration by a standard curve.

Though many variations of the composition of the Biuret reagent exist, the components rarely change. The reagent used herein is the modified reagent presented by Gornall *et al.*[86].

A stock solution of Biuret reagent was prepared by combining 1.5 g $CuSO_4 \cdot 5H_2O$ with 6.0 g $NaKC_4H_4O_6 \cdot 5H_2O$ in approximately 500 mL of DDH_2O. To this, 300 mL of 10% (w/w) NaOH was added with swirling for 5

minutes. Lastly, approximately 200 mL of DDH_2O was added to bring the total volume to 1 L. Mixed biopolymer samples were added diluted at a 5:1 ratio, and were mixed with the Biuret reagent at a ratio of 1:10 (sample:reagent). These preparations were left at ambient conditions for 30 minutes to allow full development of color.

When a Biuret reaction is developed with a protein, the resultant change in color appears to be an intensification of the blue color of the reagent. However, spectrophometric analysis reveals the presence of a protein-dependent violet-colored complex, with an absorption maximum of about 545 nm.

The characteristic color-development of the assay over a range of GL-concentrations was observed at 545 nm and formed the basis for the correlation plot of percent transmittance versus GL-concentration. The resulting plot is found in Appendix A.

4.3 Assay of Total Biopolymer Content

In absence of an adequate and simple technique to determine polysaccharide content while in aqueous mixture with protein, the total biopolymer content of mixed systems was determined. Performing a mass balance on the system enabled the determination of total polysaccharide content as a function of protein and total biopolymer contents.

The total biopolymer content of an aqueous mixed system was determined *via* dry weight analysis. A small volume (~ 3 mL) of mixed solution was weighed in an aluminum weigh dish and subsequently boiled on a hot plate at 110°C. After boiling had ceased, the remaining solid sample in the

dish was weighed. The total biopolymer content, expressed as a percentage of the total solution weight, was determined as

$$Total\ biopolymer = \frac{Weight\ of\ dry\ sample(g)}{Weight\ of\ original\ sample(g)} x100\% \quad (4.1)$$

4.4 Static Light Scattering

Biopolymer molecular weights and second virial coefficients were determined *via* static light scattering analysis (SLS) on a Brookhaven 90PDP (Brookhaven Instruments Corporation, Holtsville, New York, USA). In the limit of low concentration, the intensity of scattered light observed during SLS analysis of dilute, homopolymer solution in a single solvent may be expressed as

$$\frac{H \cdot c}{\Delta R(\theta, c)} = \frac{1}{[M_w P_Z(q)]} + 2A_2 \cdot c \quad (4.2)$$

where H is an optical constant, c is biopolymer concentration, ΔR is the excess Rayleigh factor (proportional to the intensity of scattered light), q is the magnitude of the scattering wave vector, $P_z(q)$ is the particle structure function, θ is the scattering angle, M_w is the weight-averaged molecular weight and A_2 is the second-virial coefficient of the biopolymer in the solvent[87].

When the longest dimension of the biopolymer is small compared to the wavelength of incident light, it is referred to as a Rayleigh scatterer. This negates the scattering angle term in Equation (4.2), forming the basis for a Debye plot. At a single angle (90° for the 90PDP), scattered light intensities are measured as a function of biopolymer concentration. The results from a series

of such analyses are plotted according to Equation (4.2), yielding the M_W as the inverse of the intercept and A_2 as half of the slope.

4.5 Rheology: Surface Tension and Phase Viscosity

The surface tension of dilute, neat aqueous solutions of GL and MD were measured on a Langmuir trough over a range of experimentally pertinent temperatures (Kibron Instruments Incorporated, Helsinki, Finland). The theoretical interfacial tension exhibited by these two solutions was calculated using Fowke's relationship

$$\gamma_{GL-MD} = (\gamma'_{GL}{}^2 - \gamma'_{MD}{}^2)^2 \tag{4.3}$$

where γ'_i is the experimentally-determined surface tension of the biopolymer sample.

Phase viscosities were measured on a Bohlin cone and plate viscometer (Malvern Instruments Corporation, Mississauga, Ontario, Canada). Aqueous mixed systems of GL and MD were analyzed over a range of temperatures at variable shear rates on the viscometer. The data, obtained as plots of viscosity versus shear rate, was modeled using the power law model of viscosity

$$\eta = m\dot{\gamma}^{n-1} \tag{4.4}$$

where η is sample viscosity, $\dot{\gamma}$ is the shear rate, m is the consistency coefficient and n is the flow-behaviour index. The characteristic viscosities of each of the samples were taken as the zero shear viscosities observed.

4.6 Aqueous Biopolymer Specific Volumes

The specific volumes of GL and MD in aqueous solution were determined based on the density of neat solutions of each having known concentrations. The density of each solution was taken to be a function of the weighted average of the densities of its components, *i.e.* water and biopolymer.

$$\rho_{solution} = x_{biopolymer}\rho_{biopolymer} + x_{water}\rho_{water} \quad (4.5)$$

The density of the solution, $\rho_{solution}$, was determined using a picnometer with a known mass and internal volume. The density of the biopolymer while in aqueous solution was calculated using Equation (4.5).

4.7 Confocal Laser Scanning Microscopy (CLSM)

In recent years, CLSM has seen increased use in the food science and technology arena. In brief, CLSM represents the union of a centuries-old technique with much more recent technology. Together, imaging software, fluorescent probes, and computer-controlled optical pathways have transformed the simple light microscope into a much more powerful technique. With CLSM, rather than using a lamp as with a conventional microscope, a laser source at a defined wavelength is focused by the objective lens onto a single point in the specimen plane. A subsequent X/Y raster scan of that plane produces an image. Through computer control, scans of a specific focal plane can be produced non-invasively at set heights within the sample. This is one of the trademark features of CLSM - its capacity to obtain optical sections (*i.e.*,'z-slices') of an image. By using image processing, sequential images can be assembled to yield 3-D representations of the structures studied. Reflected and

fluorescent light (if the samples autofluoresces or if such stains are used) return *via* the illumination path and are focused at the confocal point located within a pinhole. Since the spot on the pinhole and the spot on the specimen are both located in the focal plane of the imaging lens, they are said to be confocal. These pinhole apertures limit the specimen focal plane to a confined volume of ~1 μm and blocks light from planes other than the focal plane. Relatively thick specimens (*e.g.,* 100 μm) can thus be imaged by successively acquiring a series of thin sections (< 1 μm) along the optical (z) axis of the microscope.

Finally, Rhodamine B is commonly used in the microscopic analysis of phase-separated GL-MD systems. It is preferentially electrostatically bound to GL in aqueous solution[69] and readily fluoresces. Excitation occurs at approximately 543 nm and yields emission at approximately 488 nm. As such, under CLSM observation, GL-rich phases appear as bright regions whereas MD-rich regions appear dark.

Chapter 5

Modeling Biopolymer Phase Behaviour with the Flory-Huggins Theory of Polymer Mixing

5.1 Introduction

Phase separation in biopolymer mixtures occurs when thermal, pressure or compositional parameters favour solution heterogeneity. The initial manifestation of phase separation is a clouding of the solution, which is characteristic of a minority phase dispersed throughout a majority continuous phase[3;9;79]. Over time, clouding gives way to bulk separation, where two clear layers form, each rich in one polymer and poor in the other[23]. When one of the polymers in solution (typically the continuous phase) gels in the same temperature range as that of phase separation onset, the dispersed phase may become 'kinetically-trapped' in the continuous phase, resulting in a sponge-like microstructure[79]. At a given composition, system morphology will depend on the residence time spent between the phase separation temperature and the glass transition temperature[22;24;64]. In this range, unhindered thermodynamically-driven separation may proceed without kinetically-induced 'freezing' of the

solution. Controlling separation kinetics in this window permits tailoring of phase-separated system morphology and mechanical properties[36].

Germane to tailoring microstructure is the characterization of the mixed biopolymer phase behaviour, usually with the aid of a phase diagram. In solutions of small molecules (*e.g.*, glucose), the entropy of mixing is typically of greater importance than the enthalpic interactions of the dissolved components. By contrast, polymers in solution (either synthetic polymers in solvent or biopolymers in aqueous media) have a severely limited freedom of mobility, leading to a dominating enthalpy component of free energy calculation[22]. Unless molecular interaction between the different types of polymers in solution is more favourable (which is often not the case), segregation will occur as the polymers will prefer like neighboring molecules[29;82]. By determining the extent of segregation, and *de facto* polymer miscibility, the system phase diagram is constructed.

The phase behaviour of mixed biopolymers may be experimentally determined when the phase separation temperature is above that of the gelation temperatures of the components. Temperature-induced phase separation of the system begins when the temperature is quenched from the one-phase region to the two-phase region (Figure 5.1). Upon separation, clouding of the system results and is followed by the partitioning of the mixture into two, transparent uniphasic layers. Each layer will be concentrated in one polymer and poor in the other and represents a pair of points on the binodal curve (shown in green in Figure 5.1) that straddle the one-phase and two-phase regions. Compositional

analysis of the resulting layers yields the coordinates of the points on the binodal. Experimental tie-line analysis must be carefully carried out when gelation occurs, as the system kinetically traps a non-equilibrium composition[10;23].

A theoretical framework helps to elucidate the role of parameters such as polymer molecular weight, temperature and solvent quality on phase behaviour[14]. The primary factor in the theoretical analysis of phase separation is the free energy change upon mixing[82], specifically the balance between the entropy (ΔS_{mix})and enthalpy (ΔH_{mix}) of mixing, as given by

$$\Delta G_M = \Delta H_{mix} - T\Delta S_{mix} < 0 \tag{5.1}$$

Mixed polymers will strive towards minimizing Gibbs free energy, *G*. As such, polymer miscibility will occur when the change in Gibbs free energy upon mixing is less than zero. If Gibbs free energy of the individual components is greater than that of the mixed system, the net change upon mixing will promote phase separation

$$\Delta G_M = G_{mixture} - \sum G_{components} > 0 \tag{5.2}$$

From the change in Gibbs free energy of mixing, the chemical potential ($\Delta \mu_i$) is calculated for each component in the system

$$\Delta \mu_i = \frac{\partial \Delta G_M}{\partial n_i} = \Delta g_M - x_2 \frac{d\Delta g_M}{dx_2} \tag{5.3}$$

where ∂n is the change in moles of species *i*, x_2 is the mole fraction of the coexisting component and Δg_M is the molar Gibbs free energy of mixing.

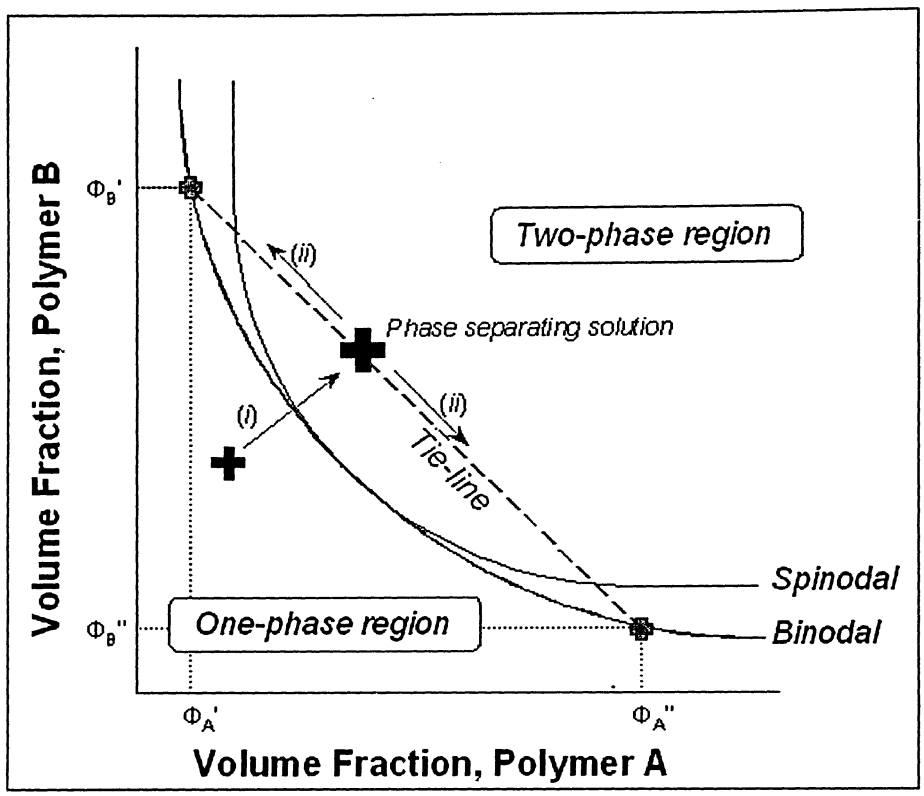

Figure 5.1: A hypothetical phase diagram for solvated mixture of polymer A and polymer B. When the one-phase system is brought into the two-phase region by process *(i)*, phase separation results. Process *(ii)* shows the newly formed phases beginning to enrich in one polymer and deplete in the next. At equilibrium, the two new phases exhibit compositions significantly different from their parent solution. All phase separating systems lying on the same tie-line will separate into the same two phases but will have different volume ratios depending on initial tie-line location. The spinodal curve further separates the two-phase region into metastable (between binodal and spinodal) and unstable (above the spinodal) regions.

The equilibrium state of a phase-separated system is characterized by the equivalence of chemical potentials of each component, *i*, in coexisting phases (denoted as μ_i' and μ_i'')

$$\mu_i' = \mu_i'' \tag{5.4}$$

The Flory-Huggins theory of polymer solution phase behaviour enables the change in Gibbs free energy of mixing to be related to composition[29].

Hence, chemical potentials can now be solved and used for calculation of phase equilibria. The original theories of Flory and Huggins developed for binary systems were extended to ternary and higher systems by Scott[27].

$$\frac{\Delta\mu_1}{RT} = \ln(\phi_1) + \left(1 - \frac{1}{P_2}\right)\phi_2 + \left(1 - \frac{1}{P_3}\right)\phi_3 + (1-\phi_1)(\chi_{ij}\phi_2 + \chi_{13}\phi_3) - \chi_{23}\phi_2\phi_3$$

$$\frac{\Delta\mu_2}{RT} = \ln(\phi_2) + (1-P_2)\phi_1 + \left(1 - \frac{P_3}{P_3}\right)\phi_3 + P_2(1-\phi_2)(\chi_{12}\phi_1 + \chi_{23}\phi_3) - P_2\chi_{13}\phi_1\phi_3$$

$$\frac{\Delta\mu_3}{RT} = \ln(\phi_3) + (1-P_3)\phi_1 + \left(1 - \frac{P_3}{P_2}\right)\phi_2 + P_3(1-\phi_3)(\chi_{13}\phi_1 + \chi_{23}\phi_2) - P_3\chi_{12}\phi_1\phi_2$$

(5.5)

where ϕ_i represents component i volume fraction, χ_{ij} represents the Flory-Huggins interaction parameter between components i and j, P_i represents the molecular weight of species i (relative to that of the solvent, where $P_{solvent}$=1). In this representation, subscript *1* indicates solvent (water) and *2* and *3* represent the polymers (*i.e.,* GL and MD). As shown, phase behaviour hinges on polymer and solvent molecular weights and energy parameters describing polymer-polymer and polymer-solvent interactions[14].

Minimizing Gibbs free energy (and thus equating the component chemical potentials amongst all phases), yields the binodal curve on the phase diagram, demarcating the one-phase, stable region from the two-phase, unstable region. The binodal corresponds to the experimentally-determined cloud-point curve, but does not give an indication of the transient stability of phase separation[27]. The condition for mixture miscibility (Equation 5.1) is necessary but insufficient alone in guaranteeing monophasic stability. This is because a

net decrease in Gibbs free energy can occur at both local and global minima. The metastable region is further demarcated from the unstable region by the spinodal curve, with the following condition

$$\frac{\partial^2 \Delta G_M}{\partial \phi_i \partial \phi_j} = 0 \tag{5.6}$$

For the ternary system of solvent(1)-polymer(2)-polymer(3), the spinodal is given by[27]

$$\left(\frac{1}{P_2\phi_2} + \frac{1}{\phi_1} - 2\chi_{12}\right)\left(\frac{1}{P_3\phi_3} + \frac{1}{\phi_1} - 2\chi_{13}\right) - \left(\frac{1}{\phi_1} - \chi_{12}\chi_{13}\chi_{23}\right)^2 \tag{5.7}$$

Other than the polymer-polymer interaction parameter (χ_{23}), all parameters required by the Flory-Huggins equations are experimentally-obtained The Flory-Huggins system of equations and equation (5.7) may then be used to construct theoretical binodal and spinodal curves for a given mixture[14;27;75].

The goal of this research was to model phase behaviour of GL-MD mixed systems by applying the Flory-Huggins theory. Such a result would fill a void in biopolymer research, where the compatibility of GL-MD solutions has been rarely investigated from a theoretical standpoint. It was hypothesized that, given the results of Flory-Huggins models of other biopolymer mixtures, a qualitative description of the phase behaviour could be obtained. This result would elucidate the role of temperature, concentration, molecular weight and the various interactions parameters in determining miscibility.

5.2 Experimental Techniques

5.2.1 Materials and Sample Preparation

The GL and MD samples and preparation techniques used were discussed previously (Chapter 2 and Chapter 4, Section 4.1, respectively). GL was classified as Type A, acid treated porcine tissue, having a bloom value of 275 (Sigma-Aldrich, Mississauga, Ontario, Canada). MD was classified as Paselli starch-derived and had a dextrose equivalency (DE) number of 5 (Tate and Lyle, Decatur, Illinois, USA).

Five aqueous system preparations were made, each having constant GL content (5% by weight) and differing in MD content (6%, 8%, 10%, 15% and 20% by weight). These systems were chosen based on preliminary micrographic evidence of the range of microstructures resulting from their separation, including GL-continuous and MD-continuous. As such, these systems were predicted to cover a broad region of the phase diagram.

5.2.2 Temperature Induced Phase Separation (TIPS)

Samples of each system were transferred into 12 mL test tubes. Each of these samples was preheated in a thermostated oven at 80°C for 10 minutes. Each test tube was then placed in incubators at temperatures set at 70°C, 60°C, 50°C or 40°C. At each of these temperatures, all samples exhibited phase separation and, after a 24 hour period, had completely bulk phase-separated. After 24 hours, each test tube was seen to have two distinct, transparent coexisting phases: the GL-rich phase on top and the MD-rich phase underneath this.

5.2.3 Biopolymer, Gelatin and Maltodextrin Phase Content

Following TIPS, the compositions of the two resultant layers were analyzed for total biopolymer (Chapter 4, Section 4.3) and GL content (Chapter 4, Section 4.2). MD content of all phases was calculated from these results by means of a mass balance on the solids in the system

$$MD\ Content\ (g) = Total\ Biopolymer\ (g) - GL\ Content\ (g) \tag{5.8}$$

5.2.4 GL and MD Specific Volumes in Aqueous Solution

The specific volumes of GL and MD in aqueous solution were determined using the procedure outlined in Chapter 4, Section 4.6.

5.2.5 Static Light Scattering (SLS)

Molecular weights and second virial coefficients were determined for GL and MD *via* SLS on a Brookhaven 90PDP light scattering device (Brookhaven Instruments Corporation) by measuring the time-averaged scattered light intensity for several samples of dilute biopolymers with varying concentrations. A_2, the second virial coefficient, was later related to the Flory-Huggins interaction parameter(s) *via*

$$\chi_{polymer-solvent} = 0.5 - \frac{v_{solvent} M_{solvent} A_{2,polymer}}{v_{polymer}^2} \tag{5.8}$$

where v is the specific volume.

5.3 RESULTS

5.3.1 Temperature Induced Phase Separation (TIPS)

A series of GL-MD solutions underwent TIPS to determine the compositions of the resulting separated phases. Turbidity in all samples (observed within a few minutes of the move to a lower hold temperature) indicated separation in the form of a dispersed droplet phase throughout a continuous phase. Upon visual inspection following the equilibration period (24 hours), all samples had bulk phase-separated into two transparent layers with a single, distinct boundary. This was taken as evidence of a coarsening process bringing the separated system in its infancy (droplets within a continuous phase) to a bulk separated system with a single interfacial boundary between the two coexisting layers.

5.3.2 Phase Composition Analysis

Samples of all resultant separated phases were gravimetrically analyzed for total biopolymer content. Analysis showed that initial systems having a given total biopolymer content separated into two phases that themselves had that same total biopolymer content (Figure 5.2). GL and MD contents of all phases were taken as the equilibrium co-solubilities of the components in aqueous solution at their given temperatures.

The specific volumes (mL/g) of neat GL and MD in aqueous solution (v_{GL}=1.551±0.009 g/mL; v_{MD}=1.538±0.005 g/mL) were used to convert phase compositions from mass percentages to volume fractions. The difference in specific volumes confirmed the initial observation that the GL-rich phase would

rest on top of the MD-rich phase in a bulk-separated system. All paired-phases (resulting from the same, initially homogeneous, parent system) yielded a single tie-line on the system phase diagram for the given temperature quench.

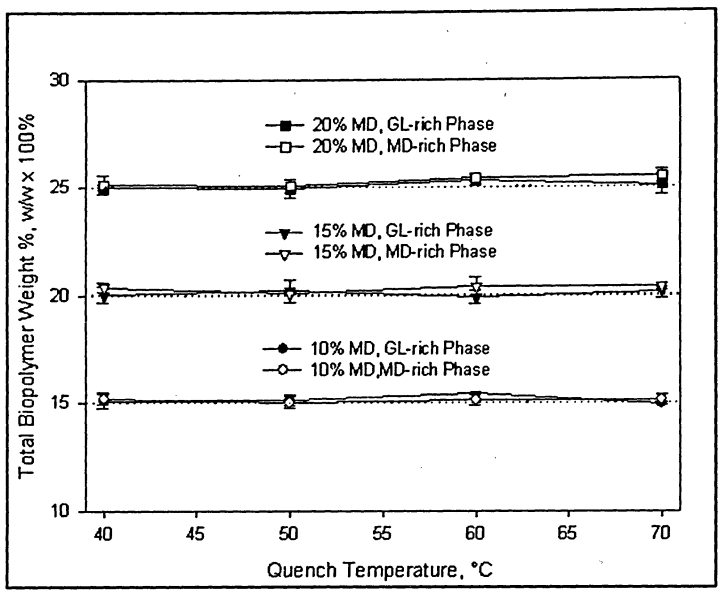

Figure 5.2: Selected results of total biopolymer content of coexisting phases following TIPS (samples containing 5% (w/w) GL and variable MD amounts) The data shows separated phases are composed of the same total biopolymer, by weight, as their parent samples.

MD-rich phases exhibited an increase in total GL content as temperature increased (Figure 5.3A). This trend of increased co-solubility was most dramatic for the 20% (w/w) MD sample. Conversely, GL-rich phases exhibited an increase in their total GL content as temperature decreased (Figure 5.3A). This drive toward biopolymer segregation was also most prevalent for the 20% (w/w) MD sample. Segregation of the phases into one purely GL-rich and one purely MD-rich would violate the equality of chemical potential criteria for equilibrium (Equation 5.4). Systems will separate such that the compositions of

the two coexisting phases are at the limits of solubility for a given temperature. Once this is attained, there is no longer a drive for further (*i.e.*, complete) segregation.

It was observed that, as the hold temperature decreased, there was a corresponding slight increase in size of the two-phase region as the compatibility curve shifted further towards the axes (Figure 5.4 A-D). In regions lying below the cloud-point curve, systems were monophasic, while above the compatibility curve into two phases connected by a tie-line and having compositions dictated by their location on the compatibility curve at that given temperature.

The general applicability of the experimental phase diagrams was investigated by preparing solutions having compositions dictated by the innermost points on the curve (as identified by circled points in Figure 5.4). The samples were left to equilibrate in incubators at temperatures 2°C above and 2°C below their requisite phase separation temperatures. All systems held at the elevated temperatures remained monophasic after the time period, whereas all of those below phase separation temperature exhibited bulk phase separation. These results were taken as evidence of the intermediate temperature acting as a transition point from miscible to immiscible behaviour for each of the investigated systems.

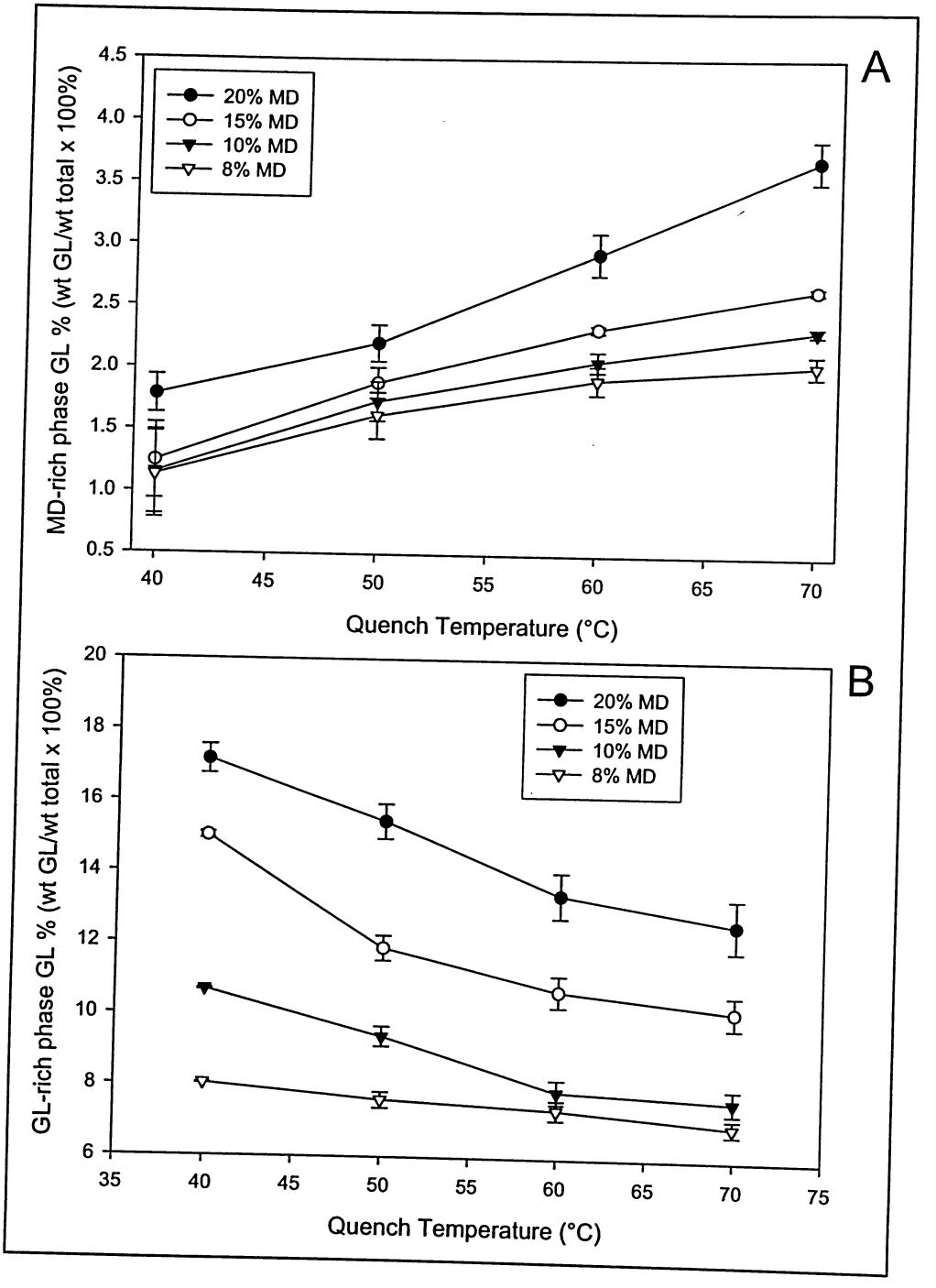

Figure 5.3: A.) Change in MD-rich phase GL weight % (all systems 5% GL, varying MD %) as a function of quench temperature. B.) Change in GL-rich phase weight % as a function of quench temperature.

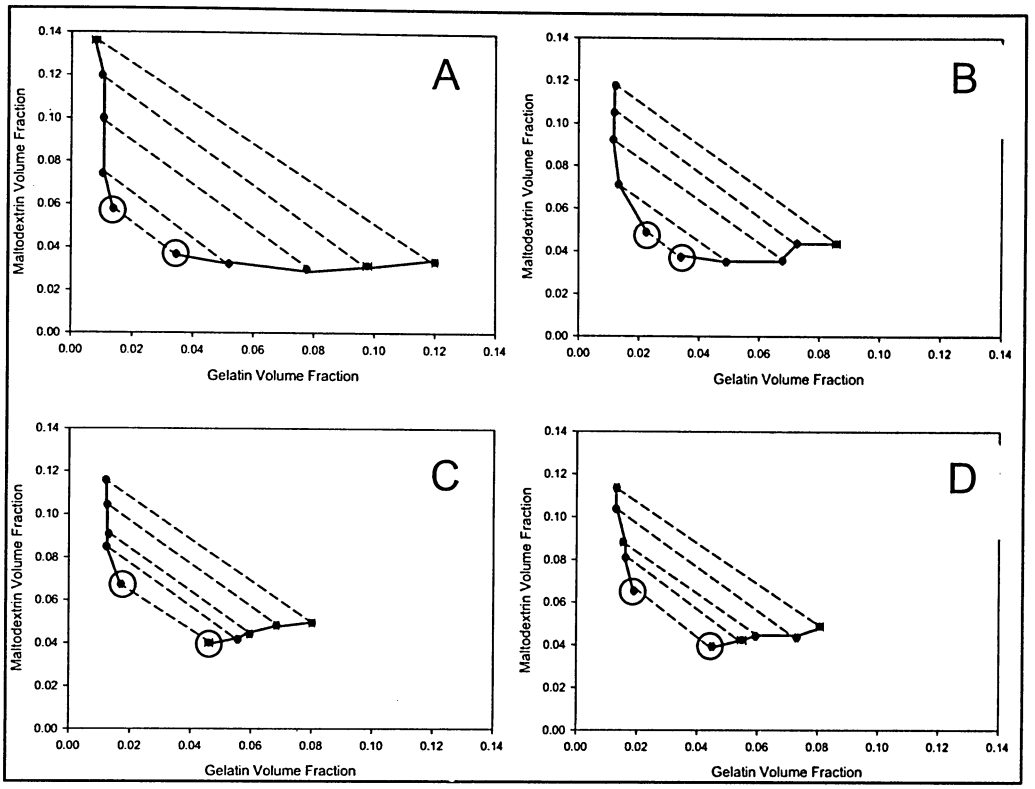

Figure 5.4: Experimentally-determined tie-line phase compositions for systems quenched to 40°C (A), 50°C (B), 60°C (C) and 70°C (D). Points on the plots indicate compositions of phases resulting from phase separation at their respective quench temperatures. Points connected by a common tie-line represent coexisting phases that originated from the same initial sample. Circled points were investigated experimentally in an effort to validate the predictive nature of the compatibility curves.

5.3.3 Experimental Determination of Model Parameters

The main parameters on which the Flory-Huggins theory is based include biopolymer volume fractions, normalized molecular weights and interaction parameters. All values, with the exception of the polymer-polymer interaction parameter, $\chi_{GL\text{-}MD}$, were determined experimentally.

Static light scattering (SLS) of neat solutions of GL and MD was undertaken. Debye plots for GL and MD were produced, showing the effect of

biopolymer concentration on the scattered intensity of incident light at 90° during the SLS experiments (Figure 5.5).

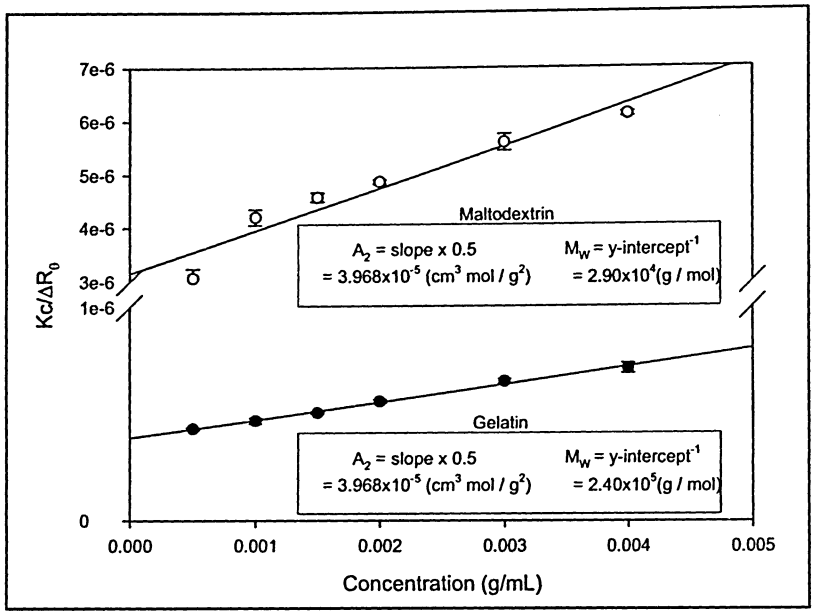

Figure 5.5: Debye plots produced from SLS experiments on neat solutions of GL and MD. The slope and y-intercept, respectively, yield the weight-average molecular weights and the second virial coefficients of the biopolymers in aqueous solution.

Polymer-solvent interaction parameters were calculated based on the second virial coefficients using Equation (5.8).

5.3.4 Polymer-Polymer Interaction Parameter ($\chi_{GL\text{-}MD}$) Determination

The polymer-polymer interaction parameter ($\chi_{GL\text{-}MD}$) was first calculated using the set of chemical potential equality equations for phase equilibrium, Equations (5.5), and the above mentioned experimentally-determined interaction parameters and molecular weights. Each set of tie-line data yielded a unique $\chi_{GL\text{-}MD}$ parameter, indicating an effect of biopolymer concentration on the interaction parameter (Table 5.1)[88]. P-values indicated a statistically

significant difference between the extreme $\chi_{GL\text{-}MD}$ values observed (both high and low) and the average $\chi_{GL\text{-}MD}$ value for each given temperature.

Table 5.1: Representative effect of biopolymer concentration on biopolymer-biopolymer interaction parameter, $\chi_{GL\text{-}MD}$, for separated samples originating from 5%GL-20%MD.

Quench Temperature (°C)	Separated Phase	GL Volume Fraction	MD Volume Fraction	$\chi_{GL\text{-}MD}$
40	MD-rich	0.0100	0.1197	0.009624**
40	GL-rich	0.1249	0.0335	0.013597**
50	MD-rich	0.0122	0.1175	0.008602**
50	GL-rich	0.0340	0.0372	0.012755**
60	MD-rich	0.0120	0.1156	0.008746*
60	GL-rich	0.0555	0.0416	0.011192*
70	MD-rich	0.0132	0.1037	0.008356*
70	GL-rich	0.0549	0.0422	0.011061*

** $P \leq 0.05$
* $P \leq 0.10$

A temperature effect was observed as the average $\chi_{GL\text{-}MD}$ for each tie-line set was found to decrease with an increase in temperature. For each cloud-point curve, the average $\chi_{GL\text{-}MD}$ value for the experimentally obtained tie-line data points was used as the final required parameter in applying Flory-Huggins theory. Once obtained, construction of theoretical phase curves was possible.

Tie-line data was next fitted to the spinodal curve equation, Equation 5.7, using $\chi_{GL\text{-}MD}$ as the lone fitting parameter. The collection of single $\chi_{GL\text{-}MD}$ values obtained from tie-line sets exhibited a similar inverse relationship with temperature as was observed earlier (Table 5.2). Values obtained for the $\chi_{GL\text{-}MD}$ parameter were similar in range and temperature dependence to comparable $\chi_{biopolymer\text{-}biopolymer}$ parameters reported elsewhere[27;75]. P values indicated a

statistically significant difference between the characteristic $\chi_{GL\text{-}MD}$ for each of the temperatures investigated.

Table 5.2: Flory-Huggins interaction parameter, $\chi_{GL\text{-}MD}$, values as determined from experimental data analysis and curve fitting.

Temperature (°C)	Average of Tie-Line Results		Curve Fitting Results	
	$\chi_{GL\text{-}MD}$, Average	Standard Deviation	$\chi_{GL\text{-}MD}$, Average	Standard Deviation
40	0.01232	0.001843*	0.01034	0.000234*
50	0.01091	0.001514*	0.00921	0.000280*
60	0.009961	0.000946*	0.008612	0.001710*
70	0.009843	0.001174*	0.008261	0.008280*

* $P \leq 0.05$

5.3.5 GL-MD Phase Behaviour Modeling Using Flory-Huggins Theory

Though the data obtained experimentally in constructing the compatibility curve represented the binodal curve of the GL-MD system, Flory-Huggins theory was used along with the stability criterion, Equation (5.6), to yield theoretical spinodal curves based on the experimental data (Figure 5.6 & 5.7). This assumption was done with experimental justification published previously, indicating a negligible difference between the binodal and spinodal in separating biopolymer systems[27]. Vinches *et al.* examined GL-oligosaccharide phase behaviour and found the metastable region to be quite small, especially in relation to the temperature-dependent shift of the phase curve. Butler *et al.* noted a similar behaviour for GL-MD aqueous mixed systems.

Figure 5.7 shows the predicted phase diagrams for the GL-MD system at 40°C, 50°C, 60°C and 70°C. In the absence of a specific temperature term in

the governing equations, the previously-mentioned effect of temperature on biopolymer compatibility was manifest in the changes of the $\chi_{GL\text{-}MD}$ parameter with temperature. The Flory-Huggins-based predictions followed the same trends observed experimentally and, furthermore, yielded a reasonable fit, with an average weighted R^2 of 0.9841 (n=10, $P < 0.0001$) for the set.

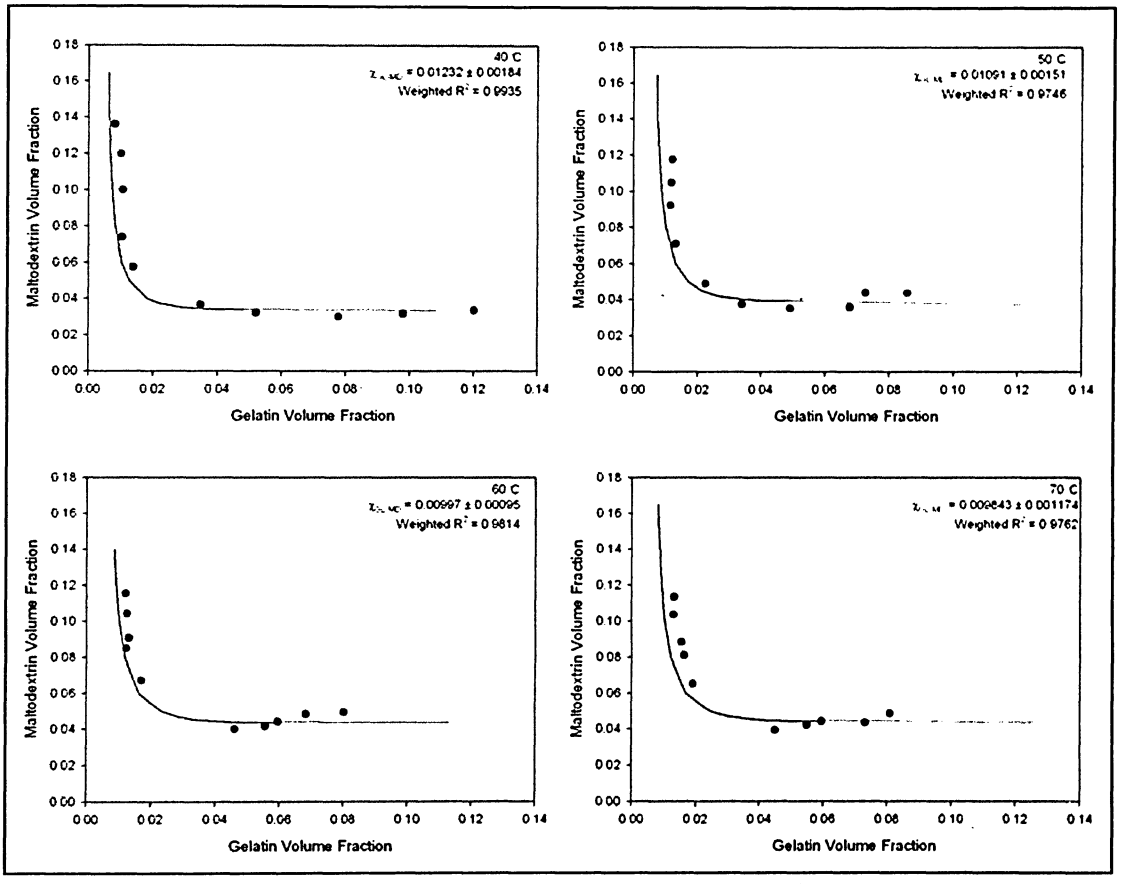

Figure 5.6: Flory-Huggins modeled compatibility curves based on the average $\chi_{GL\text{-}MD}$ from experimental tie-line sets. Points along the curve represent experimentally-determined compatibility-curve points. The smooth curve represents the Flory-Huggins-predicted phase compatibility curve.

Figure 5.8 shows similar results, this time taking the $\chi_{GL\text{-}MD}$ calculated as the fitting parameter yielded from curve fitting data analysis. Results showed a fit that was statistically reasonable based on the resulting R^2 values ($R^2 \geq 0.8572$,

n=10, P≤0.0015), but also one that was inferior to the previous method of averaging all $\chi_{GL\text{-}MD}$ values for a set of tie-lines.

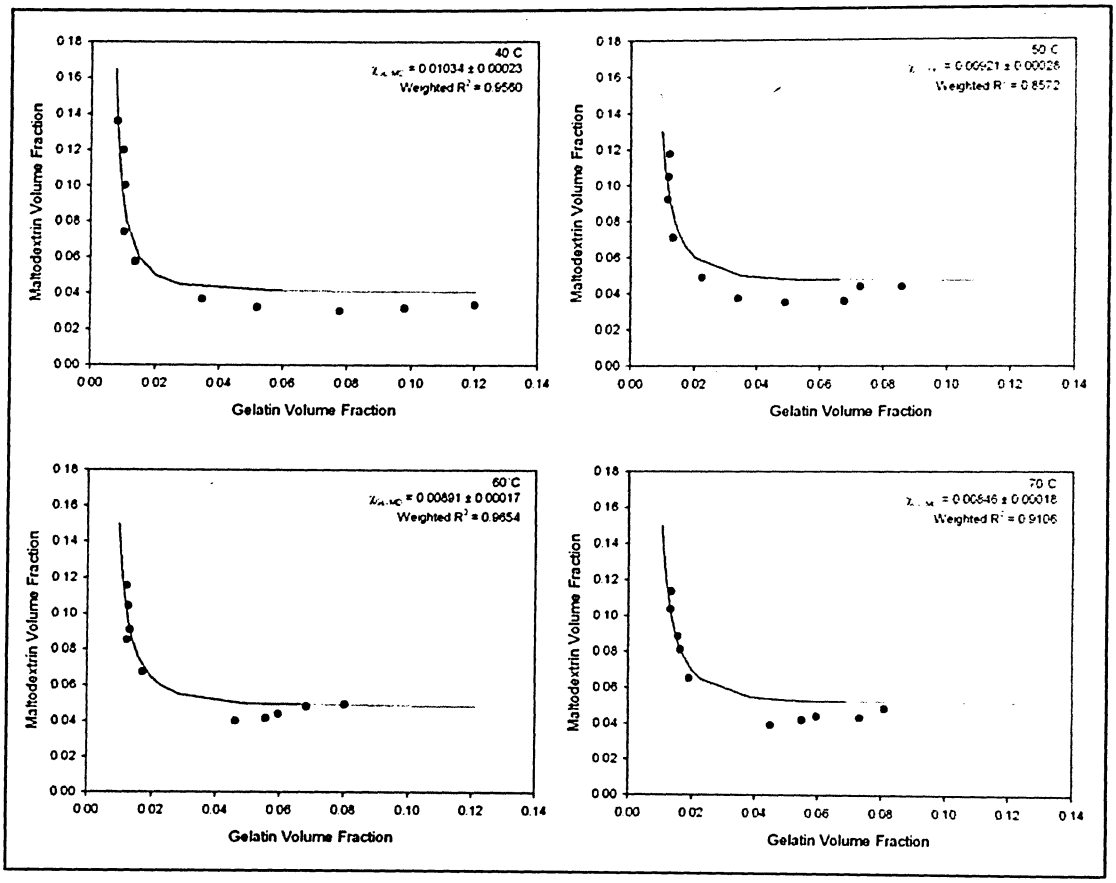

Figure 5.7: Experimental tie-line data for the typical range of temperatures, modeled with spinodal curves from the Flory-Huggins equation. The $\chi_{GL\text{-}MD}$ parameter used was determined as the fitting parameter from the curve fitting analysis of experimental results to the Flory-Huggins equations for ternary systems. Points along the curve represent experimentally-determined compatibility-curve points. The smooth curve represents the Flory-Huggins-predicted phase compatibility curve.

5.4 DISCUSSION

These results have shown that as the quench temperature decreases within the experimentally-examined range, there is a greater drive towards segregation in mixed biopolymer solutions. Though the total biopolymer content of separated phases will not differ from that of the parent system, lower temperatures will result in phases more concentrated in a single type of biopolymer. The global result of this general trend is a shift of the cloud point curve away from the axes and origin as temperature is increased. An elevated temperature yields an environment of greater miscibility, where the two-phase region will be smaller than at lower temperatures.

The modeling of experimental data using the Flory-Huggins theory of polymer mixing yielded fitted curves that were highly dependent on $\chi_{GL\text{-}MD}$, which itself was a function of temperature and biopolymer concentration (Tables 5.1 & 5.2). The physical significance and behaviour of the $\chi_{GL\text{-}MD}$ parameter remains vague, however, especially in the context of the GL-MD system, as many researchers have pointed out[14;14;27]. Researchers modeling polymer phase compatibility have broken the empirical Flory-Huggins interaction parameter into entropic and enthalpic portions which the Flory-Huggins theory normally combines in the interaction parameter. In reality, it is these terms that form the basis of the interaction parameter behaviour[89]. Though this theory had yet to be thoroughly extended into biopolymer

applications, its prediction of the compositional and temperature variations of the interaction parameter suitably match the general trends seen above.

There was often a noticeable trend in the experimentally-determined phase behaviour results. An upward shift of the GL-rich arm of the cloud-point curve was most notable in experimental data for 60°C and 70°C trials (Figure 5.4). The observed increase in MD content of increasingly enriched GL phases is counter-intuitive. Since the collection of points represent systems at equilibrium for a constant temperature, it is highly unlikely that an increase in GL content would be coupled with a concurrent increase in MD content. Instead, GL-rich phase content should be seen to increase at the expense of co-solubilized MD. This was likely attributed to experimental error, most likely that of not allowing complete bulk phase separation prior to analysis. However, inspection of the theoretically modeled phase curves indicates that disregarding these points may not be a sound approach. Figure 5.7 (specifically 50°C and 60°C) shows the modeled curve passing through these elevated points at the expense of points at lower GL contents.

In comparing the fits in Figures 5.6 and 5.7, the disparate behaviours of the model fitting techniques have noticeable effects on the predicted compatibility curve. The behaviour of the theoretically predicted spinodal curve should lie within the experimental curve, thus demarcating the unstable region from the metastable region. This is in contrast to the behaviour of the average $\chi_{GL\text{-}MD}$ method (Figure 5.7). This is borne out by the improved average-weighted R^2 (0.9814 for average $\chi_{GL\text{-}MD}$, $n=10$, $P < 0.0001$; 0.9223 for

the curve fitting technique, n=10, P=0.0001) as well as the suitable placement of the apexes of the cloud point curves between the fifth and sixth data points (best observed at 40°C, 60°C and 70°C). The poorer fit of the curve fitting method is shown by the weak approximation of the curve apexes (Figure 5.7 50°C, 60°C and 70°C). A general weakness of the average $\chi_{GL\text{-}MD}$, however, is that it is based on $\chi_{GL\text{-}MD}$ values with larger standard deviations than those observed with curve fitting. Furthermore, the utility of a predictive phase diagram that overemphasizes the two-phase region is debatable, for example in large-scale applications where the tailoring of separated microstructures is contingent on the initial phase actually phase-separating at the given temperature.

An attempt at identifying a fitting technique yielding a superior fit led to a cursory investigation of the effect of concentration on the $\chi_{GL\text{-}MD}$ interaction parameter, by examining its linear response to a series of concentration-related variables. It is important to stress that there is no theoretical basis for a linear trend between concentration and $\chi_{GL\text{-}MD}$. This assumption was made simply to investigate the behaviour of the predicted phase curves with a variable $\chi_{GL\text{-}MD}$.

A sampling of $\chi_{GL\text{-}MD}$ values from all experimental results was investigated for linear trends by Pearson correlation analysis (Figure 5.8).

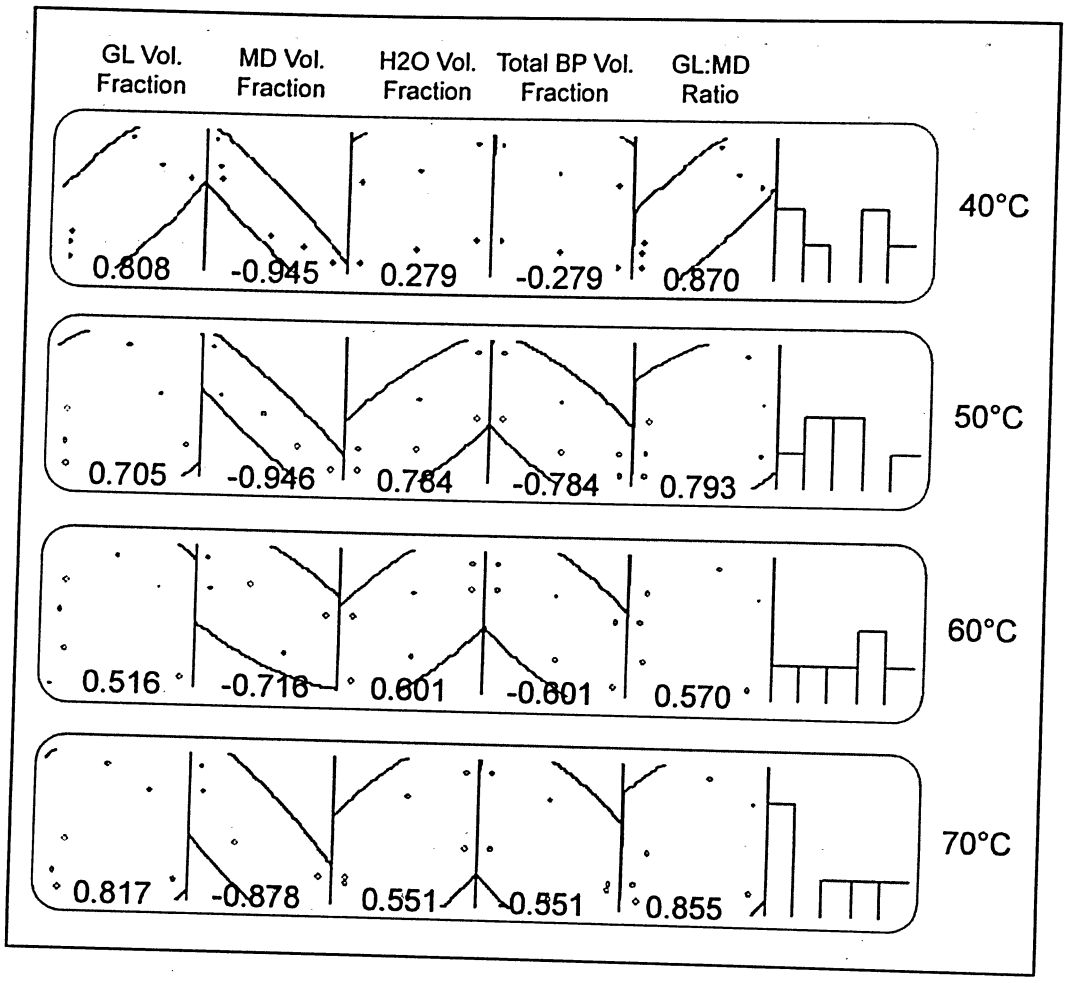

Figure 5.8: Pearson correlation analysis plots and values for the appropriateness of linear fit of $\chi_{GL\text{-}MD}$ as a function of: GL volume fraction; MD volume fraction; H_2O volume fraction; total biopolymer volume fraction; GL:MD ratio. Each block represents the relationship between $\chi_{GL\text{-}MD}$ (y-axes) and each of the concentration-related terms.

The most consistently strong linear trend was an inverse proportionality of $\chi_{GL\text{-}MD}$ with MD volume fraction, with P values between –0.716 and –0.945. Regression analysis of this relationship yielded temperature-dependent linear equations for $\chi_{GL\text{-}MD}$ as a function of MD volume fraction relationship. The resulting linear equations were used with the Flory-Huggins spinodal equation to calculate a model of experimental compatibility based on concentration-dependent $\chi_{GL\text{-}MD}$ values (Figure 5.9). The poor linear fits serve to enforce the

contention that the relationship between concentration and $\chi_{GL\text{-}MD}$ is far more complex than a linear one.

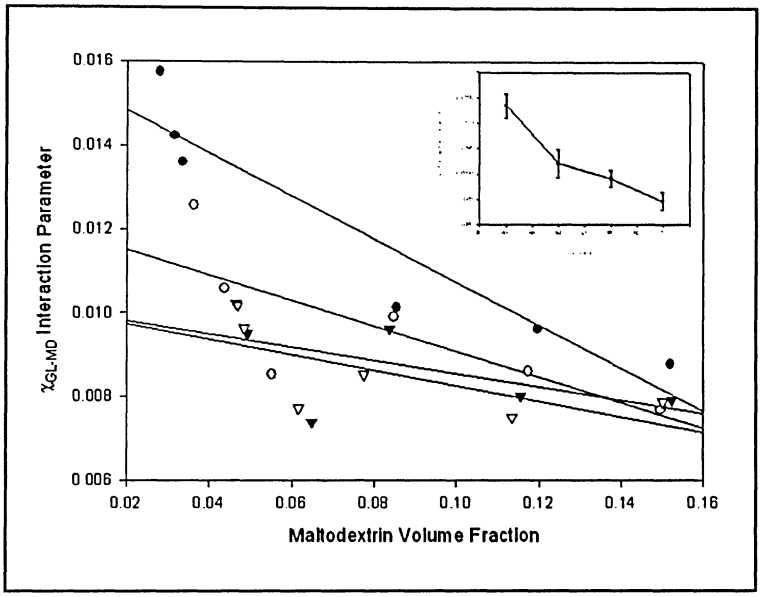

Figure 5.9: Linear regression plots of the $\chi_{GL\text{-}MD}$ = f(MD volume fraction) relationship for 40°C (●), 50°C (○), 60°C (▼) and 70°C (Δ), where: $\chi_{GL\text{-}MD,40°C}$=-0.0514[MD]+0.0159, $\chi_{GL\text{-}MD,50°C}$=-0.0304[MD]+0.0121, $\chi_{GL\text{-}MD,60°C}$=-0.0158[MD]+0.0101, $\chi_{GL\text{-}MD,70°C}$=-0.0184[MD]+0.0101

The predicted curves for this method exhibited previously unseen behaviour of the phase curves at points away from the apex (Figure 5.10). An inward curvature was apparent, to varying degrees, for all systems particularly at low GL concentrations and high MD concentrations. This behaviour is counter-intuitive, and contrary to the results of previous fitting methods. It would be expected that as the enriched biopolymer content of a given phase increased, the solubility of the minor component would decrease based on the temperature-dependent finite total solubility of biopolymers in the solution. In this situation, the variable nature of the $\chi_{GL\text{-}MD}$ parameter appears to make the predicted curve highly responsive to the locations of experimental tie-line

points, which, as discussed previously, exhibit a degree of error away from the curve apex and does not behave as the general Flory-Huggins theory would predict. The benefit of this behaviour, however, is a good fit of experimental data, yielding an average-weighted R^2 of 0.9806 (n=10, $P < 0.0001$), predicted curves generally lying within experimental data (as expected for the spinodal approximation) and reasonable placement of apexes.

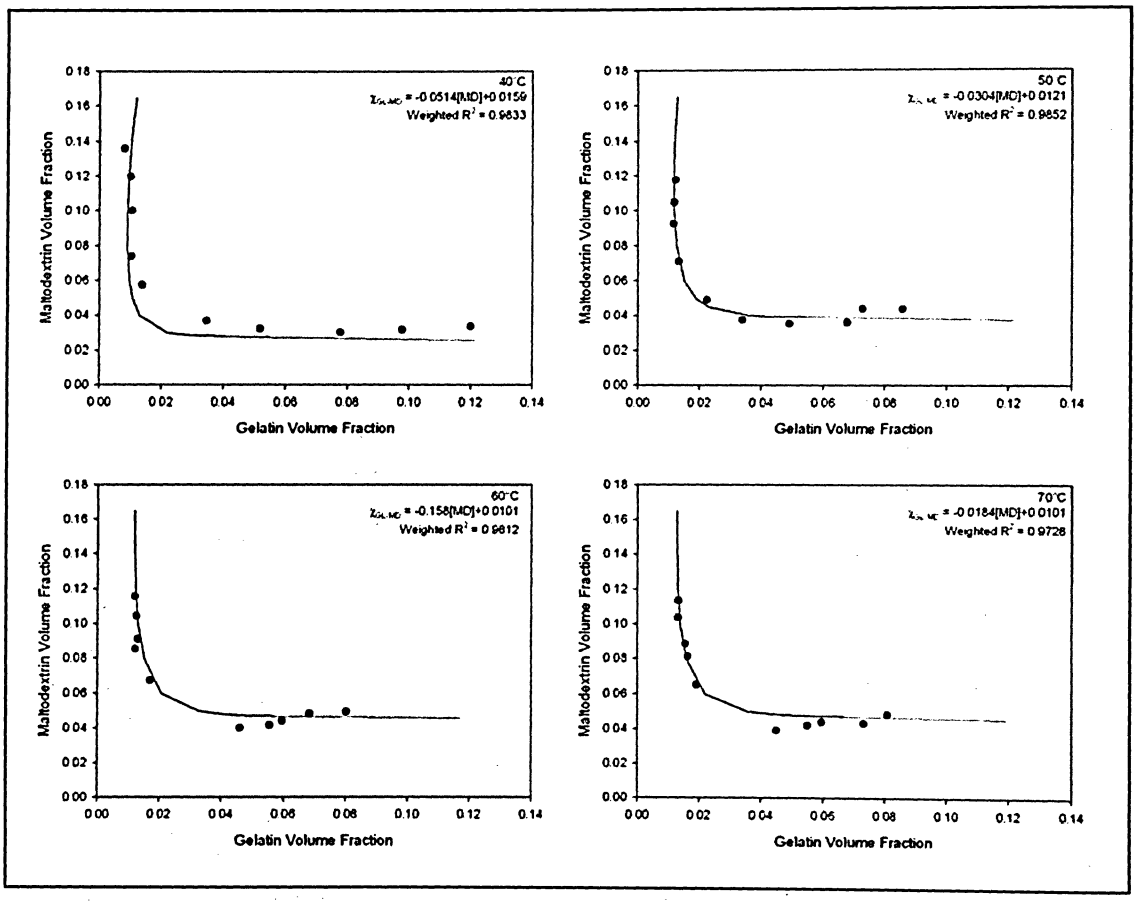

Figure 5.10: Experimental tie-line data for the typical range of temperatures, modeled with spinodal curves from the Flory-Huggins-Scott equation (Equation 5.5). Each $\chi_{GL\text{-}MD}$ parameter was determined from linear regression analysis of the relationship of $\chi_{GL\text{-}MD}$ with MD phase volume fraction. Points along the curve represent experimentally-determined compatibility-curve points. The smooth curve represents the Flory-Huggins-predicted phase compatibility curve.

5.5 CONCLUSION

The Flory-Huggins theory of polymer mixing serves as an adequate model for the qualitative description of biopolymer phase behaviour. Despite its dependence on the empirical interaction parameter, χ, and the poorly characterized concentration-dependent nature of this term[27], it predicts temperature and concentration dependent phase behaviours. The interaction parameter itself is a phenomenological term deduced by fitting experimental data to theory, a theory which is critiqued as often yielding predictions that may be in conflict with observations. Furthermore, in the context of the $\chi_{GL\text{-}MD}$, the Flory-Huggins theory leaves many practical questions unexplainable within its framework. A statistical molecular model of χ, broken down into entropic (concentration dependent) and enthalpic (temperature dependent) terms, would contribute significantly to a clearer picture of phase behaviour. Alternatively, comprehensive experimentation aimed at elucidating factors contributing to variations in χ may also aid phase behaviour prediction. From the results presented here, it is apparent the effect of both temperature and concentration are more complicated than the cursory study anticipated. Despite this, statistical fits of experimental data are acceptably good in all cases, indicating the copious work required in clarifying χ would only serve to further enhance model precision.

Chapter 6

Phase Separation and Coarsening: Experimental and Theoretically Modeled Behavior

6.1 Introduction

The presence of proteins and polysaccharides is integral to the sensory and functional properties of many processed foods (*e.g.*, in reduced-fat dairy products). Over the last few decades, it has been shown that the mixing behavior of such biopolymers may be tailored to develop novel microstructures based on water-in-water phase separation. Factors that will influence phase separation include the intrinsic properties of the biopolymers (molecular weight, profile, branching), presence of other ingredients (*e.g.*, sucrose and/or salt), and gelation condition (static or under shear, temperature and pH). Altering any one of these parameters can potentially prevent or promote segregation. In this context, the phase separation of mixed protein-polysaccharide systems follows either nucleation and growth (NG) or spinodal decomposition (SD)[69]. The main difference between these two mechanisms is in their influence of how the two

separated phases attain equilibrium compositions. From a morphological viewpoint, these mechanisms also differ in the microstructure they yield.

The aqueous biopolymer composite of phase-separated gelatin (GL) and maltodextrin (MD) is a water-in-water emulsion that undergoes some of the same coarsening processes observed in conventional oil and water emulsion destabilization[69;90]. Upon initiating phase separation, two concurrent processes aim to minimize thermodynamic instability of the system: (i) phase composition enrichment driven by diffusion of the constituent biopolymers to the newly formed phases, and (ii) coarsening of the water-in-water emulsion leading to a minimization in interfacial area between the resulting phases. A thorough understanding of these processes and of the changes in size and spatial distribution of the included phase will allow for the specific tailoring of the microstructure of a phase-separated system[19].

6.1.1 Comparison of Phase Separation Mechanisms and Early Stage Droplet Growth

Depending on composition and quench temperature, either spinodal decomposition (SD) or nucleation and growth (NG) may ensue. SD results from quenches into the unstable region, where phase separation occurs because spontaneously[12]. Systems residing in the metastable region separate *via* NG. Here, an energy barrier limits separation onset to enriched droplets which have a critical size.

Phase separation *via* SD yields a phase of dispersed droplets whose initial evolution is diffusion-limited[19]. This process is described by Tromp as resulting from fluctuations in concentration of a minority mixture component

throughout the mixture[18]. When large enough fluctuations are reached, individual concentration gradients around a global collection of particles slightly enriched in the minority polymer will develop. The enrichment of the minority polymer in the newly-formed included phase is balanced by a concurrent depletion of the same polymer from the continuous phase. Compositionally, the result is a depletion layer, depleted in the minority polymer, extending out from the droplet interface.

Early stage SD begins when a critical concentration fluctuation wavelength propagates throughout the system. Upon initiation, the characteristic length scale (wavelength) of the concentration fluctuation remains constant while the amplitude increases as the two phases begin to enrich in their majority polymer components (Figure 6.1A)[84]. Intermediate SD begins soon after, often within a matter of seconds (refer to Table 2.1)[12]. This stage exhibits a gradual shift of the wave pattern and a continued increase of amplitude (Figure 6.1B). It is during the intermediate stage that the two phases will reach their equilibrium compositions, exhibited by the attainment of maximum fluctuation amplitude. As early and intermediate stage SD progress, their rates of phase composition are largely diffusion-limited[78]. Finally, late stage SD occurs when equilibrium concentrations of the two phases are reached, and is characterized by the halting of the growth of the wave amplitude. The resulting phase-separated microstructure will continue to coarsen, typically *via* a coalescence-driven mechanism[20;28;32]. During this stage, the characteristic wavelength of the concentration fluctuation will grow as an increasing effect of

macroscopic flow tends to drive the system towards bulk phase separation (Figure 6.1C).

Quenches into the unstable region produce small concentration fluctuations that are sufficient to drive the mixture to phase separate. Initiation of SD therefore occurs without an energy barrier[12;84]. The composition fluctuations mature during separation by means of "uphill diffusion" where the gradient in composition moves from low concentration to high concentration. In contrast, in NG (described below) nuclei form and grow when the diffusional flux is inward. This process is an activated process where fluctuations not meeting a critical amplitude minimum do not overcome the energy barrier required for this type of phase separation to occur. The system is maintained in a metastable state as smaller than critical fluctuations are suppressed and unable to separate. The consistent amplitude and increasing wavelength of the fluctuation patterns developed as a function of time upon exceeding the energy barrier are characteristic of NG.

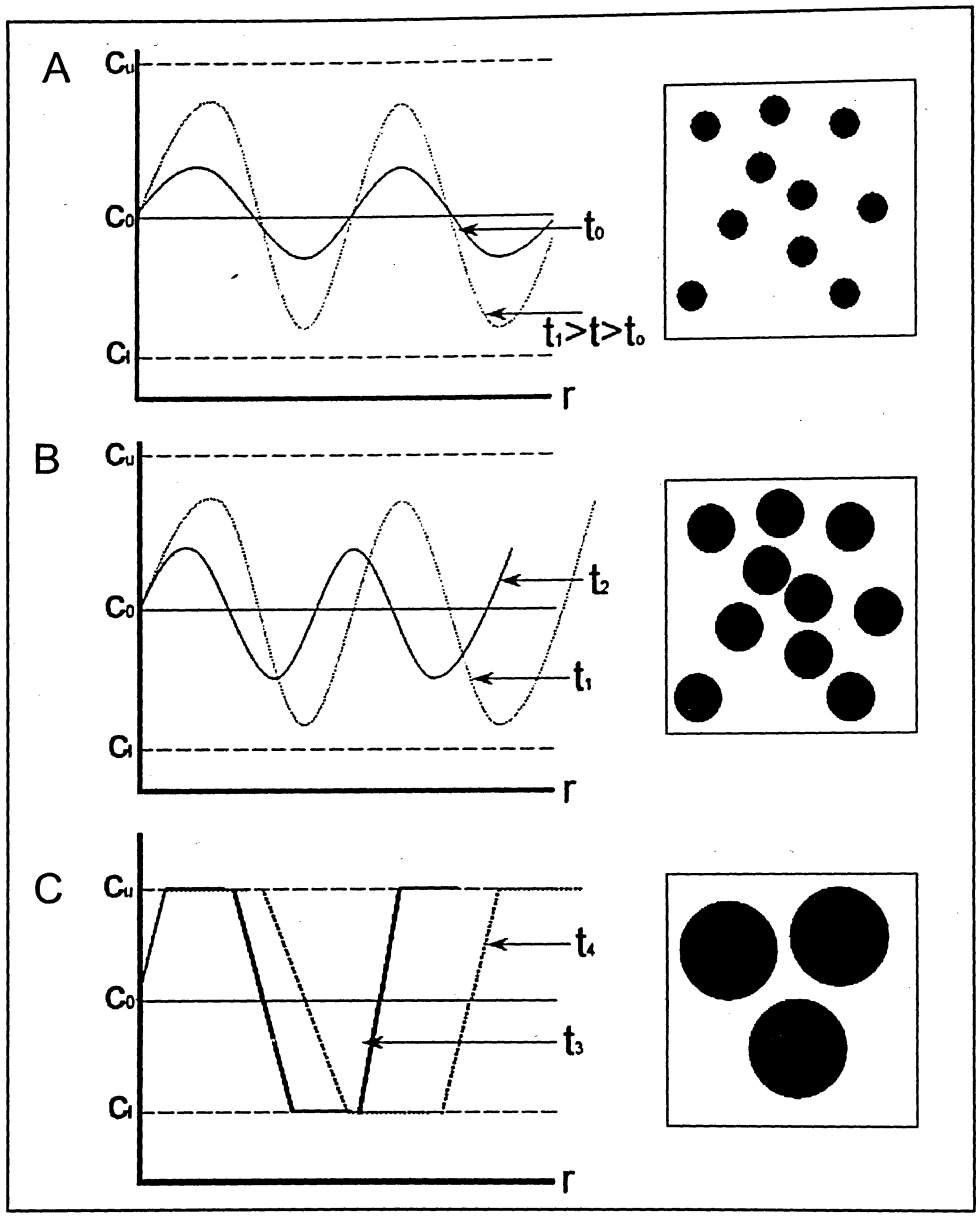

Figure 6.1: Schematic one-dimensional representations of spatial concentration fluctuations that characterize the three stages of SD phase separation, (A) early stage, (B) intermediate stage and (C) late stage. Insets represent the two-dimensional droplet sizes and distributions exhibited by each stage. Adapted from Tran *et al.*[39].

With NG, a shallow, off-critical quench, taking the system into the metastable region, will result in an included phase of dispersed droplet, rich in the minority polymer. Contrary to SD, a sufficient increase in the

compositional fluctuations characterizing the two phases will cause an increase in the free energy of the mixture, leading to phase separation by NG. Early stage phase growth by this mechanism is characterized as being reaction-limited, as only concentrated nuclei of a critical size grow. Concentration fluctuations leading to nuclei smaller than the critical size do not have sufficient activation energy to form a new phase and will be redissolved into the original mixture. Microstructural growth stemming from the NG mechanism is characterized as having a potentially wide droplet size distribution as coarsening and droplet nucleation may occur simultaneously over the period of metastability.

During coarsening *via* either SD or NG, an increase in droplet size will follow a power-law relationship, increasing proportionally with time to the power of 1/2-1/3[3]. *Via* SD, after the early and intermediate stages have completed, depletion layers will grow and reach the depletion layers of neighboring particles[84]. At this point, the two phases will have reached their equilibrium compositions and droplet growth will follow a new power law relationship[19;35]. The later stage coarsening power law behavior of the NG mechanism is less well characterized, as droplets in their infancy exhibit their maximum compositional enrichment and coarsen concurrently with the formation of additional nuclei[91].

6.1.2 Coarsening Mechanisms and Later Stage Droplet Growth

At equilibrium, phase-separated systems exhibit dynamic growth characteristic of conventional, destabilizing emulsions. As water-in-water

emulsions, separated systems of aqueous GL and MD undergo phase coarsening, a process aimed at decreasing the interfacial area between the phases. Because of the interfacial tension between the phases, minimization of the contact area between the phases serves to decrease free energy of the system. Conventional emulsions may undergo coarsening by a number of mechanisms, including sedimentation, coalescence and Ostwald ripening[21].

- Sedimentation results when a gravitational force acts upon droplets within an emulsion that exhibit a greater density than the continuous phase. Creaming is the opposite of sedimentation and occurs when the dispersed phase has a lower density than the continuous phase. Each droplet in the emulsion experiences a gravitational force, the direction of which depends on which phase has the greater density. The rate of sedimentation is dependent on the magnitude of the net gravitational force, which is composed of gravitational and buoyancy components. The strength of the buoyancy component is directly related to the magnitude of the density difference between the phases. As coarsening by this mechanism progresses, the z-direction bulk flow of the dispersed phase can lead to an acceleration of coalescence[21].
- Coalescence-driven emulsion coarsening results from the movement of dispersed particles toward one another. Merging of droplets in this fashion yields a more thermodynamically stable system through the reduction of contact area between the two phases. The formation

of larger droplets during coalescence also serves to accelerate sedimentation. The droplet collisions necessary for coalescence can result from the Brownian motion of components within the emulsion or from bulk flow in the continuous phase, often brought about by sedimentation. The rate and efficiency of coalescence are related. Here, coalescence efficiency refers to the likelihood of droplet rupture following collisions[21].

- Ostwald ripening is characterized by the diffusional mass transfer of the dispersed phase from small droplets to larger droplets through the continuous phase. Over time, the larger droplets continue to grow while smaller droplets disappear. The basis for this process is the increase in solubility of the included phase polymer accompanying the decrease in droplet size[21].

The present experimental observations indicate that GL-MD composites exhibit late-stage coarsening *via* both coalescence and sedimentation. Others have stated that both Ostwald ripening and coalescence take place during late-stage coarsening, but note that the microstructural coarsening is strongly dominated by coalescence, which proceeds more quickly than Ostwald ripening[19].

6.1.3 Droplet Growth Models and Predicted Behavior

Few studies have investigated late stage phase separation microstructural coarsening in GL-MD systems[3;65;76]. However, numerous studies have attempted to model growth behavior during this stage for synthetic polymer

mixtures. McGuire *et al.* and Martula *et al.* presented a coalescence model for synthetic polymer mixtures[28;92]. They went on to show the applicability of the model with their own experimental studies of the synthetic polymer system of isotactic poly(propylene) – diphenyl ether system[92].

The McGuire model is based on the relationship between the average droplet size and time, temperature and initial droplet concentration. Butler *et al.* have reported that the maturation of microstructure in a biopolymer phase-separated system is proportional to time to the power of some scaling factor, in accordance with the coalescence mechanism of droplet growth described by McGuire[36;92]. The general trend observed in coalescing systems is that the probability that two droplets will impinge and coalesce increases as the volume fraction of the droplets increases[20;28].

This model considers the attractive van der Waals forces that promote droplet coalescence as well as how a singular coalescence event affects the surrounding droplet population. Mechanistically, the thickness of the continuous phase film between two approaching droplets prior to coalescence consists of wave-like perturbations, where two forces act (Figure 6.2). The first, F_γ, generates and increases the perturbation wave amplitude and is strongest where the film is thinnest, implying that as two droplets approach, the interface between the two will thin where they contact one another. The second force, F_{vw}, is perpendicular to the droplet interface and acts to promote a shape of least minimal contact area between the dispersed and continuous phases.

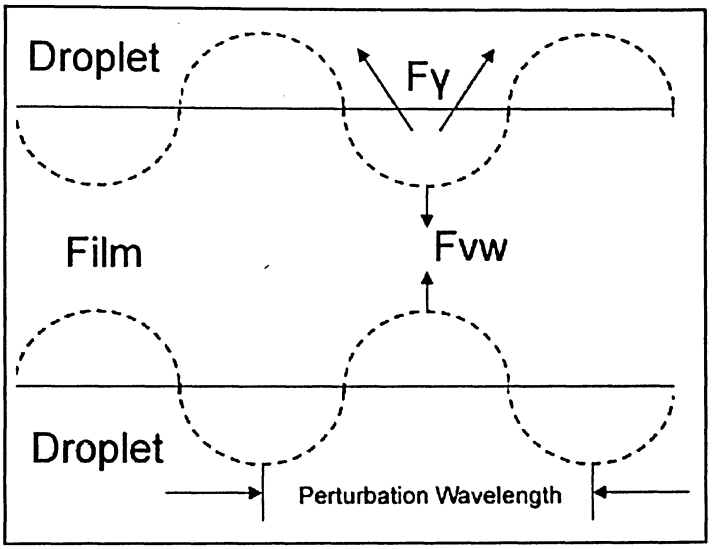

Figure 6.2: Schematic of the continuous-phase film between two approaching droplets prior to coalescence. The solid line represents the time-averaged location of the droplet interface, while the dotted line represents its perturbations. Adapted from McGuire *et al.*[30].

Figure 6.3 shows the approach and coalescence of two droplets. As the fluid film between the droplets ruptures, it is forced out and may promote neighbouring droplets to undergo subsequent coalescence.

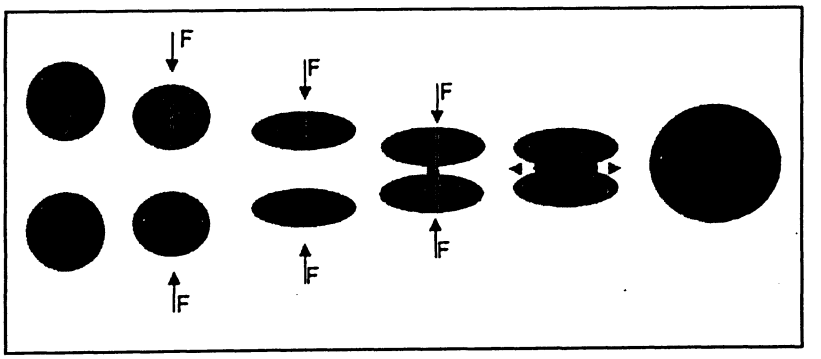

Figure 6.3: Schematic representation of coalescence of two droplets, beginning with approach and ending with a single droplet having a total volume equal to the sum of the original droplets. Adapted from McGuire *et al.*[30].

From start to finish, the coalescence process, as depicted in Figure 6.3 consists of 5 steps. Two droplets first approach one another under the influence of some external force and, when close enough, *via* van der Waals attractive

forces. The continuous phase film is squeezed out from between the approaching droplets, which begin deforming. When the film decreases to a critical thickness, it ruptures and the droplets begin to merge. The size of the inter-droplet connecting bridge increases in an attempt to minimize its curvature. As the interconnecting bridge rapidly widens in an attempt to minimize the droplet surface area, the fluid film is expelled into the continuous phase. Finally, the coalesced droplets form a new, larger droplet with a minimized surface area and a volume equal to the sum of the parent droplet volumes. This coalescence model indicates that hydrodynamic flow within the continuous phase will lead to greater mass flow within the system than by Brownian motion alone.

The important components in this model include: calculation of the ejected fluid velocity profile; the time required for post-rupture fluid expulsion; determination of the movement of droplets neighbouring a coalescence event; and calculation of the number resultant collisions. Finally, the number of collisions is related to the average size of droplets in the system as a function of time. Taking the continuous phase viscosity, interfacial tension, droplet volume fraction, initial average droplet radius and time after phase separation as input parameters, the model yields the time-dependent change in droplet radius

$$\frac{d<r>}{dt} = \frac{\nu C^*}{4(t+t_s)} \int_V \left(v_r^{\,2} + v_z^{\,2}\right)^{1/2} dV \qquad (6.1)$$

where $<r>$ is the average droplet radius, υ is the dispersed phase volume fraction, C^* is the fitting parameter, v_r and v_z are the radial and axial velocity profiles of expelled fluid and V is the working volume upon which the system is

modeled. The definition of time, t, is arbitrary and is taken as the time at which coalescence becomes dominant. The value t_s is the time between phase separation onset and coalescence. The single fitting parameter, C*, is the volumetric number of coalescence events occurring at a given time, t. A more detailed derivation of this model is presented in Appendix D.

6.2 Experimental Methods

6.2.1 Materials and Sample Preparation

The GL and MD samples and preparation techniques used were discussed previously (Chapter 2 and Chapter 4, Section 4.1, respectively). Two sets of samples were made, each with a microstructure: i) GL-continuous and ii) MD-continuous, with volume fraction compositions of 0.043GL-0.054MD and 0.020GL-0.070MD, respectively. Compositions of these systems were obtained from the theoretical phase diagrams described in Chapter 5. Samples prepared for microscopy were supplemented with the fluorescing dye Rhodamine B (Sigma-Aldrich, Mississauga, Ontario, Canada) at a concentration of 0.01% (w/w).

6.2.2 Rheology: Surface Tension and Phase Viscosity

Surface tensions for dilute (2% by weight) neat aqueous solutions of GL and MD were measured using the techniques outlined in Chapter 4, Section 4.5. Dilute solutions were analyzed so as to minimize the formation of gelled networks at lower temperatures.

Phase viscosities were measured on a cone and plate viscometer using techniques discussed in Chapter 4, Section 4.5. A system composed of 5wt%

GL and 15wt% MD was allowed to bulk phase separate at 70°C, 60°C, 50°C and 40°C. The two resulting coexisting phases of each sample were extracted and measure at their respective temperatures on the rheometer. Logarithmic plots (Appendix C) of viscosity (mPa·s), η, against shear rate (s^{-1}), $\dot{\gamma}$, yielded the consistency coefficient, m, and the flow-behavior index, n, from the power law model of viscosity, Equation 4.4. Shear rate was incrementally increased to a maximum ($2.18x10^{2}$ s^{-1}) then decreased gradually to the initial shear rate ($2.60x10^{1}$ s^{-1}), yielding a forward and backward sweep of the shear rate range. The characteristic viscosities of the samples were taken as the apparent viscosities at 1 s^{-1}, m, based on the assumption of *very* low shear rates acting between the two coexisting phases during coarsening.

6.2.3 Confocal Laser Scanning Microscopy (CLSM)

Inclusion growth profiles were investigated by CLSM on a temperature controlled stage (Instec Research Instrument Corporation, Boulder, Colorado USA). The microscope used was a Zeiss Axioplan-2 with an Achroplan 63x/0.9 water-immersion objective and a LSM 510 confocal module (Zeiss Instruments, Mississauga, Ontario, Canada). The laser was operated at 543 nm, which provided excitation of the fluorescing dye. Emitted light was detected using a KP 680 main beam splitter and a KP 685 filter. Samples (volume = 0.5 mL) were placed onto a welled microscope slide (1 mm well depth, 133 mm well diameter 13.3 cm D??), heated to 80°C to minimize the risk of premature separation. Samples were placed onto the heated microscope stage and held at 72°C for 5 minutes to reach thermal equilibrium. The stage temperature was

then rapidly dropped to the predetermined quench temperature at a rate of 30°C/minute. CLSM images were captured every minute at a depth of 50-100 μm below the cover slip.

6.2.4 Image Analysis

Micrographs were analyzed in a consistent fashion to extract average inclusion size data. Images were adjusted using Fovea Pro image enhancement software (2006 Edition, Reindeer Graphics, California, USA) by autoleveling contrast and brightness, followed by a Gaussian blur (27 pixel radius) subtraction, then finally by applying a Fourier transform with a 0.1 radius Butterworth filter. This rigorous combination of adjustments was found to provide the best possible image quality and ensure consistent treatment of all micrographs. All visible droplets were completely masked individually by visual inspection and the image background was deleted. Masked droplets were measured for average area based on the assumption that drop cross-sections were circular[20]. Bi-continuous samples were analyzed for their average characteristic dimension, which was determined by randomly placing a series of ten line segments on each micrograph extending across one of the phases from interface to interface. The average length of these lines was taken as the average characteristic length for that respective micrograph.

6.3 Results

6.3.1 Rheology: Surface Tension and Phase Viscosities

The interfacial tensions (Figure 6.4), calculated using Fowke's relationship, exhibited an effect of temperature on interfacial tension, $\gamma_{GL\text{-}MD}$. The sharp increase of $\gamma_{GL\text{-}MD}$ at 40°C was likely the result of the proximity of the investigated temperature to the temperature of network formation of GL.

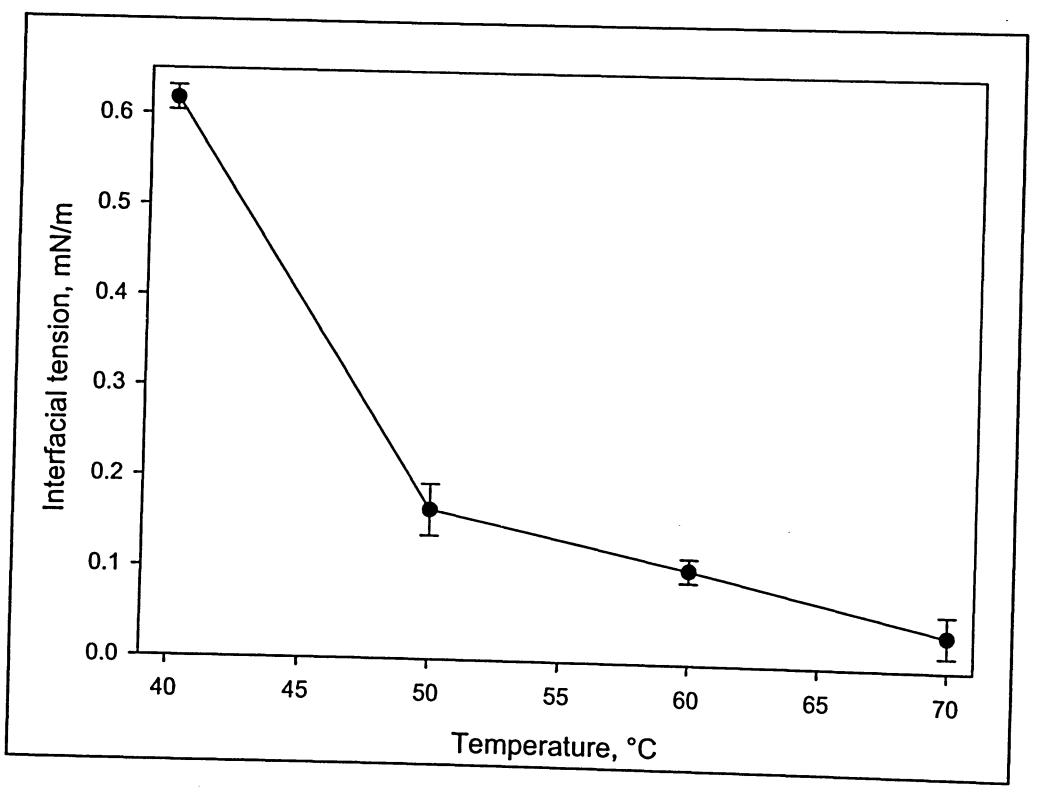

Figure 6.4: Effect of temperature change on the interfacial tension between GL-rich and MD-rich phases (n=5).

The viscosities of the GL-rich and MD-rich phases at key temperatures (Figure 6.5) show that the GL-rich system gelled close to 30°C. Thus the lowest temperature at which viscosity for this system was recorded was 32.5°C.

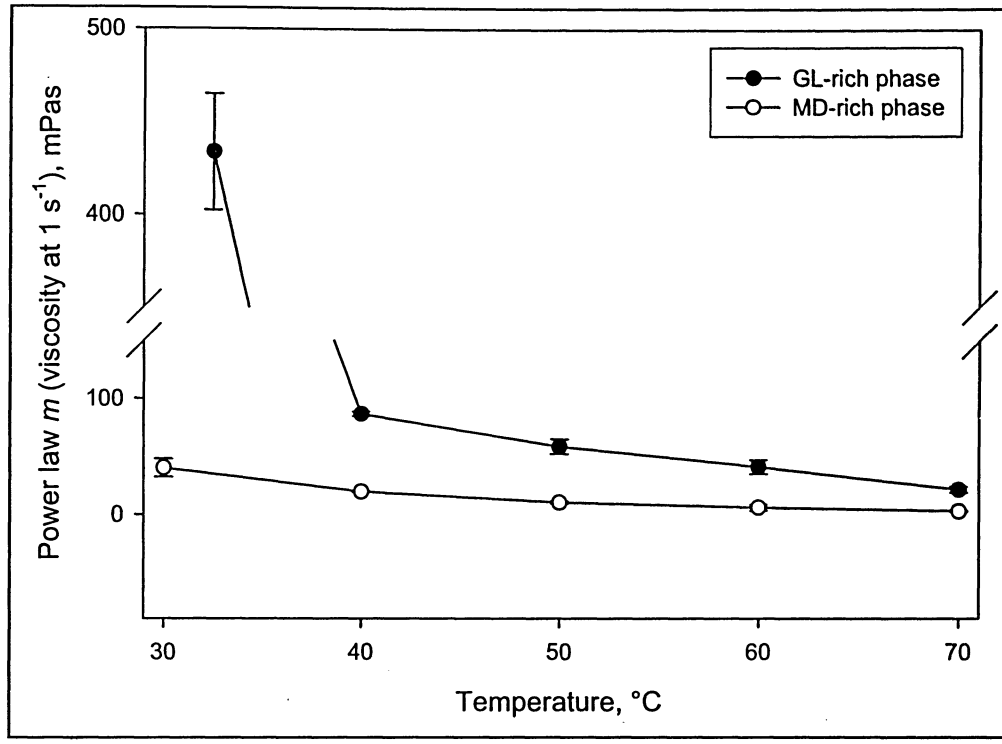

Figure 6.5: Phase viscosities for the phase-separated system (5%GL-15%MD) at varying temperatures. The GL-rich system gelled at 30°C and was therefore examined as low as 32.5°C. The increase in viscosity at 32.5°C is evidence of a degree of pre-gel molecular ordering.

6.3.2 Droplet Growth Profiles

The characteristic growth of phase-separated droplets over time depended on continuous phase type and quench temperature. Figure 6.6 shows representative behavior of the GL and MD continuous systems.

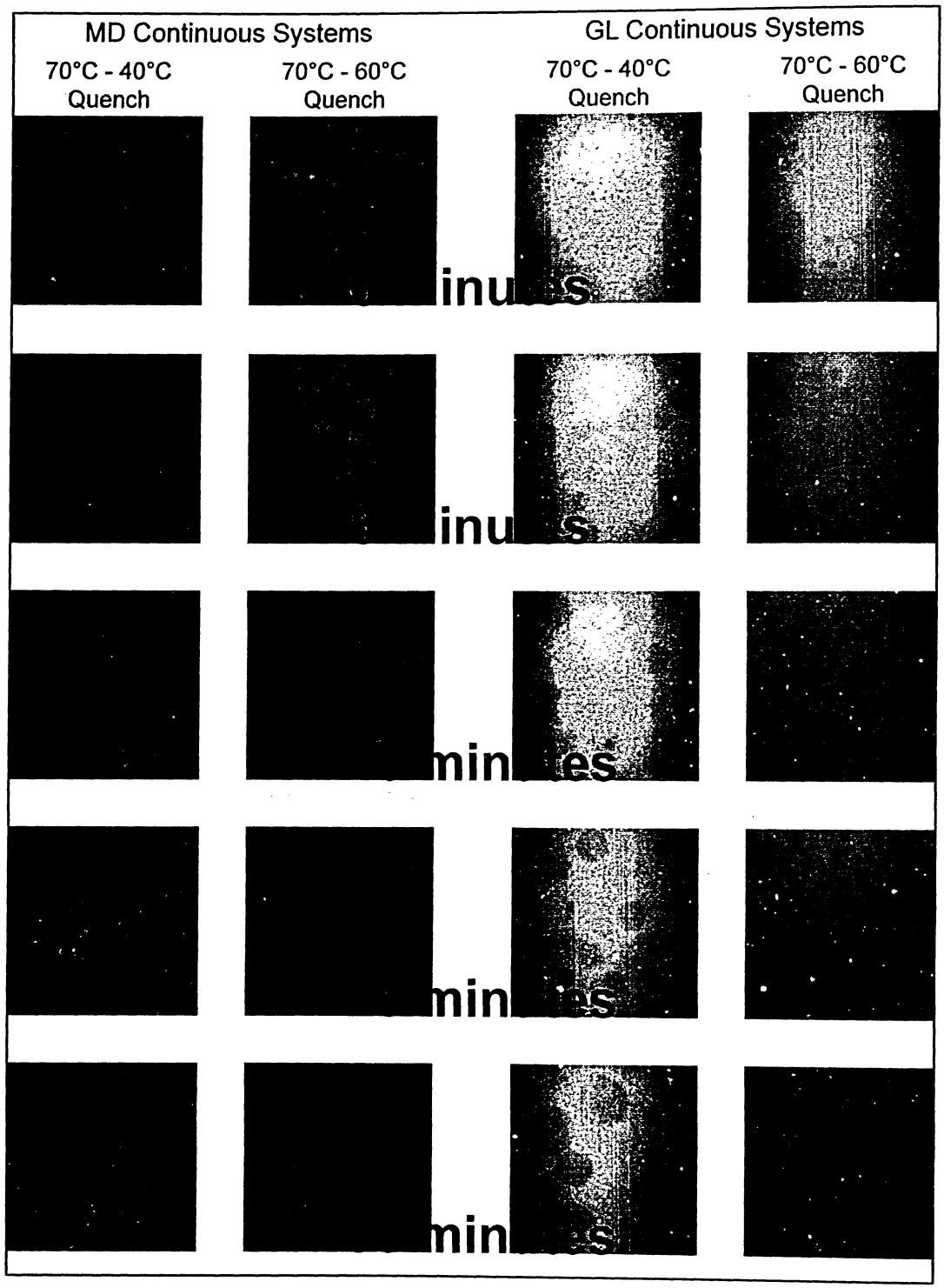

Figure 6.6: Representative images of the growth sequences of MD-continuous and GL-continuous systems for the two quench depths investigated. The micrographs are 152 μm x 152 μm.

Droplet size analysis yielded characteristic growth curves for each system (Figure 6.7). The lower temperature quench (40 *vs.* 60°C) yielded larger droplets and inclusions in the GL-continuous systems grew at a decreased rate compared to MD-continuous systems within the experimental time frame. There was an abrupt change in growth curve trajectory observed in GL- and MD-continuous systems, which indicated different growth processes early/intermediate and late stage phase separation.

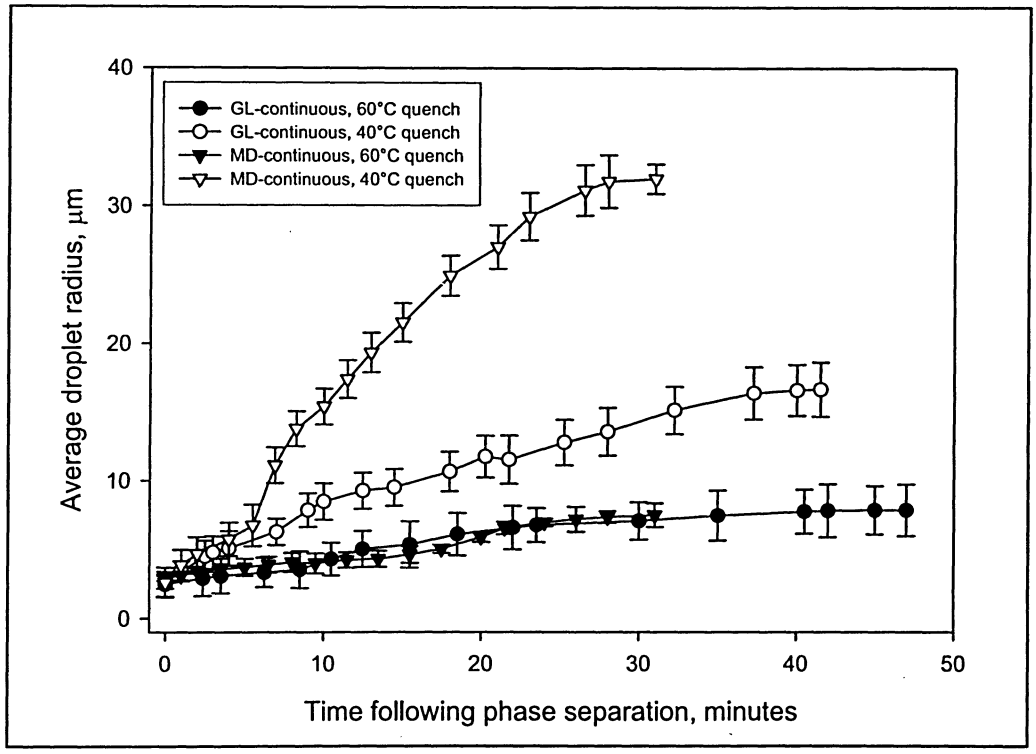

Figure 6.7: Droplet growth regimes for MD-continuous and GL-continuous systems quenched to 60°C or 40°C, based on droplet radii extracted from CLSM micrographs. Data points indicate the averaged droplet radius for growth runs conducted in triplicate.

6.4 Discussion

Early and intermediate stages of phase separation have been characterized by a growth exponent, α, with values in the range of 1/3 in a power law relationship of average droplet size with time[3]

$$r(t) \sim t^{\alpha} \tag{6.4}$$

These separative periods are followed by a change in growth exponent that accompanies the transition from intermediate to late stage phase separation, which is characterized by an increased hydrodynamic effect and a change in the growth exponent (ranging from 0.1 to 1), which depends on the participating mechanism(s).

In an effort to differentiate the two regimes (each characterized by a unique α), growth profiles of the investigated GL-continuous and MD-continuous systems were charted on semi-logarithmic plots (Figure 6.8).

The natural logarithmic semi-plots of droplet radius with time were iteratively matched with a pair of best fit lines to yield a pair of fits (exhibiting the best correlation coefficient values), with each representing either the early/intermediate or late stage of separation. Figure 6.8 also shows that the time-dependent behavior of the primary phase separation stage was dependent on temperature quench depth. Systems quenched to 40°C had a shorter primary stage and a subsequent sharper rise in droplet growth than the quench to 60°C. Lower temperatures (*i.e.*, a deeper quench) yield greater thermodynamic incompatibility, manifested in a higher population of dispersed phase droplets which transit through the primary phase of separation more rapidly. The

observation of a higher population of droplets for deeper quenches, and the subsequent increase in droplet growth rate, indicated that droplet growth was dominated by coalescence.

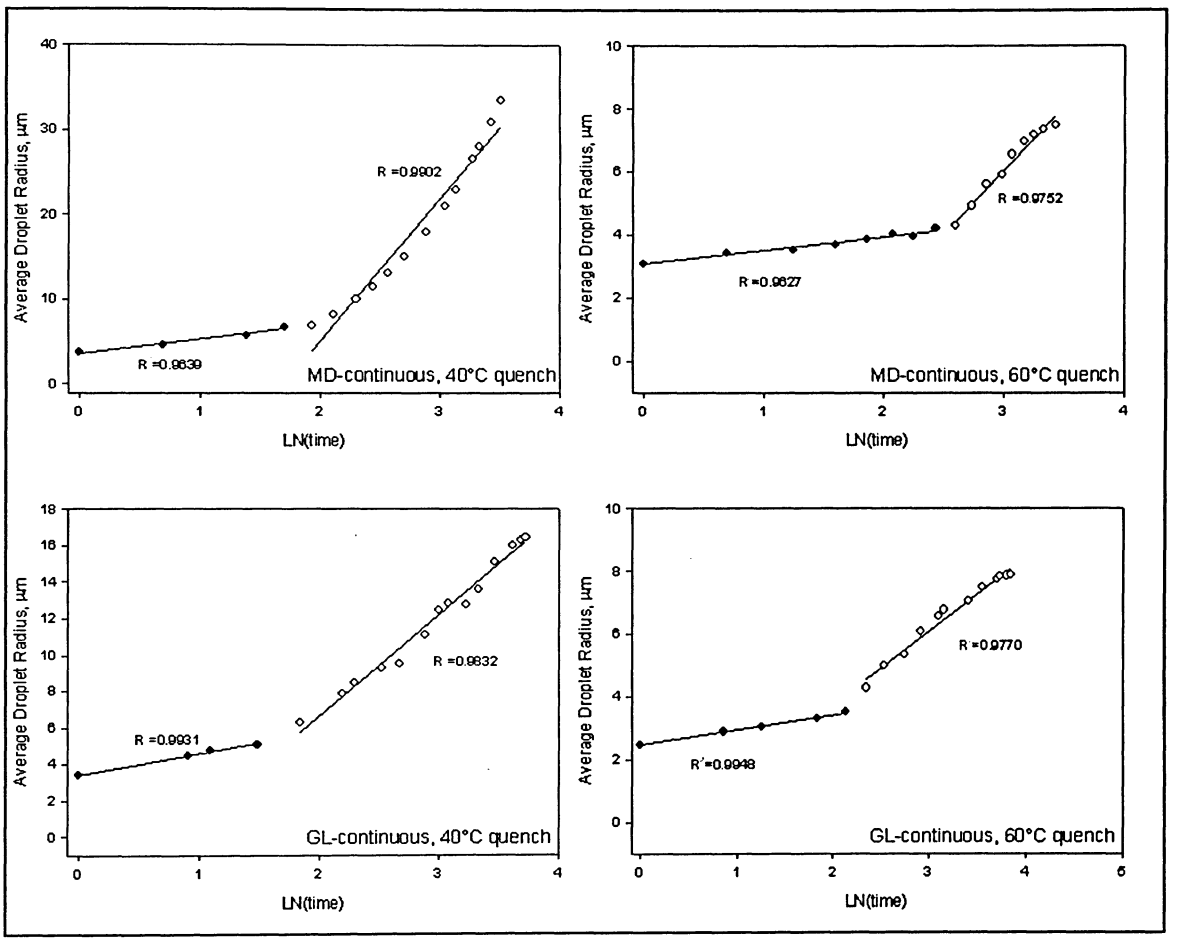

Figure 6.8: Power law growth curves for MD-continuous and GL-continuous systems coarsening under a deep or shallow quench. The occurrence of a sharp increase in the slope of the power law growth curve is taken to be indicative as a crossover from early/intermediate (diffusion-limited) growth to late (coalescence-dominating) growth.

Evidence of coalescence was substantiated by microscopy observations of actual droplet coalescence events in later stages of phase separation (Figure 6.9). As described by the McGuire model, there was rupture of the thin film

between two approaching droplets. Within a few seconds, a single, larger droplet remained.

Experimental phase growth curves were modeled in their later stages using the coalescence-induced-coalescence model of phase-separated phase growth discussed in section 6.1.3. The coalescence-dominant regime of droplet growth was taken to begin at the statistically-determined point where the growth regime went from the early/intermediate to the later, coalescence-dominated, stage (Figure 6.10).

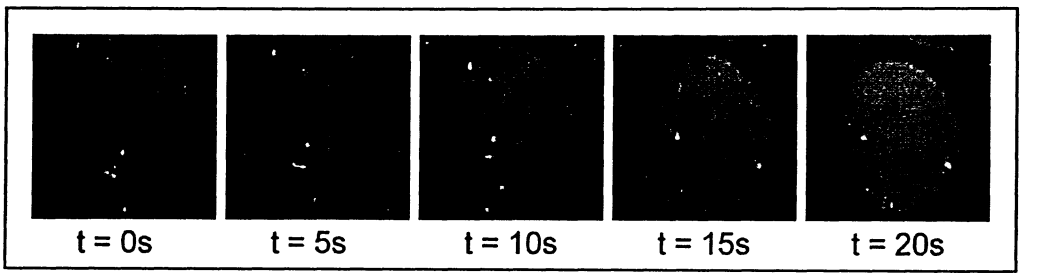

Figure 6.9: Coalescence event occurring during the later stages of coarsening in a MD-continuous system. Images are 152 μm x 152 μm.

The behavior of the growth profiles was explained reasonably well ($R^2 \geq 0.93$, $n \geq 17$, $P < 0.0001$ for all systems). The difference between the deep (40°C) and shallow (60°C) quenches was contrary to expectations. It was expected that the increased viscosity at the deep temperature quench would inhibit or slow down droplet mobility, and hence droplet coalescence. Instead, at the deeper temperature quenches for both GL-continuous and MD-continuous systems, a greater droplet growth rate, as well as final droplet size, was observed. This effect was likely due to the increase in the dispersed phase volume fraction and the increased droplet population with a deeper quench.

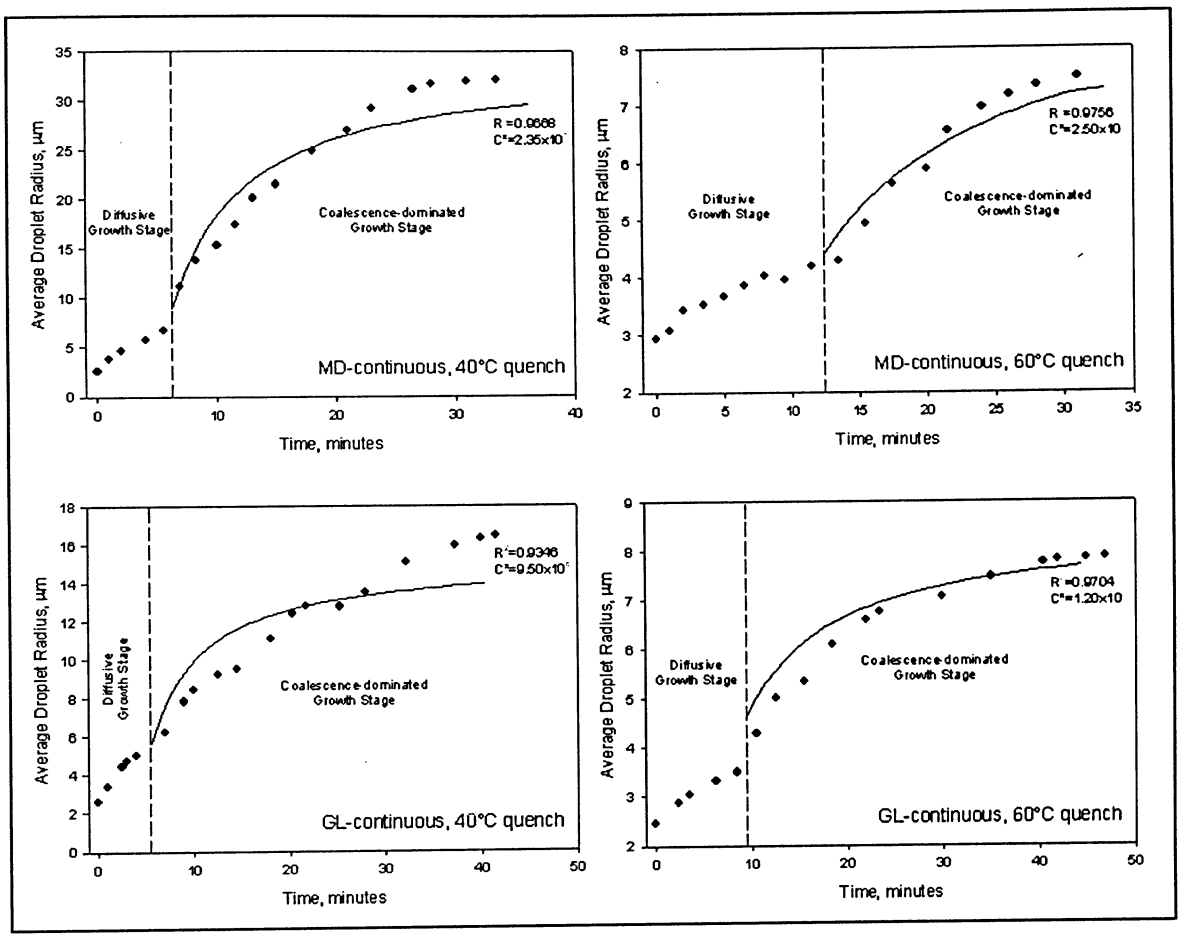

Figure 6.10: Plots of experimentally observed and simulated increases in droplet radius for coarsening systems. Values for R^2 and the fitting parameter, C*, are presented for each system investigated.

A general trend in observed deficiencies of the model fits indicates a likely existence of a number of confounding coarsening mechanisms occurring subsequently and, to a certain extent, along with the coalescence mechanism. The consistent crossover of experimental points surpassing the modeled curve (Figure 6.10) could be indicative of sedimentation simultaneously occurring in the late stages of coarsening. Such a mechanism would accelerate as droplet size increased, thereby increasing the hydrodynamic flow within the system necessary for sedimentation.

The parameter-dependent behavior of the coalescence-induced coalescence model elucidates the importance of various factors on late stage droplet growth. These factors include continuous phase viscosity, included phase volume fraction, interfacial tension and initial average droplet size. The results of this analysis are presented in Appendix B.

6.5 Conclusion

Post-phase separation coarsening was investigated and shown to be qualitatively simulated by a coalescence model of growth in its later stages. Differing quench depths led to different time and structure growth scales in the early and intermediate stages of phase separative growth. Late stage growth exhibited a good fit with model-predicted coalescence behavior. The eventual deviation from this model was theorized to be indicative of competing coarsening mechanisms. These concurrent processes commence and accelerate when droplets reach a sufficiently large size. Along with the coalescence-induced bulk flow in the continuous phase, the increase in droplet size past a critical point initiates gravity-driven bulk flow in the z-direction. Despite this deviation, it is apparent that there is a utility of the presented model in predicting late stage microstructural growth.

Chapter 7

Gelation-Induced Kinetic Trapping in Biphasic GL-MD Gels

7.1 Introduction

Over the last few years, there has been substantial interest in the demixing behavior of protein-polysaccharide mixtures in the food industry, primarily for the creation of reduced-fat dairy products. A key requirement for the development of controlled biopolymer microstructures based on proteins and polysaccharides is the control of microstructure. Within this context, the possibility of halting incipient phase-separated microstructures has been shown to hold promise[12].

The morphology of a phase-separating mixed biopolymer system will be highly dependent on the residence time of the system in the two-phase liquid region of a temperature-composition phase diagram. Above this zone, a single homogeneous phase will result, while below this zone phase separation, and perhaps, gelation of one or both components will ensue. Upon TIPS induction, the microstructure of a separated system will continue to coarsen so long as a certain degree of molecular mobility and/or hydrodynamic (bulk) flow exists.

The ultimate utility of phase behavior information, along with droplet growth profiles, is contingent on the ability to arrest microstructural coarsening when the desired morphology has been reached.

Kinetic trapping of protein-polysaccharide systems undergoing phase separation provides a rational means of controlling microstructure[4;22]. Halting phase separation at a point away from thermodynamic equilibrium is often achieved by a rapid and deep temperature quench below the gelation temperature of one of the components. It is possible that the constituent phases will exhibit compositions far away from the equilibrium compositions dictated by theory. More commonly, kinetic trapping is carried out in an effort to minimize the likelihood of bulk phase separation. Such a system will likely have attained its equilibrium compositions, but is nonetheless thermodynamically unfavored as a result of the unminimized interfacial area shared between the dispersed and continuous phases. High rates of gelation are able to freeze the composite network in a non-equilibrium arrangement, preventing osmotic diffusion of solvent between the phases[62].

Inquiries on kinetic trapping of separated gelatin (GL) – maltodextrin (MD) systems have generally focused on the interplay between the separation process and gelation of one of the phases[4;22;32;79]. A number of studies, however, have been conducted in an effort to identify the transient nature of phase enrichment following gelation. Rapid trapping initiated soon after, or in tandem with, phase separation onset yields a separated system away from its thermodynamically-dictated phase compositions. In such a case, it may be

concluded that the continuous phase, regardless of its biopolymer identity, holds a disproportionate amount of solvent[22]. The transient nature of phase compositions, as opposed to relative phase sizes, is indicative of a spinodally decomposing (SD) - separating system, which is all the more likely given the depth of quench required to initiate kinetic trapping.

The general trends exhibited by concurrent gelation and phase separation are present throughout most investigations of the synergistic effects of these two processes. The morphology of the trapped, separated system will be mainly influenced by the gelling properties of the biopolymer that gels first[93]. Furthermore, from a processing condition standpoint, the average size of dispersed phase droplets will increase as the cooling rate of the system decreases. Similarly, the same droplets will exhibit a larger average size when the pre-quench hold time is increased[79]. These two results are in accordance with the oft-mentioned relationship of morphology with residence time in the two-phase liquid region of the comprehensive phase diagram.

The first component of the chapter reasserts these findings whereas the second component investigates the feasibility of kinetic trapping of the GL-MD system by a chemically-induced crosslinking reaction. Numerous researchers have discussed the use of a covalent chemical crosslinker in tandem with GL-based systems intended for food or pharmaceutical applications. The utility of gelled GL is limited by the relatively small range of temperatures suitable for gelation, which in turn limits processing and storage conditions. Fixation of GL with a chemical crosslinker would eliminate this issue and would also impart

favorable characteristics to the system, including modified textural properties and potentially enhanced shelf-life stability. Genipin (GP) has recently come into prominence as the chemical crosslinker of choice for GL-based systems[43;58;59]. These studies have revealed that its potentially rapid rate of reaction, high extent of crosslinking and accompanying increase in system viscosity make it a viable chemical crosslinker for studies of the GL-MD separating system. With this in mind, the second component of the present work was undertaken to investigate the kinetic trapping of phase-separated systems to which GP has been added.

7.2 Experimental Methods

7.2.1 Materials and Sample Preparation

The GL and MD samples and preparation techniques used were discussed previously (Chapter 2 and Chapter 4, Section 4.1, respectively). A single system type was investigated having a GL-continuous nature and composed of 4.30% GL and 5.40% MD, by weight. This sample was chosen due, in part, to the fact that its continuous phase formed physical gels. Such a system would be most effective in kinetically trapping microstructure.

Samples undergoing chemical crosslinking were treated with GP to a final concentration of 15 mM (approximately 0.35% w/w). A literature review of studies examining GL crosslinking with GP showed this concentration to be close to the maximum effective concentration of GP. A summary of this review is found in Appendix E.

7.2.2 Determination of Gelation Temperature and Rates of Gelation

The concentration dependence of the temperature of instantaneous gelation of neat GL was investigated over an experimentally pertinent range of concentrations (5%, 4% and 3% GL solutions, by weight) using a Bohlin cone and plate oscillatory rheometer (Malvern Instruments Corporation, Mississauga, Ontario, Canada). Samples were placed into the rheometer and storage (G') and loss (G'') moduli were monitored at 40Hz during a temperature quench (0.5°C/minute) beginning above the gelling region. The temperature of crossover of the values of G' and G'' was noted for each sample as the characteristic temperature of gelation.

The time-dependent nature of gelation was next determined *via* rheological analysis of a GL solution (5% GL, w/w). A sample (volume ≈ 0.5 mL) was placed into the rheometer and the time dependent behavior of the G' was monitored at constant temperature. Onset of gelation was similarly defined as in previous experiments. The time required for gelation onset was observed for the range of temperatures, beginning with the generally-accepted temperature of gelation (30°C) down to the experimentally determined temperature of instantaneous gelation.

7.2.3 Kinetic Trapping and Gelation-Induced Phase Separation Evaluation

The efficacy of gelation-induced kinetic trapping and the occurrence of gelation-induced phase separation were initially investigated *via* a simple deep quench of phase-separated systems. Two factorial experimental designs were carried out to further clarify gelation and kinetic trapping by means of physical

and chemical crosslinking of the continuous phase. Samples were treated to specific thermal profiles (outlined below) and subsequently imaged using CLSM (Zeiss Instruments, Mississauga, Ontario, Canada) at 50 μm and 150 μm below the coverslip. Images were analyzed for average droplet size using previously-mentioned techniques (Chapter 6, Section 6.2).

The first experimental design was carried out on GP-untreated aqueous solutions of GL and MD. Samples were held at 75°C, above phase separation temperature (70°C), for a five minute period to erase all previous thermal history. Subsequently, a rapid thermal quench (30°C/minute) to 40°C was undertaken. Samples were then held at this temperature for a predetermined period of time to allow phase separation to progress in the liquid state. Next, samples were quenched to the final temperature (15°C) and held for a period of five minutes. Table 7.1 provides a breakdown of the treatments and levels used, as well as the total time for each experimental run and the residence time of each system within the two-phase liquid region. Samples numbered 5, 6 and 7 were repeats of the same conditions to give an indication as to the repeatability of the procedure. All other thermal regimes were conducted once, with six CLSM images per sample analyzed.

Table 7.1: Factorial experimental design grid for uncrosslinked (non-GP) systems.

Sample ID	Hold time at 40°C (minutes)	Ramp rate to 15°C (°C/minute)	Total experimental time (minutes)	Two-phase liquid region residence time (minutes)
1	0	0.7	40.7	14.29
2	10	0.7	50.7	24.29
3	20	0.7	60.7	34.29
4	0	2	17.5	5
5	10	2	27.5	15
6	10	2	27.5	15
7	10	2	27.5	15
8	20	2	37.5	25
9	0	10	7.5	1
10	10	10	17.5	11
11	20	10	27.5	21

The second factorial design was carried out on GP-treated aqueous solutions of GL and MD. Samples were held above phase separation temperature (70°C) for a five minute period to erase all previous thermal history. At this point, GP solution was dispersed throughout the sample yielding a concentration of 15 mM. The temperature of the system was maintained at 70°C for a predetermined period of time, during which crosslinking was initiated. A subsequent rapid temperature quench (30°C/minute) to 40°C was followed by a second holding period at this temperature. Following this predetermined period of time, all systems were finally quenched into the gelling region at a rate of 2°C/minute to 15°C. Table 7.2 provides a breakdown of the treatments and levels used, as well as the total time for each experimental run and the residence time of each system above the physical gelation temperature. Samples numbered 2, 3 and 4 were repeats of the same conditions to give an indication as to the repeatability of the

procedure. All other thermal regimes were conducted once, with six CLSM images per sample analyzed.

Table 7.2: Factorial experimental design grid for GP-treated crosslinked systems.

Sample ID	Hold time at 70°C (minutes)	Hold time at 40°C (°C/minute)	Total experimental time (minutes)	Two-phase liquid region residence time (minutes)
1	0	0	12.5	5
2	0	10	22.5	15
3	0	10	22.5	15
4	0	10	22.5	15
5	0	20	32.5	25
6	7.5	0	20	12.5
7	7.5	10	30	22.5
8	7.5	20	40	32.5
9	15	0	27.5	20
10	15	10	37.5	30
11	15	20	47.5	40

7.3 Results

7.3.1 Gelation Temperature and Rate Determination

The instantaneous gelation time of GL solutions, characterized as the point of crossover of G' and G'', was found to be influenced by concentration (Figure 7.1A). These results indicated that gelation of GL was a time-dependent process which may proceed over a long period of time. As such, the relationship between temperature and the time dependence of gel formation was investigated, with results shown in Figure 7.1B. The temperature of instantaneous gelation was determined to be 17.8°C. From the previously-constructed phase diagram, it is apparent that there exists the potential to have a GL-rich phase (continuous or dispersed) separated phase with a concentration

below 5% (w/w). As such, a lower temperature (15°C) was chosen as the minimum final quench temperature for all kinetic trapping experiments to ensure rapid gelation.

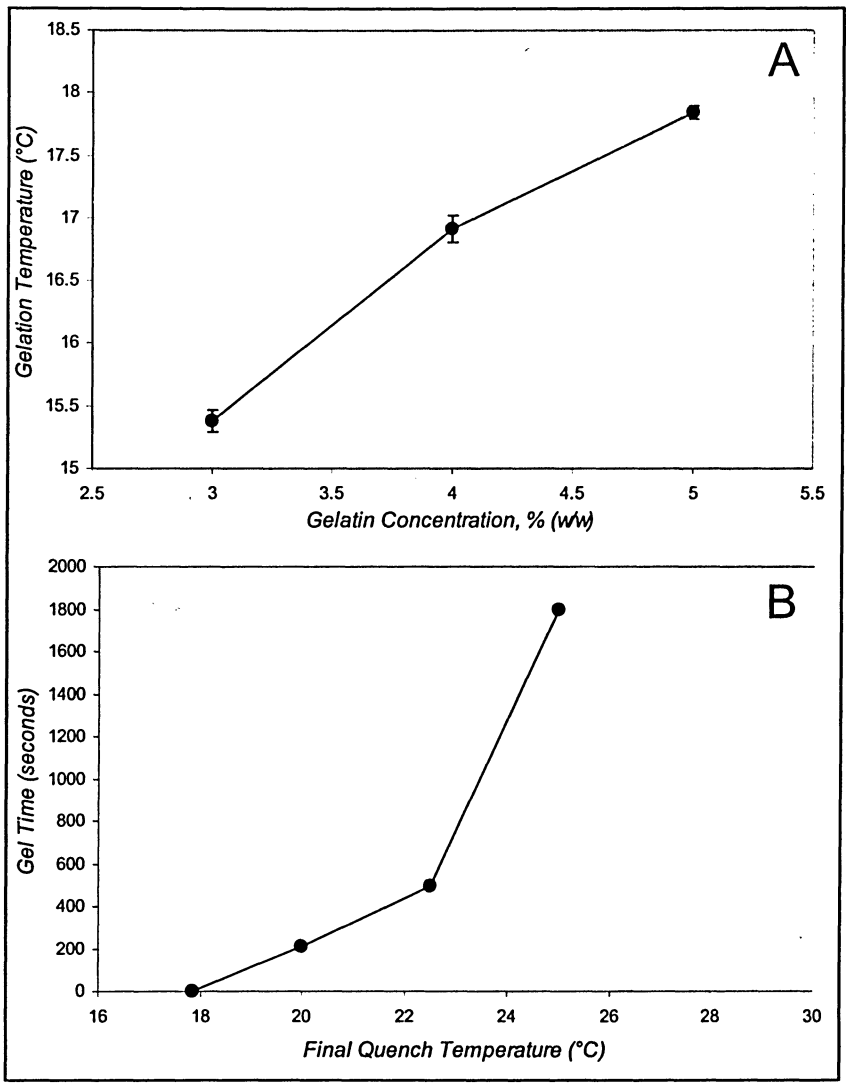

Figure 7.1: Results of rheological investigations conducted to elucidate the thermal and temporal behavior of a gelling GL solution. (A) The maximum temperature at which a gelled network began to form for a series of differently composed systems. (B) Temperature-dependent rate of gelation.

7.3.2 Kinetic Trapping and Phase Separation-Induction *via* Physical Crosslinking

Preliminary investigation of the efficacy of gelation as a means of kinetic trapping was conducted on separated systems following a period of coarsening. Rapid quenches (30°C/minute) were seen to induce gelation (by visual inspection of the samples). Micrographs taken immediately before and after the final quench revealed little change in the size and spatial distribution of droplets originally present in the first image (Figure 7.2).

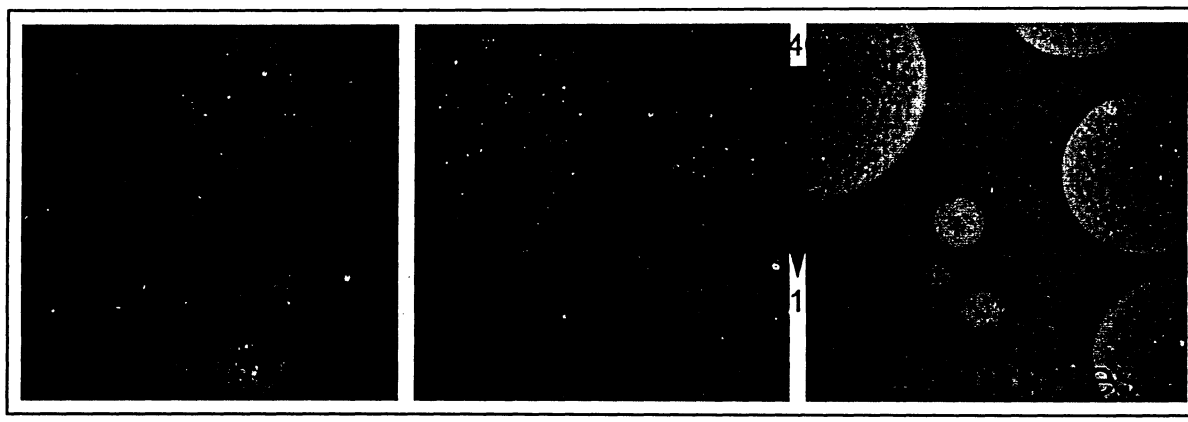

Figure 7.2: Representative micrograph series depicting the kinetic trapping of phase-separated microstructure *via* gelation (in this case of the dispersed phase). System microstructure is seen to mature over a period of 30 minutes at a temperature above that of gelation. Instantaneous gelation was induced and shown to effectively inhibit droplet coarsening. All images are 152 μm x 152 μm.

In the absence of kinetic trapping, the 15-minute time frame between the second and third images in Figure 7.2 would be sufficient to coarsen the microstructure, with bulk phase separation being a possible outcome. Instead, the main droplets observed in the second image remain at the same size and in the same location in the third image. For all samples undergoing this thermal treatment, kinetic trapping by these means was found to inhibit coarsening in

both GL-continuous (on average, a 3.20±0.33% change in average original droplet area) and MD-continuous (on average, a 5.40±0.42% change in average original droplet area systems). The continuous-phase specific efficiencies of kinetic trapping were found to be statistically significant ($P < 0.05$) and are likely a result of the increased concentration of GL. The appearance of a population of smaller, regularly-sized droplets was observed in all samples. This phenomenon, secondary phase separation, forms the basis for Chapter 8.

The first experimental design was conducted to reiterate the general findings of others, namely the interdependence of two-phase liquid region residence time and droplet size. Two factors were investigated (hold time at 40°C; quench rate from 40°C to 15°C) at three levels each (hold times of 0, 10 and 20 minutes; quench rates of 0.7, 2 at 10°C/minute). The results are shown in plots of the main effects of the two factors (Figures 7.3A and 7.3B). ANOVA testing showed a significant effect on the average droplet diameter for both hold time ($P < 0.01$) and quench rate ($P < 0.05$).

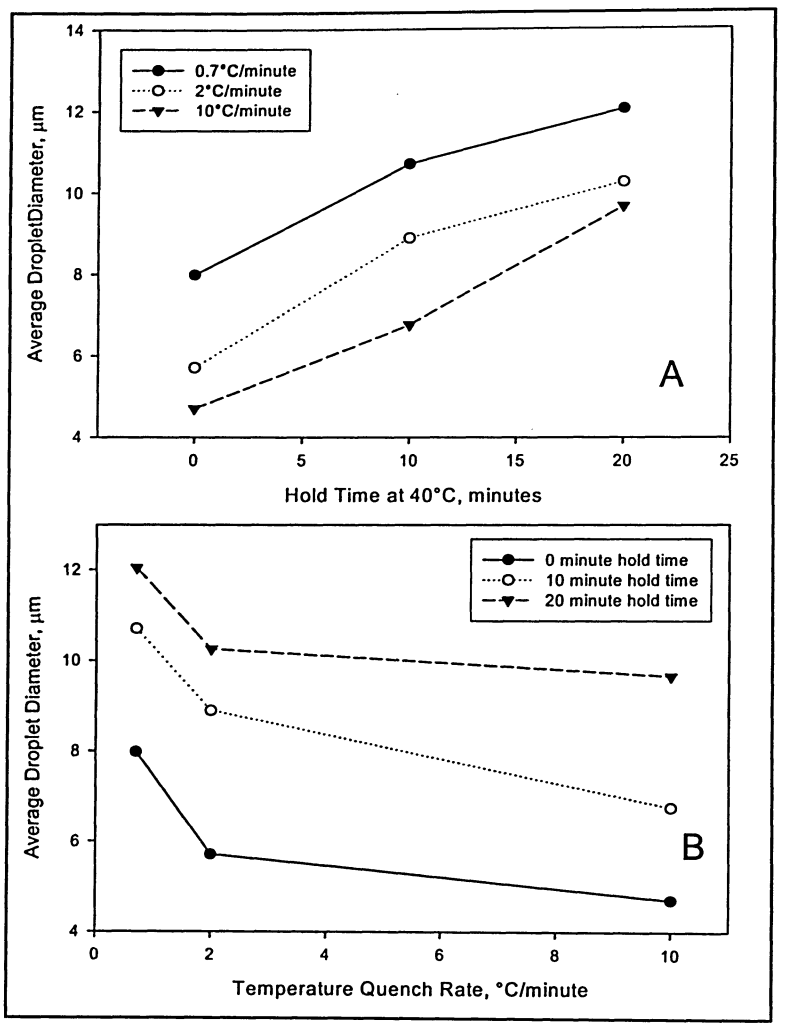

Figure 7.3: Plots indicating the overall main effects of the experimental design on the factors hold time at 40°C and quench rate. (A) An increase in the hold time of systems at 40°C yielded larger droplets relative to shorter hold times. (B) An increase in the rate at which systems were quenched to the temperature of instantaneous gelation yielded smaller droplets than systems quenched slower.

Only main effects were examined, and any replication carried out was in order to evaluate the repeatability of experimental results. Table 7.3 shows the results of multiple trials of a particular thermal regime and indicate negligible variability between sample runs of the same type.

Table 7.3: Representative replicate data for uncrosslinked sample investigation.

Sample ID	40°C Hold Time (minutes)	Quench Rate (°C/minute)	Average Droplet Area at 50 μM Depth (μm^2)
5	10	2	67.30
6	10	2	60.98
7	10	2	58.35
			62.22±4.69

7.3.3 Kinetic Trapping *via* Chemical Crosslinking

The second experimental design was conducted to investigate the contributing effects of chemical crosslinking on the kinetic trapping and gelation-induced phase separation of a biopolymer mixed system. The direct relationship between temperature of crosslinking and the resulting rate of reaction was taken into account in designing the experiment. Two factors were investigated (reaction time at 70°C; reaction time at 40°C) at three levels each (0, 7.5 and 15 minutes; 0, 10 and 20 minutes). The results are shown in plots of the main effects of the two factors (Figures 7.4A and 7.4B). ANOVA testing showed a significant effect on average droplet diameter for only holding periods at 40°C ($P < 0.05$).

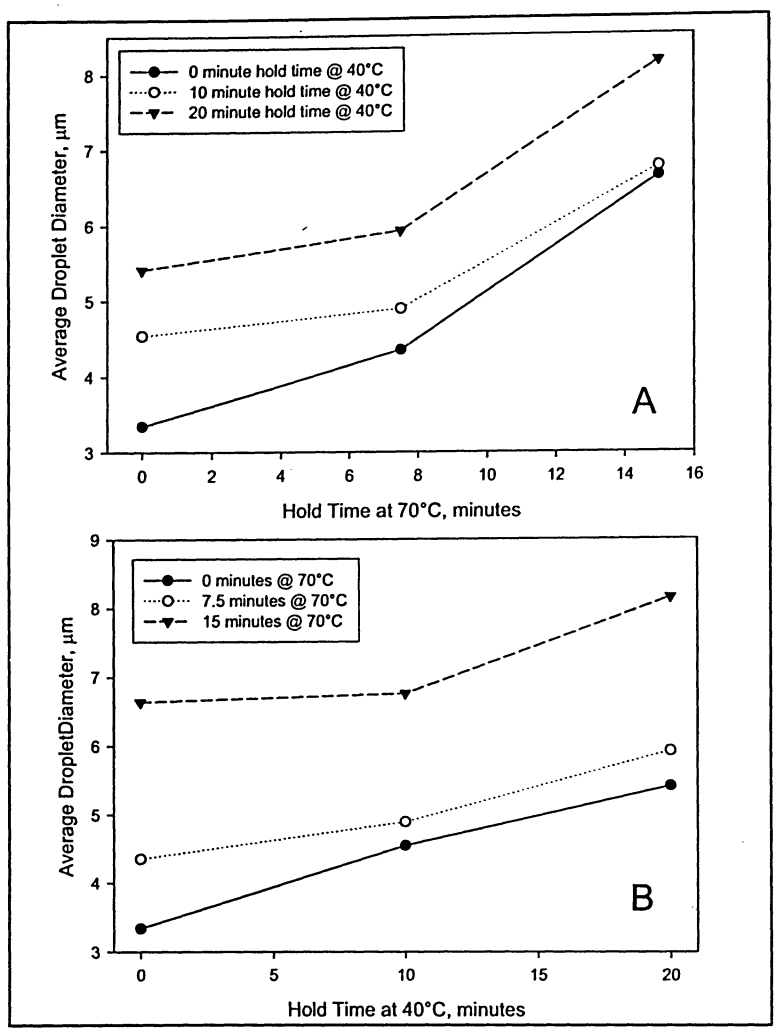

Figure 7.4: Plots indicating the main effects of the experimental design on the factors hold time at 70°C and 40°C in systems treated with GP. (A) Increases in the hold time of systems at 70°C are shown to yield larger droplets relative to shorter hold times. (B) Increases in time for which systems are held at 40°C are shown to increase average droplet diameter.

7.4 Discussion

The results of Figures 7.2 indicate the effectiveness of gelation-induced kinetic trapping and reiterate the direct relationship between residence time in the two-phase liquid region and average inclusion size. The direct linear response of the two tested factors indicate that effective kinetic trapping was

independent of quench rate and was solely contingent on instantaneous gelation of the GL-rich phase. Slower quenches into the gelling region serve only to allow for a greater period of time of microstructural coarsening. The direct relationship between coarsening period and droplet size is best seen in a composite plot of all data point collected in the experiment (Figure 7.5A).

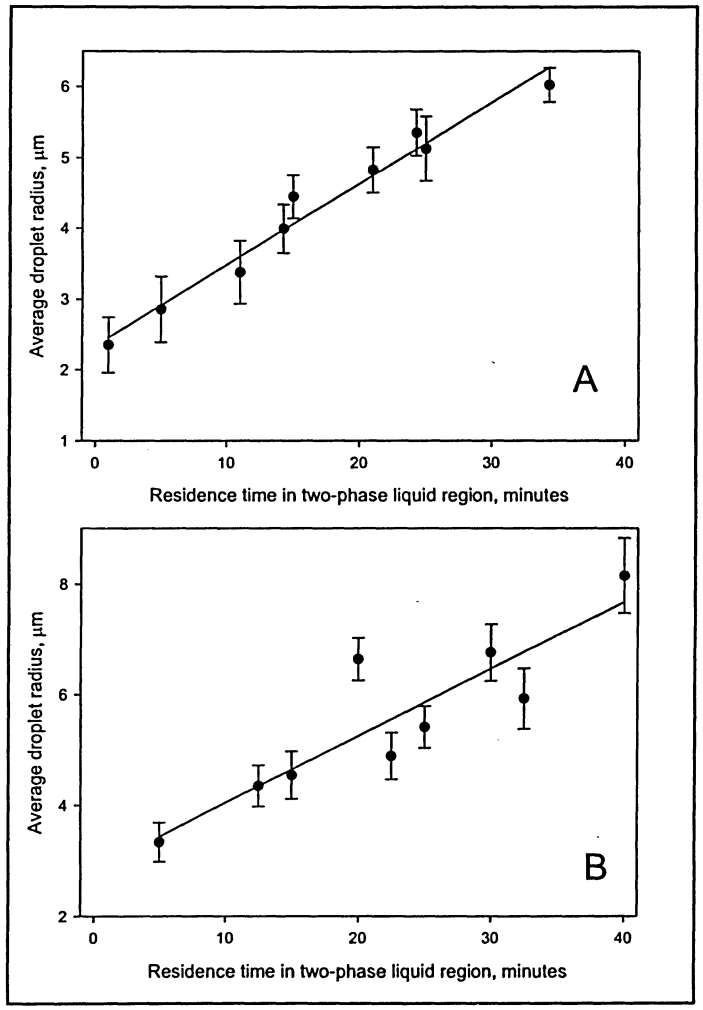

Figure 7.5: Plots of average droplet size as a function of system residence time in the two-phase liquid region (*i.e.*, above gelling temperature) for (A) the uncrosslinked system and (B) the GP crosslinked system.

Gelling of a GP crosslinking solution introduced another aspect of kinetic trapping, namely the potential to trap systems at elevated temperatures. The rapid rate of network fixation and the resultant gelling of the system were proposed to serve as a second possible mechanism for halting microstructural coarsening. The trend observed in Figure 7.5B indicates the unsuitability of this of this theory. The average droplet size in systems having similar residence times as those in uncrosslinked systems were consistently larger in the GP treated systems. Figure 7.6 further confirms that not only was GP treatment an ineffective method of kinetic trapping, but it also has the effect of slightly increasing the inclusion size average relative to what would have resulted in the absence of the crosslinker. Given the comparable residence times, it is apparent that another mechanism is acting to accelerate phase separation during the GP crosslinking reaction.

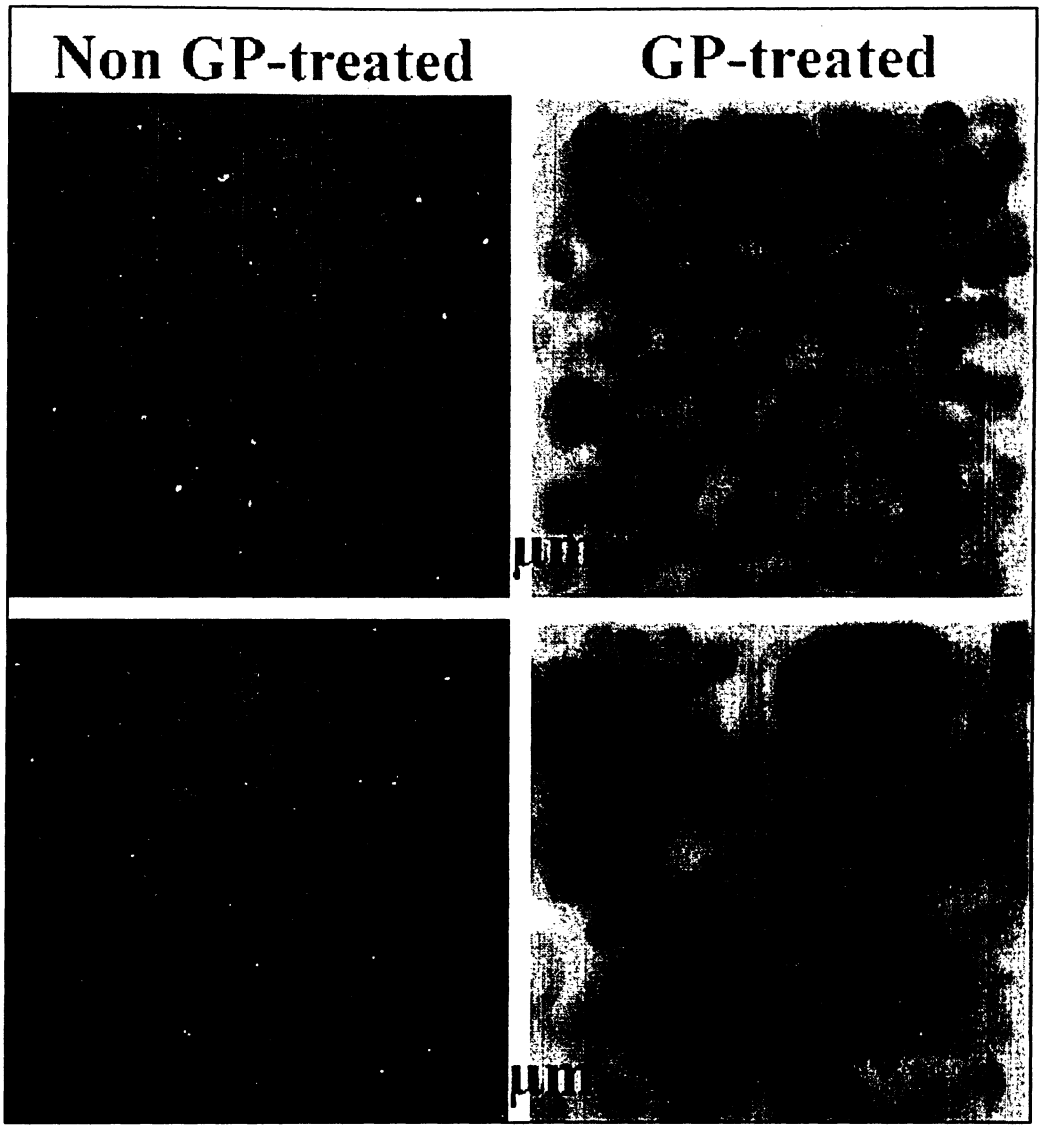

Figure 7.6: Micrographic comparison of the representative microstructures resulting from growth and kinetic trapping in non GP-treated and GP-treated systems having identical residence times within the two-phase liquid region. Images presented are taken at 50 μm and 150 μm below the coverslip to provide evidence of sedimentation. All images are 150 μm x 150 μm.

It has been shown previously (Chapters 5 and 6) that an increased biopolymeric molecular weight will increase the tendency of a system towards separation. Later results (Chapter 8) confirm this by showing that an effective increase in molecular weight upon physical gelation induces phase separation. The implication here is that the extent of network formation of GP treated

systems plays a role in the development of phase-separated structures. This role is likely similar to that observed for physically-gelling GL. The effective increase in GL molecular weight resulting from crosslinking (chemical or physical) alters the thermodynamic state of the system and can induce phase separation in the absence of a temperature quench. Furthermore, droplet growth behavior (Chapter 6) indicates that the microstructure resulting from a thermal profile that includes a growth period at 70°C would be expected to be less mature than that of one primarily growing at 40°C. This trend is not observed in the GP-treated system, further implying another effect is at play.

GL gelation has been shown to be an effective method to kinetically trap microstructure. Given this, it is apparent that the increase in viscosity resulting from gelation effectively inhibits the hydrodynamic flow required for late stage coarsening. Though GP treatment at elevated temperatures had been theorized to occur at a rate in the time range required for kinetic trapping, it is apparent that the degree of network formation within this time frame is inadequate for this end result. However, there appears to be a degree of network formation that acts to effectively increase the GL molecular weight, accelerating phase separation. Systems typically separating at 70°C (as was the case for the investigated system) left to separate and coarsen at 70°C would exhibit a slow rate of both separation and coarsening. The position of the system on the binodal curve would lead to metastable NG separation, where it is necessary for separating nuclei to overcome an energy barrier prior to separation. As well, it has been shown that systems undergoing a shallow quench will coarsen in their

late stages at slower rates than deeply-quenched systems (Chapter 6). These two trends would indicate that the GP-treated system, in complete absence of network formation at 70°C, would be characterized by a relatively small degree of phase separation in the form of small inclusions. Instead, these systems exhibited a great degree of phase separation. Clearly, while network formation did occur in GP-treated samples, its crosslinking rate was not high enough to kinetically trap the system, though it did accelerate phase separation at unusually elevated temperatures.

Kinetic trapping of separating systems was also investigated against sedimentation-dependent coarsening. Effective microstructural trapping should ideally inhibit droplet growth in all directions. Figure 7.6 also gives a representative picture of the relative degrees of sedimentation in systems with and without GP treatment. The average droplet size in both micrographs shows an increase relative to that of the images just under the coverslip, indicating a coarsening effect in the downward direction. Similar to the effect of increased average droplet size observed previously, the GP-treated system exhibited a great deal of sedimentation in the form of larger droplets lower in the sample.

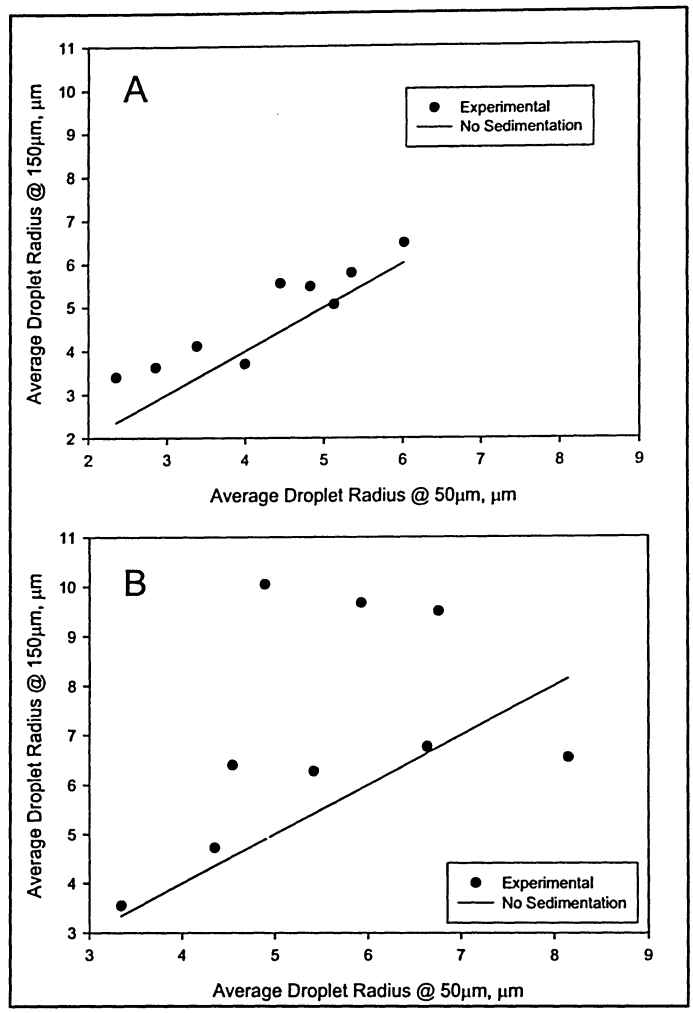

Figure 7.7: Sedimentation plots for systems undergoing physical (A) and chemical (B) crosslinking during microstructural coarsening. Average droplet diameters at a depth of 50 μm are plotted on the x-axis, while average droplet diameters at 150 μm appear against the y-axis. The solid line represents a plot of ideal, non-sedimentation behavior and serves to give an indication as to the extent of sedimentation. Points lying above the line exhibit sedimentation.

Sedimentation occurred in both systems, though the extent of sedimentation was far greater in the GP-treated system. The results in Figure 7.7A confirm the hypothesis (Chapter 6) that coalescence-dominated droplet growth is not the only mechanism occurring during late stage phase separation. The high degree of sedimentation in the GP-treated system (Figure 7.7B)

indicates the treatment of separating GL-MD systems with GP accelerates phase separation and coarsening. From this standpoint, treatment with GP at temperatures above that of gelation serves as a replacement for an extended residence time in the two-phase liquid region. If kinetic trapping of a GP-treated GL-MD composite is desired, a rapid temperature quench to the temperature of instantaneous gelation is by far the most effective method.

7.5 Conclusion

Kinetic trapping of separated and coarsening GL-MD composite systems was shown to be feasible through simple gelation of the GL-rich phase. The efficiency of trapping was shown to be relatively weak when systems were slowly quenched into the gelling region. Instead, rapid gelation, brought about by temperature quenches below the temperature of instantaneous gelation, quickly and effectively trapped further coarsening of the separated microstructure. Droplets maintained their pre-quench sizes and spatial distributions.

While the utility of GP in crosslinking GL-MD systems has been previously discussed, rapidity of its network formation is insufficient to provide any degree of kinetic trapping[43]. Instead, GP reaction serves to effectively increase the molecular weight of GL, which has a similar effect as quenching the system well into the phase separation region. The microstructure resulting from GP treatment exhibits characteristics in line with systems having undergone much lengthier phase separation.

Chapter 8

Microstructural Characterization of a Two-step Phase Separation in Biopolymer Mixtures

8.1 Introduction

Phase separation is a process that leads to the formation of heterogeneous microstructures in incompatible mixed biopolymers. The dynamics and morphology of phase separation are strongly dependent on composition and temperature quenching conditions. Phase separation mechanisms may be classified as spinodal decomposition (SD) or nucleation and growth (NG) droplet growth regimes. In the case of SD, phase separation may be further subdivided into bicontinuous and droplet SD.

In the study of food-related phase separation, the focus has been on ordering processes encountered during single temperature quench from the stable one-phase region of a phase diagram to the metastable or unstable two-phase region. Since the 1980s, there has been intensive research in manipulating the phase separation of protein-polysaccharide mixtures, such that today, the kinetics and thermodynamics are reasonably well-understood.

Industrially, this process is used to develop biopolymer composites with a wide range of textural properties.

Quench conditions are one of the key factors that will determine the phase separation pathway. In this regard, in the polymer field, there has been considerable interest in generating novel phase-separated microstructures through complex temperature modulations. An example of this is periodic spinodal decomposition, where microstructure is influenced by both inducing and depressing subsequent phase separations in both the included and continuous phases of an initial TIPS[17;57].

The purpose of the present investigation is the off-critical double quench, which is composed of a first quench from the one-phase to a two-phase metastable or unstable region followed by a second quench deeper within the two-phase region. This second quench is deeper than the initial quench and as such initiates further thermodynamic instability within the system.

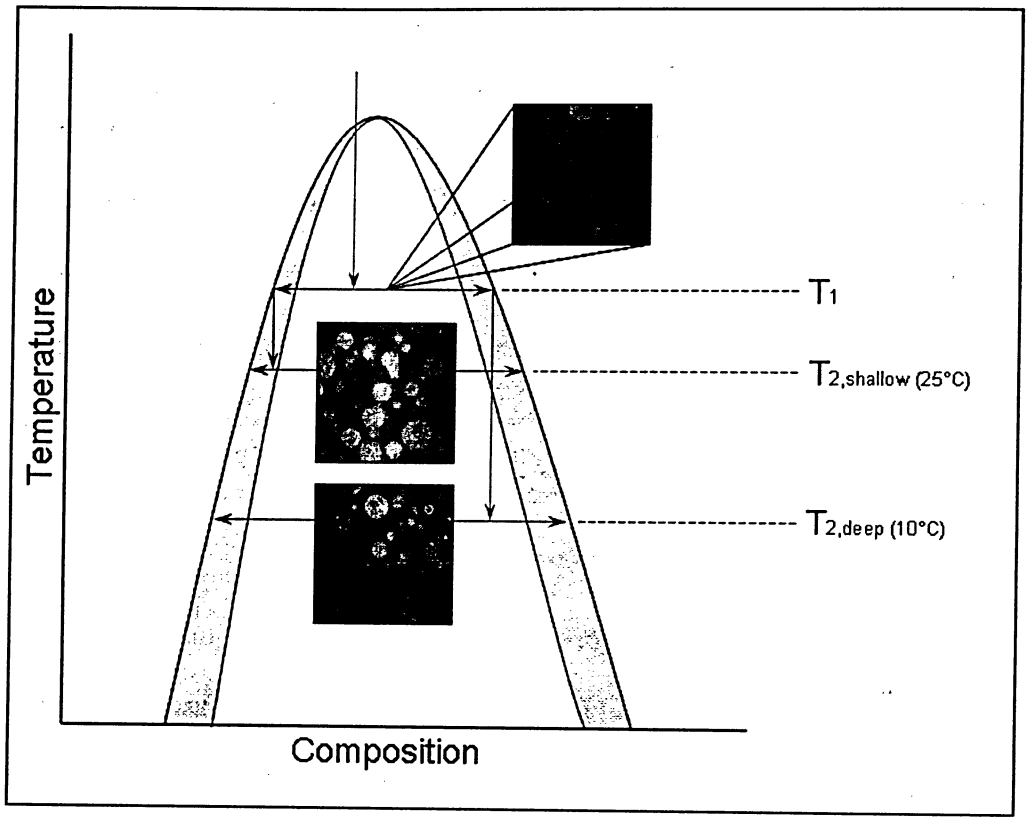

Figure 8.1: Schematic representation of the double temperature quench process in biopolymer systems. Initial samples reside in the monophase region, above the binodal. With the first temperature quench, samples are brought into the two-phase region (unstable or metastable, depending on quench depth). Over a sufficiently long period of time, phase separation will result in a two-phase microstructure, each phase enriched in one type of biopolymer. These coexisting phases are characterized by points on the binodal. The second temperature quench returns these phases to the two-phase region, and secondary phase separation results. The mechanism of the second quench will depend on whether the system ultimately lies in the metastable (shallow quench) or unstable region (deep quench).

Comprehensive studies of secondary phase separation in biopolymeric systems remain rare. In contrast, much work has been done in investigating the process in synthetic polymer systems, both experimentally and theoretically[17;17;55;94]. The majority of these studies have investigated the growth profile of structure growth factors following a double quench. The

structure factor is a characteristic measurement of systems separating *via* SD. It represents the dominant length scale within the system. Theoretically, this value takes the form of the wavelength of the concentration profile depiction of SD growth outlined based on the theories of Cahn[84]. Experimentally, the structure factor is the characteristic distance between inclusions in a separating system. In the experimental work of Tanaka *et al.*, the second quench was carried out at both the intermediate and late stages of the primary phase separation regime[17;95;95]. The theoretical studies of Ohnaga *et al.* investigated the effects of secondary quenches at three different stages of phase separation, namely SD onset, upon appearance of well-developed concentration fluctuations and, finally, when the concentration fluctuations reached their equilibrium values (*i.e.*, when separated phases attained equilibrium compositions, dictated by the initial temperature quench)[65]. In these studies, SD was the mechanism of the second phase separation regime. Hashimoto *et al.* observed experimentally an adherence to the linear theory in the relationship between the characteristic structure factor with time on a logarithmic plot[17]. Hashimoto *et al.* observed an effect of the initial included dispersed phase size on the rate of growth of the secondary structures[17]. It was observed that larger initial inclusions favored a more rapid development of secondary structure. In the context of the concentration profile model used to depict SD, Ohnaga *et al.* proposed a mechanism of constructively and destructively interfering wave patterns for a secondary phase separation regime (Figure 8.2)[96;97]. The presence of two length scales in the system has a confounding effect on the concentration

fluctuation profiles throughout the system. The resulting concentration profile is discussed in the context of experimental observations later in the chapter[6].

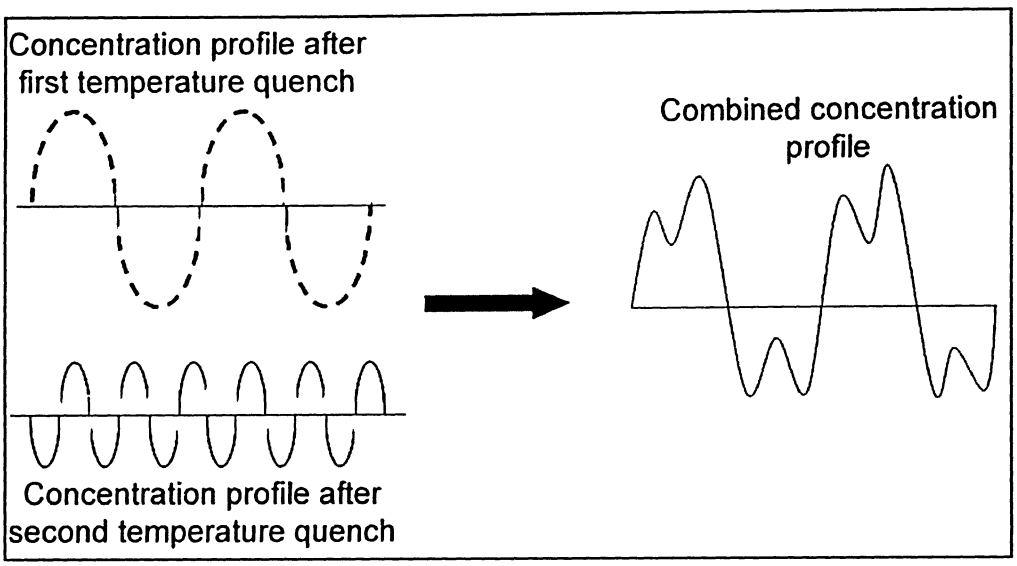

Figure 8.2: Schematic representation of the proposed constructive and destructive interfering concentration profiles present following a double quench regime. Adapted from Ohnaga *et al.*[96].

Tanaka presented a rare look at the coarsening behavior of a system having undergone a double temperature quench where the second quench was deeper than the first[98]. They observed a complex coarsening behavior characterized by three distinct regimes, each differing in the time evolution behavior of the structure factor of the system[17]. Upon secondary quenching, small droplets appeared and coarsened with time in the large droplets, which behaved as isolated systems made unstable by the second quench. The second regime exhibited a change in the coarsening behavior of the droplets, as they stopped growing *via* the SD mechanism and began to interact *via* a diffusion mechanism with the larger droplets that contained them. During the third stage, small droplets disappeared *via* Ostwald ripening (OR). OR was evidenced by

the growth of droplets at the expense of neighboring droplets through a mechanism of diffusion.

Double quenches in food biopolymers will tend to drive secondary phase separation when the quench depth is within the gelling region. While gelation has been shown to inhibit coarsening on the macroscopic level, it does not necessarily do so to the same extent at all length scales. Macroscopic kinetic trapping rapidly follows gelation, while molecular motion leading to phase enrichment and a degree of phase separation may still occur. Furthermore, gelation has been observed to stimulate phase separation on small length scales due to effectively increasing the molecular weight of the gelling component through physical crosslink formation. This occurrence enhances the driving force for phase separation. Near-critical quenches of GL-dextran have exhibited gelation-induced secondary phase separation. A low temperature quench well into the gelling region of GL was observed to give more intense higher angle light scattering, implying presence of an increase in concentration inhomogeneities on small length scales that were not present prior to the second quench[18].

The objectives of this study were to observe the secondary phase separation behavior resulting from quenches below gelation temperature in GL-MD systems and to clarify how composition affects the kinetic pathway of phase separation and the resulting microstructural hierarchy. Systems were analyzed for extent of secondary phase separation and its presence in both the continuous and dispersed phases.

8.2 Experimental Methods

8.2.1: Materials and Sample Preparation

The GL and MD samples and preparation techniques used were discussed previously (Chapter 2 and Chapter 4, Section 4.1, respectively). Two sample compositions were analyzed, each having phase separation temperatures of 70°C. Each sample had a different continuous nature upon primary separation, one yielding a GL-continuous composite system (4.23% GL and 3.45% MD, w/w) and the other an MD-continuous system (2.86% GL and 6.82% MD, w/w).

8.2.2 Double Quench Sample Treatment.

A volume (0.5 mL) of sample was placed onto a welled microscope slide, which was placed onto a heated CLSM stage (Zeiss LSM-510 confocal microscope, Zeiss Instruments, Mississauga, Ontario, Canada). Samples were first maintained at 70°C before being rapidly quenched (30°C/minute) to 40°C. Phase separation and coarsening were followed at this temperature for a period of 20 minutes. Afterwards, the temperature of the system was decreased *via* a second rapid quench (30°C/minute) to either 10°C or 25°C. Images were captured every minute until no noticeable change in microstructure was seen. Micrographs were analyzed (sp) for average droplet size and size distribution using previously mentioned techniques (Section 5.2).

8.3 Results

8.3.1 Initial Observations of Secondary Phase Separation

Secondary phase separation in the GL-MD system was first observed as an unexpected result of kinetic trapping experiments (Chapter 7). Samples were allowed to phase-separate and coarsen for a period of time, after which gelation was induced by a secondary quench. The desired effect of kinetic trapping was observed (halting of microstructural evolution), along with a substantial degree of secondary phase separation (Figure 8.3).

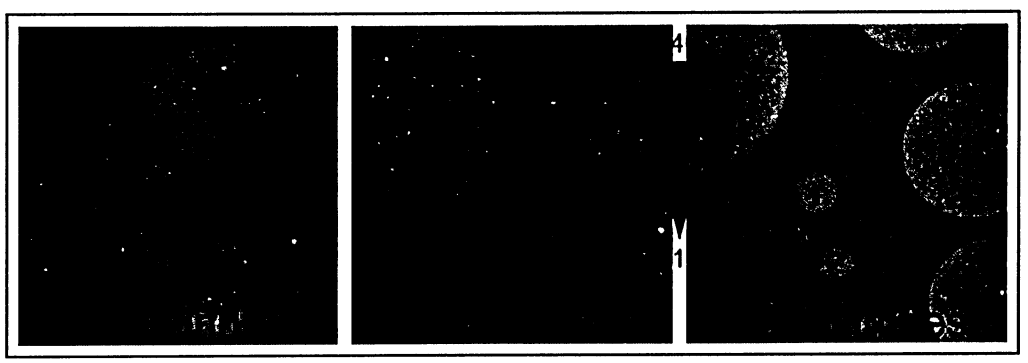

Figure 8.3: Secondary phase separation resulting from a second thermal quench of a separating system into the gelling region observed during kinetic trapping experimentation. Droplets resulting from the initial phase separation are seen to grow in size for 30 minutes, when the system is quenched below the gelation temperature. The initial droplets maintain their size and configuration while a second population of droplets is formed within the original continuous and dispersed phases. Images are 152 μm x 152 μm. Secondary droplets observed in the originally-included GL phase are classified as "inner droplets". Secondary droplets formed in the originally-continuous MD phase are classified as "outer droplets".

Figure 8.3 shows secondary phase separation in both the dispersed and continuous phases. This result had not been previously reported in literature. Observations, like those in Figure 8.3, were the motivation for a more

controlled analysis of secondary phase separation in GL-continuous and MD-continuous systems.

8.3.2 Secondary Phase Separation in MD-continuous Systems

The depth of the second quench greatly influenced the microstructure of the phase-separated mixture. Though secondary phase separation was present in both phases for both quenches, the droplet population attributed to this separation for the two quenches differed.

Figure 8.4 shows the differing growth profiles exhibited by shallow- and deeply-quenched MD-continuous systems following a period of coarsening. The appearance of secondary separation structures was apparent as early as 3 minutes in the deeply-quenched system. In comparison, their appearance in the shallow-quenched system lagged until the 7-minute mark. Secondary phase separation was observed in both the continuous and dispersed phases for both quench depths, though not to the same extent.

The concurrent gelation of the system halted morphological maturation in both systems, with little change observed beyond 9 minutes in the deeply-quenched system; a similar effect was apparent in the shallow-quenched system at 21 minutes. The time of kinetic-trapping onset, however, was clearly not related to the extent of secondary phase separation generated, as the deeply-quenched system exhibited a larger population of secondary structures than the shallow-quenched system.

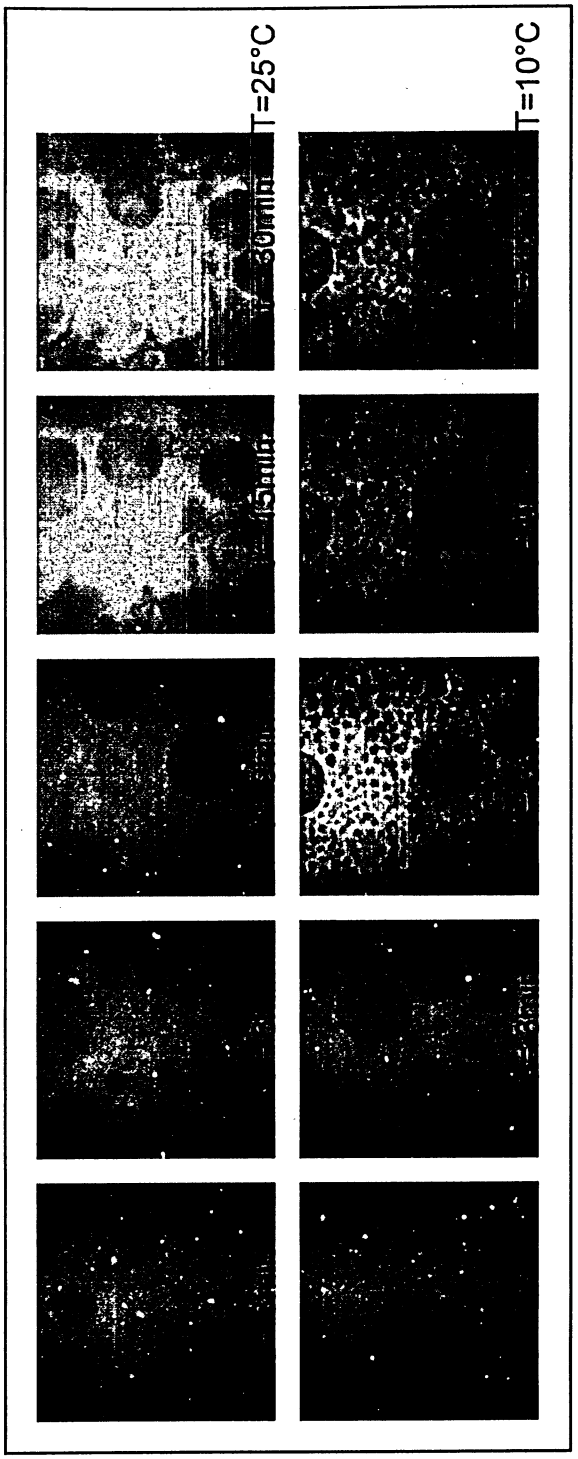

Figure 8.4: Micrographs of MD-continuous systems undergoing thermally induced secondary phase separation following T_2 quenches to 25°C and 10°C. Images are 152 μm x 152 μm. Times shown are relative to t=0 minutes, the time at which the second quench temperature, T_2, was achieved.

The change in droplet population exhibited by MD-continuous systems following a secondary quench showed a strong dependence on the quench depth (Figure 8.5). Shallow-quenched systems showed a lag time of ~10 minutes before the population increase accompanying secondary phase separation was observed. The increase in population of secondary structures residing in the original dispersed phase began much later (at ~20 minutes) and remained relatively unchanged while the major population continued to evolve. A gradual decrease in the outer, continuous phase structure population was observed. This was seen as a likely indication of sedimentation or coalescence occurring concurrently during the experimental time frame.

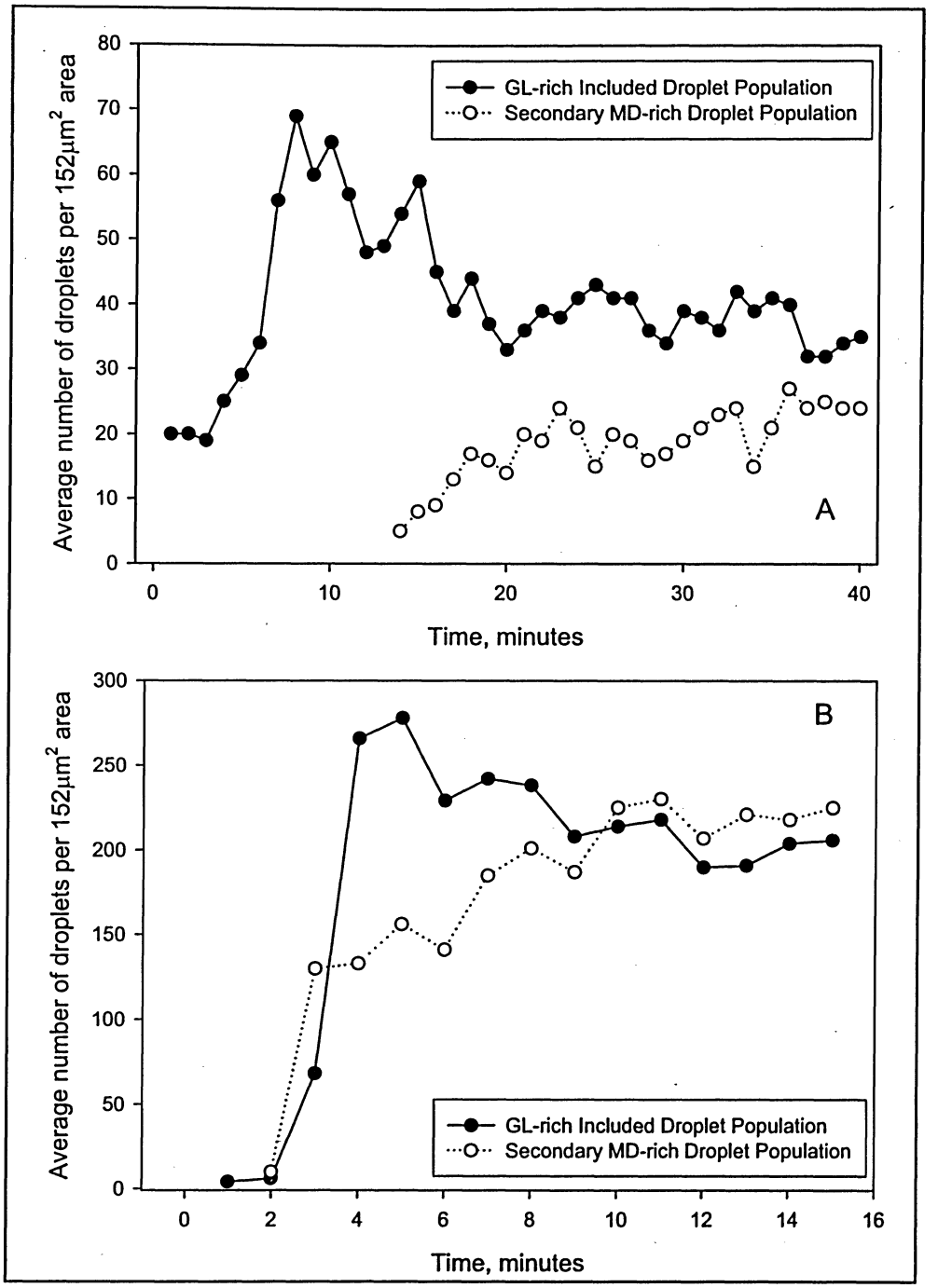

Figure 8.5: Droplet population profiles for MD-continuous systems undergoing secondary phase separation upon quenches to (A) 25°C and (B) 10°C.

Growth of the secondary phase structures resulting from a deep quench occurred almost immediately upon reaching the secondary quench temperature. Almost simultaneously, the inner structures (within the included GL phase) formed and their population evolved similarly to that of the major structures. Based on droplet population growth profiles, the relative amount of phase separation between the two quench depths is noticeably disparate. The deeper quench was observed to have a higher degree of secondary phase separation based on the greater number of secondary droplets.

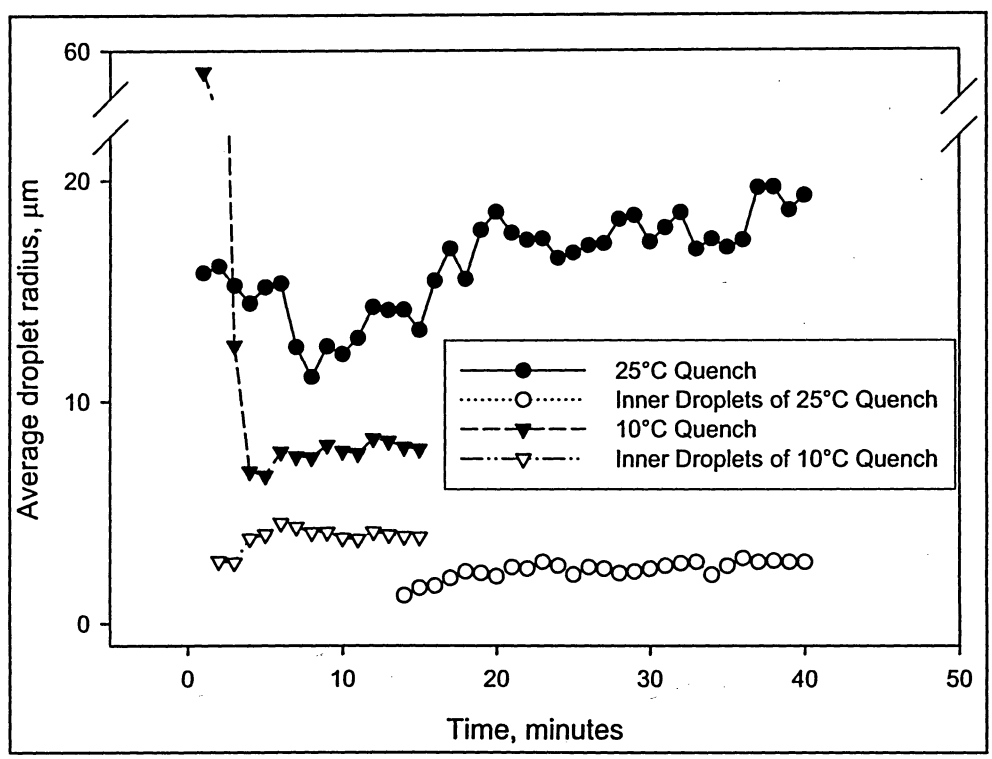

Figure 8.6: Average droplet radius profiles for MD-continuous systems quenched to 25°C and 10°C.

The evolution of the average droplet radius exhibited by the two systems was another measure by which the two quench depths differed. The average

size of the outer structures of the shallow quench did not change following the appearance of secondary structures. The small dip in the curve at approximately 10 minutes coincides with the spike in population in Figure 8.5A. However, the effect of this decrease was only local in nature, as the droplets began to rapidly grow as the total population fell. This may have resulted from the presence of sedimentation or coalescence acting primarily on the original phase-separated structures.

Inner droplet growth for the shallow quench was initiated at a different time than the observed decrease in size of the outer droplets. This indicated that secondary phase separation was not proceeding within the same time scale for coexisting original phases.

The average droplet size accompanying the deep quench showed a steep decline from its value at t=0, indicating the rapid development of a large population of small droplets (Figure 8.6). The appearance of these droplets coincided with the appearance of droplets within the original dispersed phase.

8.3.3 Secondary Phase Separation in GL-continuous Systems

The depth of the second temperature quench had a profound influence on the rate of secondary phase separation, as well as on separation within the initial dispersed phase. Figure 8.7 shows characteristic time course morphologies resulting from the secondary quench of GL-continuous systems.

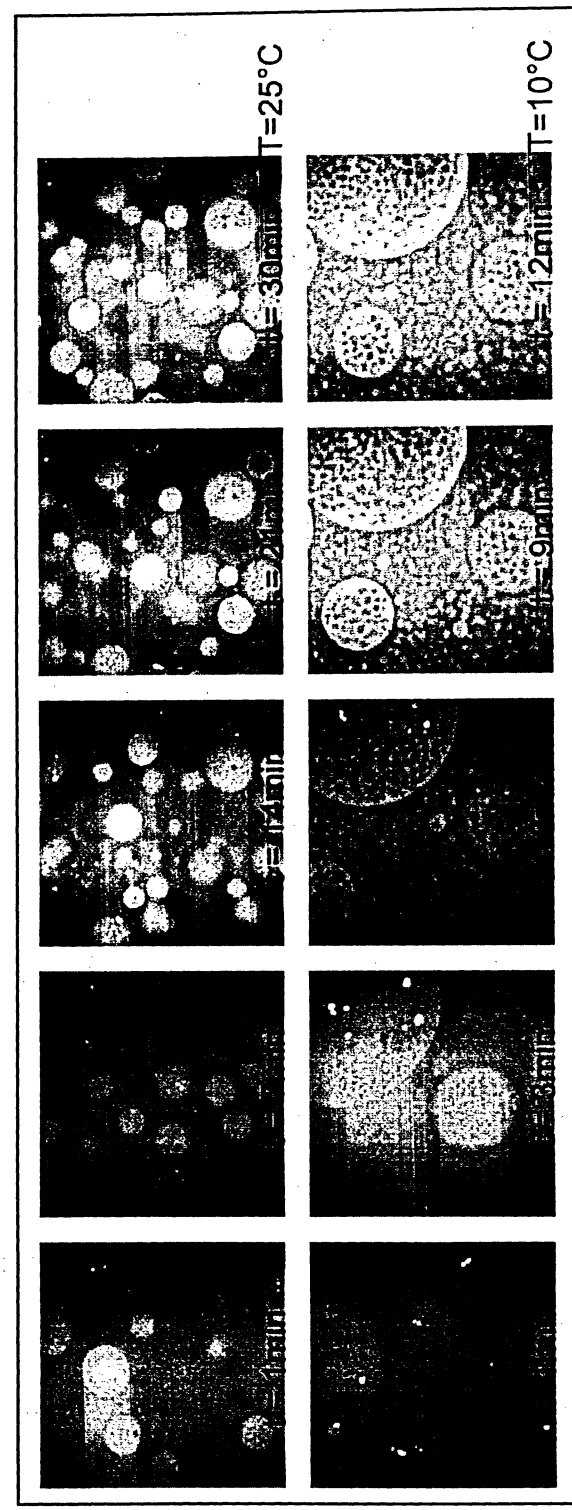

Figure 8.7: Micrographs of GL-continuous systems undergoing TIPS following T_2 quenches to 25°C and 10°C. Times shown are taken in regard to t=0 minutes being the time at which the second quench temperature was achieved. Images are 152 μm x 152 μm.

Shallow second quenches led to a longer lag prior to the onset of secondary phase separation. Deeply-quenched GL-continuous systems showed signs of secondary phase separation after ~3 minutes with little change in microstructure soon after. Shallow-quenched systems began separating at 9 minutes and continued to evolve (in number of? secondary phase-separated structures and the size and spatial distribution of the original inclusions) for a period of ~30 minutes. Systems quenched to 10°C exhibited a higher degree of secondary phase separation, as was evidenced by the greater droplet population in the GL-continuous phase relative to the 25°C quench. Phase separation within the initial dispersed phase was most prominently observed in the deeply-quenched system, where small GL-rich inclusions with a narrow size distribution appeared soon after secondary phase separation onset. Secondary structures in the dispersed phase of the 25°C sample were faintly noticeable on the micrographs. They were few in number and did not appear to evolve over the course of experimentation.

The droplet population growth profiles (Figure 8.8) for the GL-continuous system showed that the quench depth influenced the time of secondary phase separation onset and the time required for phase separation to yield an unchanging system. The appearance of inner GL-rich droplets coincided with the period of rapid dispersed phase droplet population growth?, at ~4 minutes. The curves exhibited a similar time plateau attainment, as well, at approximately 7 minutes. These behaviors are contrasted by the population growth curve of the shallow quenched system, which begins growth at

approximately 9 minutes and, within the experimental timeframe, does not exhibit a noticeable plateau in population.

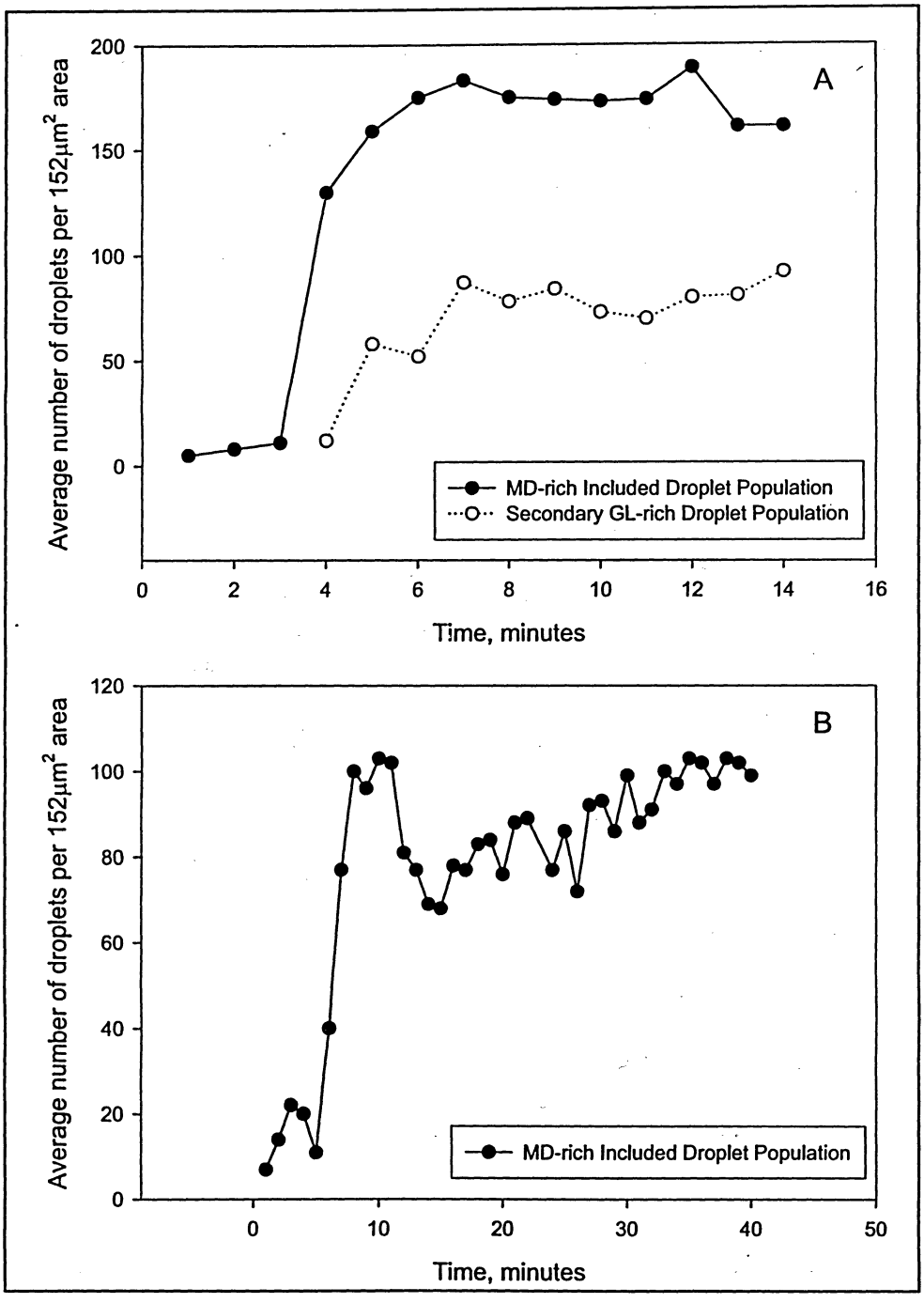

Figure 8.8: Droplet population profiles for GL-continuous systems undergoing secondary phase separation upon quenches to (A) 10°C and (B) 25°C.

The change in the average radius of the included droplet population is shown in Figure 8.9. The behavior of the average droplet radius profiles was opposite that of the population curves. While total droplet population was found to increase over time, average droplet size decreased with time. The downward trend in average droplet radius for the system quenched to 25°C, coupled with the concurrent upward trend of the system's droplet population, indicated that secondary phase separation continued beyond the experimental timeframe.

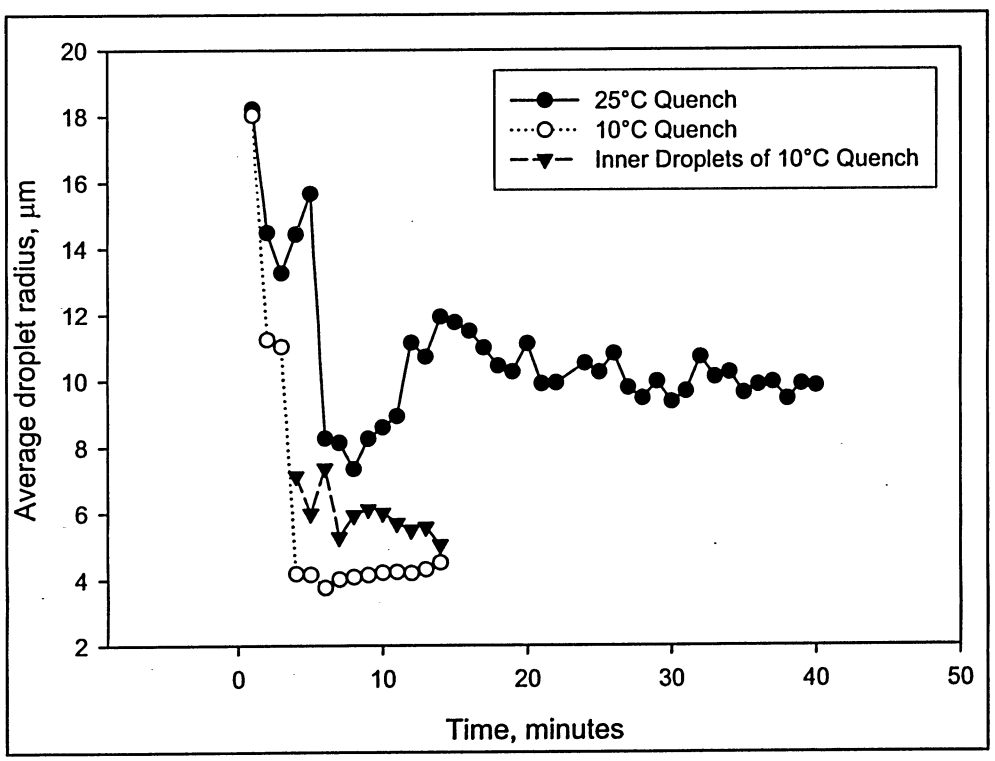

Figure 8.9: Average droplet radius profiles for GL-continuous systems quenched to 25°C and 10°C. The low occurrence and visibility of inner droplet formation in the 25°C sample prohibited.

8.4 Discussion

8.4.1 Evolution of Secondary Phase Separation Structures

Secondary phase separation was observed in all systems undergoing secondary quench regimes. The wide array of characteristics that differed between varying quench depths and continuous phase nature included: existence of secondary phase separation in both the continuous and dispersed phases of the parent system; time after T_2 attainment that secondary phase separation began; behavior of the evolution of the droplet population and average droplet size evolution.

The differing behaviors exhibited by systems undergoing a shallow or deep quench provided insight into the competing mechanisms driving secondary phase separation. As was observed in Chapter 7, an almost inevitable result of kinetic trapping *via* gelation was the occurrence of secondary phase separation, which was more prevalent in deeply-quenched systems. Given that all systems exhibited compositional stability at 40°C, both quenches drove the samples well into the SD region. Despite this, shallow quenches severely reduced secondary phase separation relative to deep quenches. MD-continuous systems undergoing shallow quenches showed minor secondary phase separation, especially within the continuous phase. It is possible that either of these systems were not quenched into the 2-phase region of the phase diagram, though this is unlikely given their equilibrium state at 40°C. Alternatively, it is likely that the secondary quench brought these systems into the metastable region. This would be in accordance with the behavior observed by the shallow

quenched GL-continuous system (Figure 8.8B) which exhibited a gradual increase in population indicative of NG. It is possible that the observed decrease in droplet population within the shallow-quenched MD-continuous systems was insufficient to overcome the required energy barrier for phase separation. The differing evolution of secondary microstructures observed for shallow and deep quenches exhibited behaviors unique to NG (shallow quench) and SD (deep quench) phase separation mechanisms.

Secondary phase separation in deep-quenched systems exhibited a far more complex behavior. The rapid development of a large population of closely monodisperse droplets in both phases indicated a deep quench into the unstable region, yielding phase separation *via* the SD mechanism. However, was the effectiveness of this quench solely attributed to the final temperature of the system or the effective increase in the GL molecular weight upon gelation? Given the highly unstable nature of the secondary phase separation observed and the proposed metastable nature of the shallow quench, it is possible that the temperature quench was not alone in driving phase separation. It is readily apparent that the significant difference between the two temperatures is the instantaneous rate of gelation occurring with the quench to 10°C. It would then be this gelation, concurrent with a quench into the two-phase region, that would drive the highly unstable phase separation observed.

8.4.2 Proposed Explanation of Interfacial Depletion Zones

The depletion areas at the interfaces of the original continuous and dispersed phases were features that were readily exhibited, to varying degrees,

by all deeply-quenched systems (Figure 8.3). It was in these zones that no evidence of secondary structures was observed. Z-axis micrograph stacks of secondary phase-separated systems showed this as an actual depletion layer and not a visual effect resulting from imaging, as had been proposed in previous observations of double phase separation[69]. The combined concentration profile model of secondary temperature quench laid forth by Ohnaga *et al.* provides a possible explanation of these zones[96]. The micrographs presented indicate a microstructure with a concentration profile characterized by an extremely large wavelength (itself a representation of the 2D cross-sectional inclusion size). Upon initiation of unstable secondary phase separation, a second concentration profile appears throughout the system, characterized by a very small wavelength. The resulting combined concentration profile would still exhibit the broad, large wavelength pattern of the original fluctuations. In addition, though, the superimposed patterns would yield smaller peaks and valleys within this main wave, each representing inclusions of the second concentration profile. The smaller, superimposed fluctuations residing at the peaks and valleys of the original profile would be representative of SD droplets formed as the second phase within the original phases. Figure 8.1 depicts this behavior for a system with a small population of secondary droplets. Depletion zones are proposed to exist at the edges of the original peaks and valleys where local extrema in the peaks and valleys reside immediately beside one another (Figure 8.9).

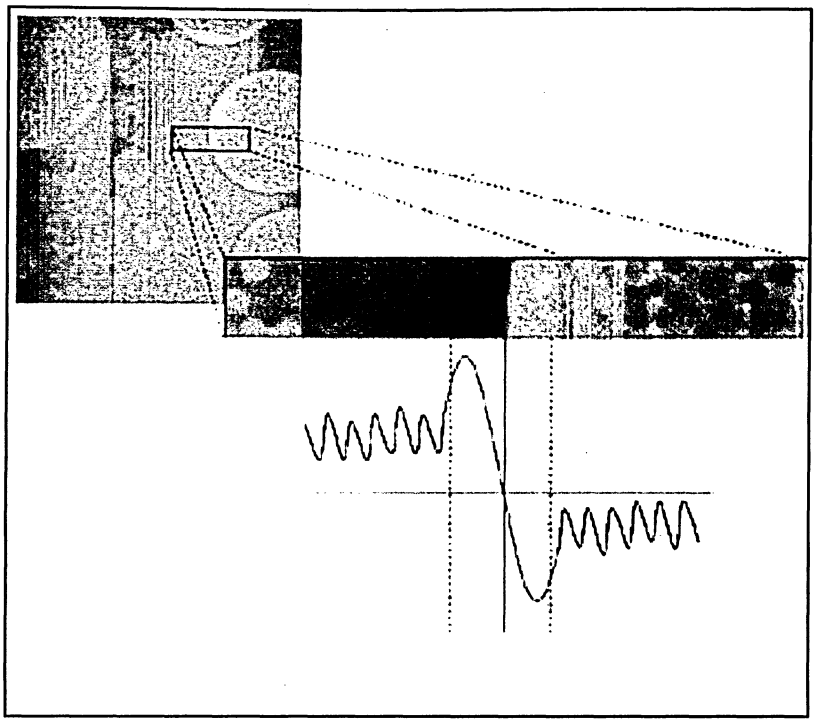

Figure 8.9: Proposed explanation of the observed depletion zone based on the composite wave model of secondary phase separation of Ohnaga *et al* [97]. A possible model of the behavior exhibited by the deeply quenched systems was presented in Figure 8.1.

8.5 Conclusions

The key appeal of the secondary phase separation process in tailoring microstructure lies in its ability to further differentiate separated morphology from that of non-phase-separated systems. Secondary phase separation was observed in GL-continuous and MD-continuous systems. The differing evolution of secondary microstructure observed for shallow and deep quenches were characteristic of NG (shallow quench) and SD (deep quench) phase separation mechanisms (shown diagrammatically in Figure 8.1). Gelation of the microstructure was found to act concurrently with the deep temperature quench to yield a highly-unstable system which underwent rapid separation yielding a

large number of similarly-sized droplets. The development of these droplets introduced another length scale to the system, which others have observed as a new peak in the scattering vector and we have presented as a pronounced decrease in the average droplet size within the system[35].

The dependence of secondary phase separation on gelation of the system is an important result. The observation that secondary phase structure development varied greatly between relatively closely-spaced shallow and deep quenches indicated the contributing effect of gelation on secondary separation. Given the disparate mechanisms of separation observed for the two quenches (slow developing NG and evenly distributed SD), it is readily apparent that the effective increase in quench depth resulting from gelation helps drive separation.

Chapter 9

Conclusion

Phase separation in GL-MD mixed biopolymer systems was observed for a range of compositions and temperatures. In the context of phase-separated microstructures, a number of processes were shown to combine and form the complex collection of behaviors exhibited by separating systems. Each of these processes was shown to be predictable, and as such the fundamentally important in the tailoring of microstructure.

Flory-Huggins theory was shown to qualitatively model the compatibility behavior of GL-MD mixed systems at temperatures above the point of gelation. The inherent trends in phase behavior resulting from changes in temperature and mixture composition were well described. Future work in this area demands that attention be given to the biopolymer-biopolymer interaction parameter, specifically in defining its concentration-dependent variation. Despite this glaring omission in contemporary biopolymer research, it is likely that a limited improvement in model functionality would result from such comprehensive and involved studies.

A predictive model based on coalescence-induced coalescence provided a good fit of experimental data in the later stages of phase-separated

microstructure evolution. Divergence from modeled behavior was eventually observed and was explained as the onset of other coarsening mechanisms, namely sedimentation and possible Ostwald ripening. The goodness of fit of the model in the early coalescence region, however, emphasizes its usefulness as a tool in predicting microstructural evolution.

Having established the theoretical predictability of thermodynamic compatibility (phase separation onset) and phase-separative growth (coarsening) in the GL-MD system, it became apparent that a process halting microstructural evolution would complement these techniques in tailoring morphology. Kinetic trapping was shown to be an effective means of accomplishing this. However, the transient change in microstructure was found to dominate kinetic trapping unless samples were brought into a region of instantaneous gelation. Chemical crosslinking was refuted as an effective mechanism for kinetic trapping. However, the unique phase separative behavior of a chemically-crosslinking system may provide a further mechanism to control microstructure. Formation of chemical crosslinks was theorized to alter the thermodynamic parameters of the mixture components, thereby enhancing phase-separative behavior at previously unobserved rates and temperatures.

The secondary quench required to trap the system was also shown to drive a secondary phase separation process. The morphology (a manifestation of the characteristic mechanism of phase separation occurring) was found to be highly influenced by the depth of the quench. As was observed in chemically-crosslinked samples, introduction of physical crosslinks, resulting from deep

quenches into the gelling region, was a likely contributor to the observed accelerated separative behavior. The operative depth of the quench was increased by the effective increase in molecular weight of networking components. This resulted in a greater than expected degree of thermodynamic incompatibility.

In the context of microstructural tailoring, the results presented herein are shown to elucidate the behaviors of the characteristic processes that turn a homogeneous biopolymer system into a bulk phase-separated system of uniquely composed coexisting phases. Furthermore, the influences of processing parameters, from temperature to component molecular weight, are shown to be predictable, leading to a greater control of the processes of phase separation, microstructural evolution, kinetic trapping and secondary phase separation.

References

1. V. Tolstoguzov, *Journal of Thermal Analysis and Calorimetry* 61, 397-409 (2000).

2. S. Kasapis, E. R. Morris, I. T. Norton, C. R. T. Brown, *Carbohydrate Polymers* 21, 261-268 (1993).

3. M. F. Butler and M. Heppenstall-Butler, *Food Hydrocolloids* 17, 815-830 (2003).

4. N. Loren and A. M. Hermansson, *International Journal of Biological Macromolecules* 27, 249-262 (2000).

5. C. G. de Kruif and R. Tuinier, *Food Hydrocolloids* 15, 555-563 (2001).

6. T. Tran, P. Chan, D. Rousseau, in *Unpublished Book Chapter*, 2006).

7. F. Tanaka and T. Koga, *Bulletin of the Chemical Society of Japan* 74, 201-215 (2001).

8. S. A. Madbouly and T. Ougizawa, *Journal of Macromolecular Science-Physics* B41, 271-287 (2002).

9. V. Tolstoguzov, *Nahrung-Food* 44, 299-308 (2000).

10. N. Loren, A. Altskar, A. M. Hermansson, *Macromolecules* 34, 8117-8128 (2001).

11. V. Tolstoguzov, *Biotechnology Advances* 24, 626-628 (2006).

12. L. Lundin, M. Williams, B. Foster, in *Texture in Food: Volume 1 - Semi-solid Foods*, B. McKenna, Ed. (Woodhead Publishing Ltd., Cambridge, England, 2003) ,chap. 3.

13. T. S. Nordmark and G. R. Ziegler, *Food Hydrocolloids* 14, 579-590 (2000).

14. A. H. Clark, *Carbohydrate Polymers* 42, 337-351 (2000).

15. E. Amici, A. H. Clark, V. Normand, N. B. Johnson, *Biomacromolecules* 3, 466-474 (2002).

16. N. Loren et al., *Macromolecules* 34, 289-297 (2001).

17. T. Hashimoto, M. Takenaka, H. Jinnai, *Journal of Applied Crystallography* 24, 457-466 (1991).

18. R. H. Tromp and R. A. L. Jones, *Macromolecules* 29, 8109-8116 (1996).

19. M. A. K. Williams et al., *Langmuir* 17, 3412-3418 (2001).

20. K. S. McGuire, A. Laxminarayan, D. S. Martula, D. R. Lloyd, *Journal of Colloid and Interface Science* 182, 46-58 (1996).

21. K. Mootoosingh and D. Rousseau, unpublished book chapter (2006).

22. S. Alevisopoulos, S. Kasapis, R. Abeysekera, *Carbohydrate Research* 293, 79-99 (1996).

23. S. Alevisopoulos and S. Kasapis, *Carbohydrate Polymers* 40, 83-87 (1999).

24. N. Loren, M. Langton, A. M. Hermansson, *Journal of Chemical Physics* 116, 10536-10546 (2002).

25. L. Piculell, C. Viebke, P. Linse, *Journal of Physical Chemistry* 99, 17423-17430 (1995).

26. K. Bergfeldt, L. Piculell, P. Linse, *Journal of Physical Chemistry* 100, 3680-3687 (1996).

27. C. Vinches, A. Parker, W. F. Reed, *Unknown* 607-622 (1997).

28. D. S. Martula, T. Hasegawa, D. R. Lloyd, R. T. Bonnecaze, *Journal of Colloid and Interface Science* 232, 241-253 (2000).

29. Flory and P, Principles of polymer chemistry (Cornell University Press, Ithaca, New York, 1953).

30. Binder, K., Frisch, H. L., and Jackle, J. Kinetics of phase separation in the presence of slowly relaxing structural variables. Journal of Chemical Physics 85(3), 1505-1512. 8-1-1986.

31. W. J. Chen, X. L. Li, T. Dong, M. Jiang, *Macromolecular Chemistry and Physics* 199, 327-333 (1998).

32. V. J. Anderson and R. A. L. Jones, *Polymer* 42, 9601-9610 (2001).

33. F. Tanaka and N. Ishida, *Macromolecules* 32, 1271-1283 (1999).

34. J. L. Doublier, C. Garnier, D. Renard, C. Sanchez, *Current Opinion in Colloid & Interface Science* 5, 202-214 (2000).

35. R. H. Tromp, A. R. Rennie, R. A. L. Jones, *Macromolecules* 28, 4129-4138 (1995).

36. M. F. Butler, *Biomacromolecules* 3, 676-683 (2002).

37. M. F. Butler and M. Heppenstall-Butler, *Biomacromolecules* 4, 928-936 (2003).

38. E. C. Needs et al., *Journal of Dairy Research* 67, 329-348 (2000).

39. M. F. Butler, *Biomacromolecules.* 3, 1208-1216 (2002).

40. V. Tolstoguzov, *International Review of Cytology - A Survey of Cell Biology, Vol 192* 192, 3-31 (2000).

41. S. B. Ross-Murphy, *Abstracts of Papers of the American Chemical Society* 219, U401 (2000).

42. P. D. A. Pudney, T. M. Hancewicz, D. G. Cunningham, C. Gray, *Food Hydrocolloids* 17, 345-353 (2003).

43. M. T. Nickerson et al., *International Journal of Biological Macromolecules* 38, 40-44 (2006).

44. M. T. Nickerson et al., *Pending Publication* (2005).

45. F. Cuppo, M. Venuti, A. Cesaro, *International Journal of Biological Macromolecules* 28, 331-341 (2001).

46. S. Kasapis, E. R. Morris, I. T. Norton, A. H. Clark, *Carbohydrate Polymers* 21, 243-248 (1993).

47. I. T. Norton and W. J. Frith, *Food Hydrocolloids* 15, 543-553 (2001).

48. C. Joly-Duhamel, D. Hellio, M. Djabourov, *Langmuir* 18, 7208-7217 (2002).

49. C. Joly-Duhamel, D. Hellio, A. Ajdari, M. Djabourov, *Langmuir* 18, 7158-7166 (2002).

50. S. Al Assaf, G. O. Phillips, P. A. Williams, *Food Hydrocolloids* 20, 369-377 (2006).

51. S. Kasapis, E. R. Morris, I. T. Norton, M. J. Gidley, *Carbohydrate Polymers* 21, 249-259 (1993).

52. V. J. Morris, A. R. Kirby, A. P. Gunning, *Scanning* 21, 287-292 (1999).

53. I. S. Chronakis, *Critical Reviews in Food Science and Nutrition* 38, 599-637 (1998).

54. V. Tolstoguzov, *Food Hydrocolloids* 18, 873-877 (2004).

55. C. H. Yao, B. S. Liu, C. J. Chang, S. H. Hsu, Y. S. Chen, *Materials Chemistry and Physics* 83, 204-208 (2004).

56. S. Vieth, thesis, Ryerson University (2004).

57. A. Bigi, G. Cojazzi, S. Panzavolta, N. Roveri, K. Rubini, *Biomaterials* 23, 4827-4832 (2002).

58. J. L. Wang and R. J. Sadus, *Fluid Phase Equilibria* 214, 67-78 (2003).

59. M. F. Butler, Y. F. Ng, P. D. A. Pudney, *Journal of Polymer Science Part A-Polymer Chemistry* 41, 3941-3953 (2003).

60. Y. S. Chen et al., *Biomaterials* 3911-3918 (2004).

61. M. Rao, in *Texture in Food: Volume 1 - Semi-solid Foods*, B. McKenna, Ed. (Woodhead Publishing Ltd., Cambridge, England., 2003) ,chap. 2.

62. A. Cesaro, F. Cuppo, D. Fabri, F. Sussich, *Thermochimica Acta* 328, 143-153 (1999).

63. S. Bruin, *Fluid Phase Equilibria* 160, 657-671 (1999).

64. L. I. Khomutov, N. A. Lashek, N. M. Ptitchkina, E. R. Morris, *Carbohydrate Polymers* 28, 341-345 (1995).

65. D. Leisner, M. C. Blanco, M. A. L. Quintela, *Macromolecular Symposia* 190, 93-115 (2002).

66. C. B. Closs, B. Conde-Petit, I. D. Roberts, V. B. Tolstoguzov, F. Escher, *Carbohydrate Polymers* 39, 67-77 (1999).

67. C. Schmitt, C. Sanchez, S. Desobry-Banon, J. Hardy, *Critical Reviews in Food Science and Nutrition* 38, 689-753 (1998).

68. M. G. Semenova and L. B. Savilova, *Food Hydrocolloids* 12, 65-75 (1998).

69. M. F. Butler and M. Heppenstall-Butler, *Biomacromolecules* 2, 812-823 (2001).

70. Y. A. Antonov and M. P. Goncalves, *Food Hydrocolloids* 13, 517-524 (1999).

71. P. D. A. Pudney, T. M. Hancewicz, D. G. Cunningham, *Spectroscopy-An International Journal* 16, 217-225 (2002).

72. M. F. Butler, *Biomacromolecules* 3, 1208-1216 (2002).

73. R. Tuinier, J. Rieger, C. G. de Kruif, *Advances in Colloid and Interface Science* 103, 1-31 (2003).

74. Y. S. Zhu and Z. H. Xu, *Fluid Phase Equilibria* 162, 19-29 (1999).

75. F. Simonet, C. Garnier, J. L. Doublier, *Carbohydrate Polymers* 47, 313-321 (2002).

76. P. Aymard, M. A. K. Williams, A. H. Clark, I. T. Norton, *Langmuir* 16, 7383-7391 (2000).

77. A. Keller and S. Z. D. Cheng, *Polymer* 39, 4461-4487 (1998).

78. M. Tokuyama and Y. Enomoto, *Physica A* 220, 261-276 (1995).

79. N. Loren, M. Langton, A. M. Hermansson, *Food Hydrocolloids* 13, 185-198 (1999).

80. V. Normand, P. D. A. Pudney, P. Aymard, I. T. Norton, *Journal of Applied Polymer Science* 77, 1465-1477 (2000).

81. V. Y. Grinberg and V. B. Tolstoguzov, *Food Hydrocolloids* 11, 145-158 (1997).

82. V. Tolstoguzov, *Food Hydrocolloids* 17, 1-23 (2003).

83. C. Vinches, A. Parker, W. F. Reed, *Biopolymers* 41, 607-622 (1997).

84. J. W. Cahn, *Journal of Chemical Physics* 42, 93-99 (1965).

85. J. W. Cahn and J. E. Hilliard, *Journal of Chemical Physics* 28, 258-267 (1957).

86. A. Gornall, C. Bardawill, M. David, *Journal of Applied Chemistry* 15, 751-766 (1948).

87. Brookhaven Instruments Corporation, 90PDP Instruction Manual - 90Plus Debye Plot Option for Molecular Weight Determination

(Brookhaven Instuments Corporation, Holtsville, New York, ed. 1, 2004).

88. A. Kumar and R. Gupta, Fundamentals of Polymer Engineering (Marcel Dekker, Inc., New York, New York, ed. Second, 2003).

89. B. Smit, *Fluid Phase Equilibria* 116, 249-256 (1996).

90. B. Wolf, R. Scirocco, W. J. Frith, I. T. Norton, *Food Hydrocolloids* 14, 217-225 (2000).

91. Y. Enomoto and M. Tokuyama, *Physica A* 232, 304-314 (1996).

92. K. S. McGuire, A. Laxminarayan, D. R. Lloyd, *Polymer* 36, 4951-4960 (1995).

93. S. Kasapis, E. R. Morris, I. T. Norton, A. H. Clark, *Carbohydrate Polymers* 21, 269-276 (1993).

94. R. Gupta, R. Mauri, R. Shinnar, *Industrial & Engineering Chemistry Research* 38, 2418-2424 (1999).

95. F. Tanaka and M. Ishida, *Journal of the Chemical Society-Faraday Transactions* 91, 2663-2670 (1995).

96. T. Ohnaga and T. Inoue, *Journal of Polymer Science Part B-Polymer Physics* 27, 1675-1689 (1989).

97. T. Ohnaga, W. J. Chen, T. Inoue, *Polymer* 35, 3774-3781 (1994).

98. F. Tanaka, *Macromolecules* 22, 1988-1994 (1989).

Appendices

Appendix A

Biuret Assay for Total Protein Content – Experimentally-compiled Standard Curve

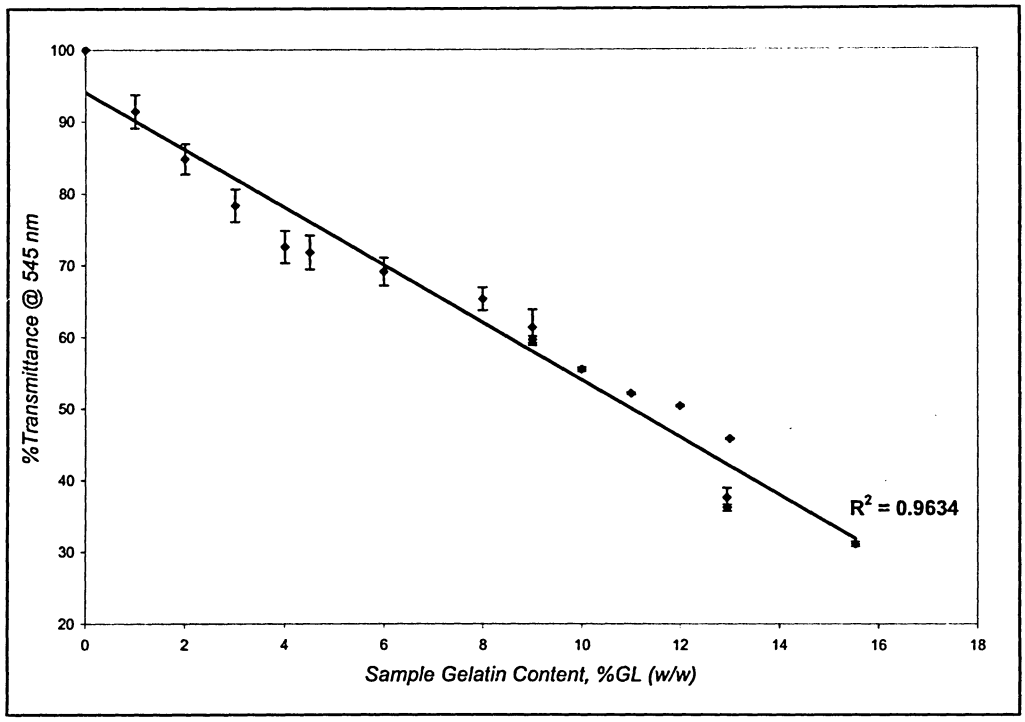

Appendix A-1: Experimentally-determined calibration curve for the Biuret assay of GL content in mixed biopolymer systems (R^2=0.9634, n=5, P=0.005).

Appendix B

Influence of Various Parameters on Coalescence-based Droplet Growth Curves

The overall goodness of fit of the coalescence model indicates that it is appropriate in at least qualitatively outlining coarsening of GL-MD composite systems. The following figures illustrate the characteristic behavior of the growth model resulting from changes in its key parameters, including: (1) continuous phase viscosity; (2) interfacial tension; (3) dispersed phase volume fraction and (4) average initial droplet radius.

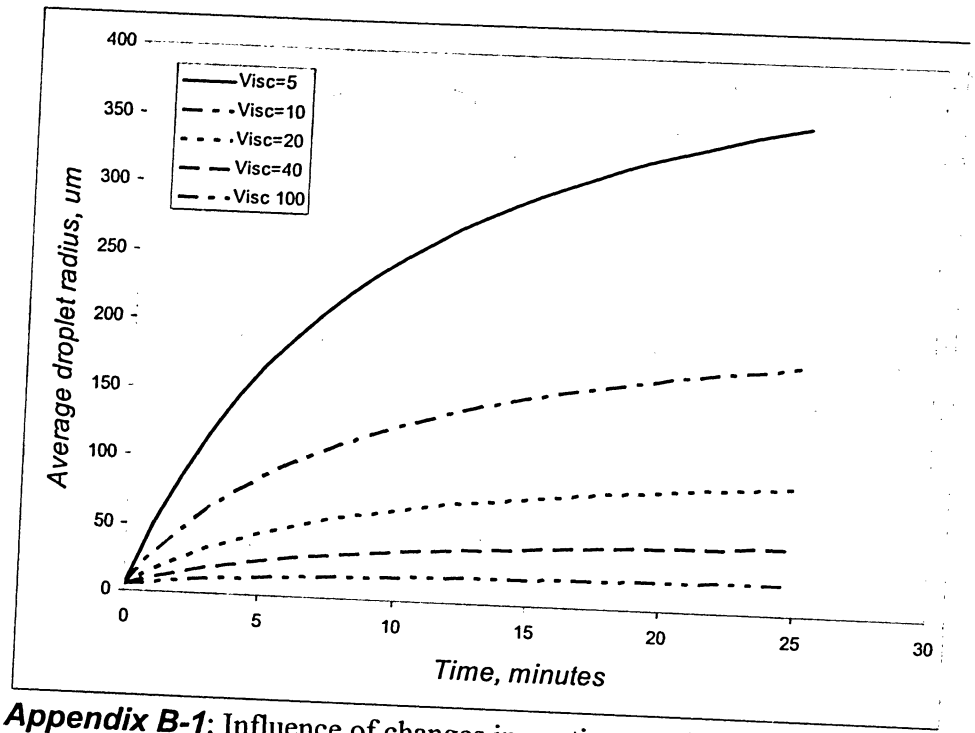

Appendix B-1: Influence of changes in continuous phase viscosity on the characteristic growth curve of droplets undergoing coalescence-induced coalescence.

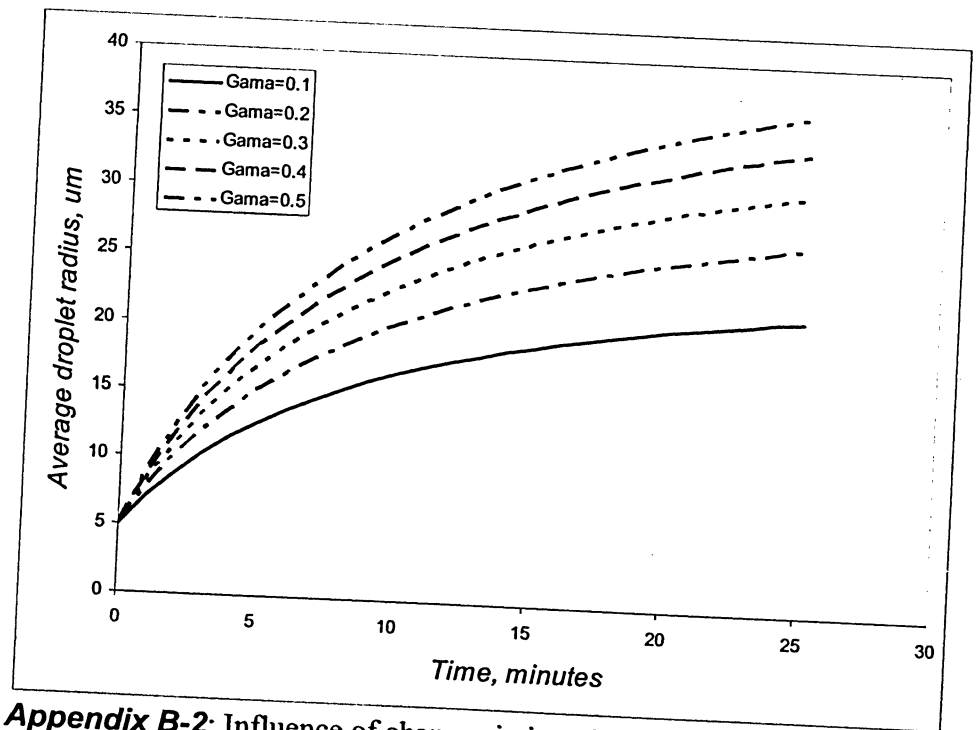

Appendix B-2: Influence of changes in interfacial tension on the characteristic growth curve of droplets undergoing coalescence-induced coalescence.

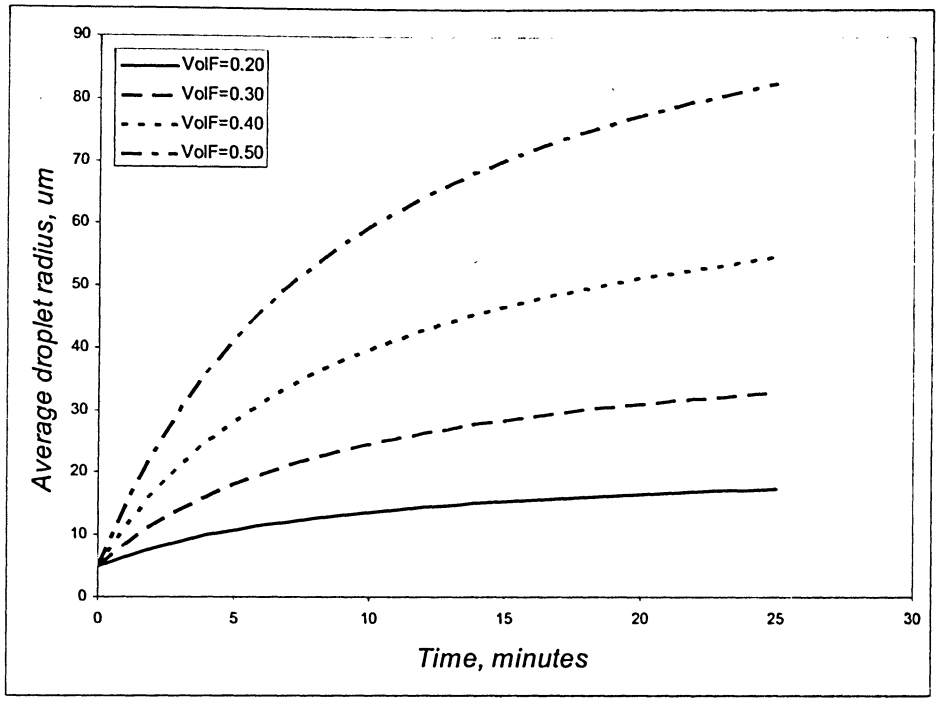

Appendix B-3: Influence of changes in dispersed phase volume fractions on the characteristic growth curve of droplets undergoing coalescence-induced coalescence.

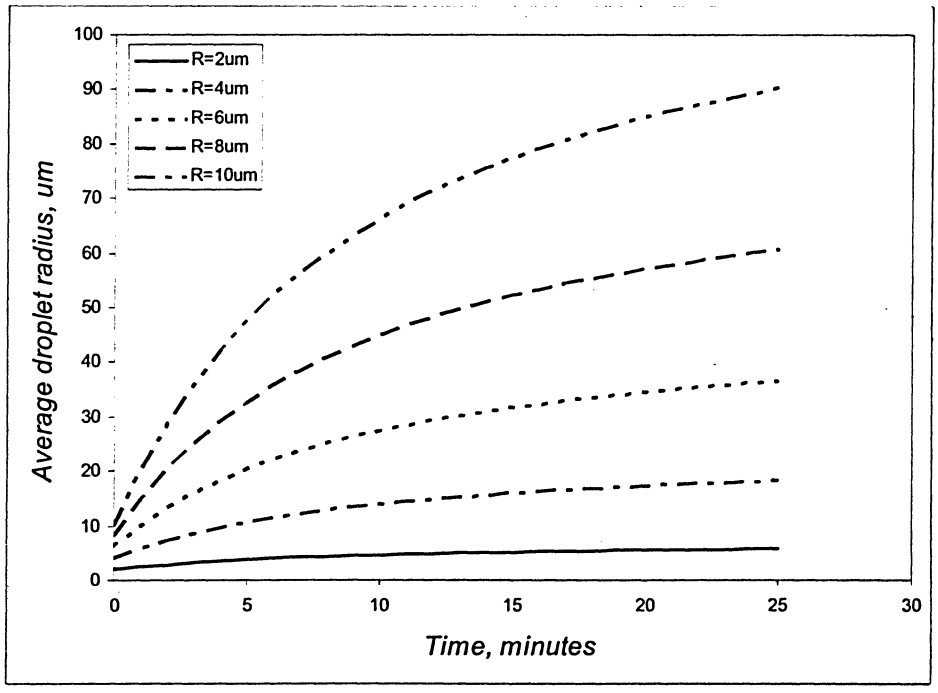

Appendix B-4: Influence of changes in the average initial droplet radius on the characteristic growth curve of droplets undergoing coalescence-induced coalescence.

Appendix C

Rheological Raw Data Plots and Eldridge-Ferry Power-law Curves

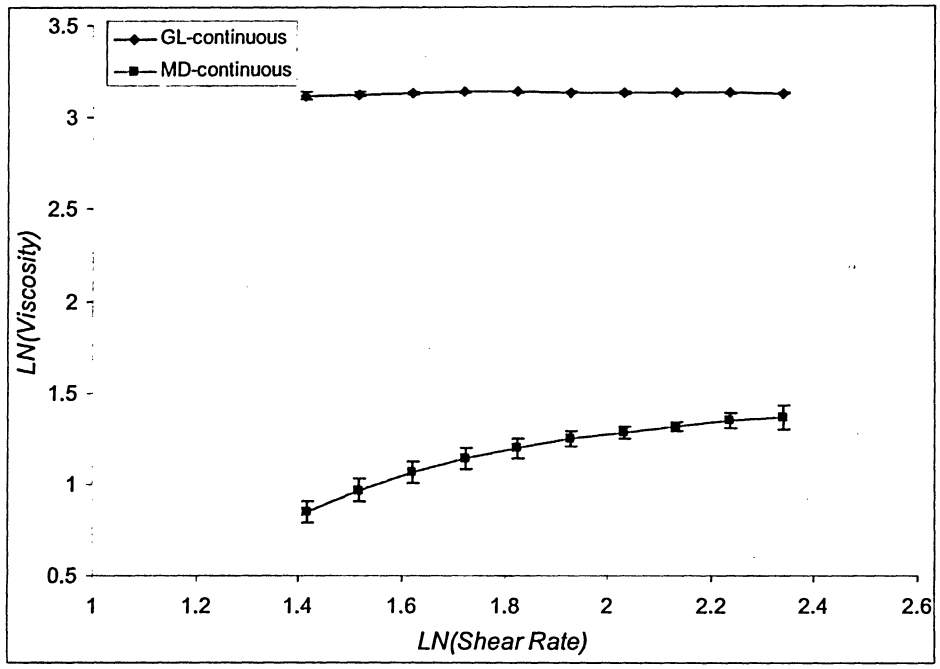

Appendix C-1: Power law plot of cone and plate viscometer results for analysis of shear-dependent viscosity of GL-rich and MD-rich phases at 70°C.

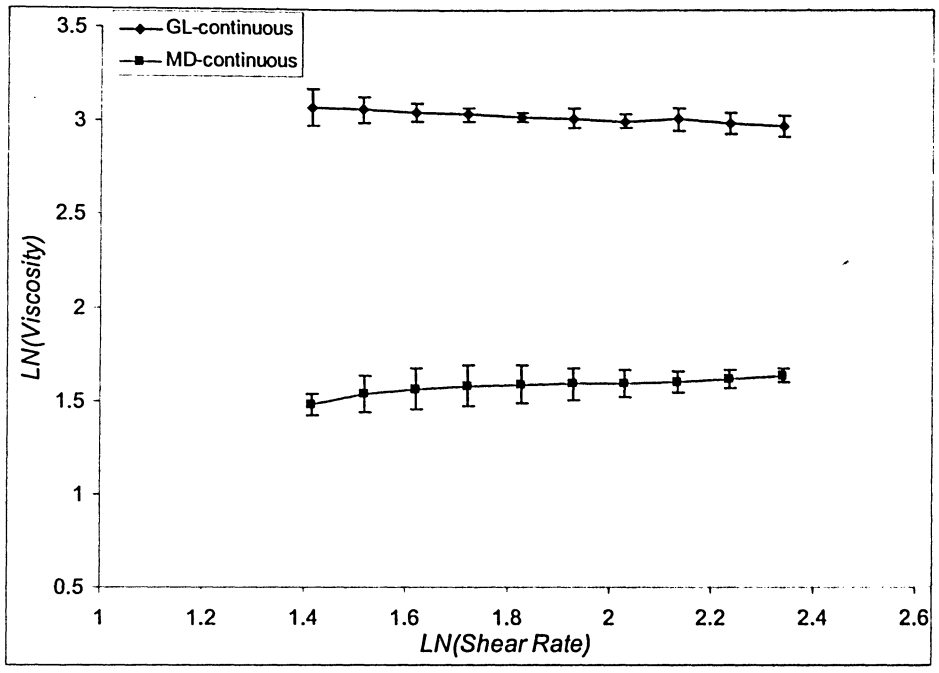

Appendix C-2: Power law plot of cone and plate viscometer results for analysis of shear-dependent viscosity of GL-rich and MD-rich phases at 60°C.

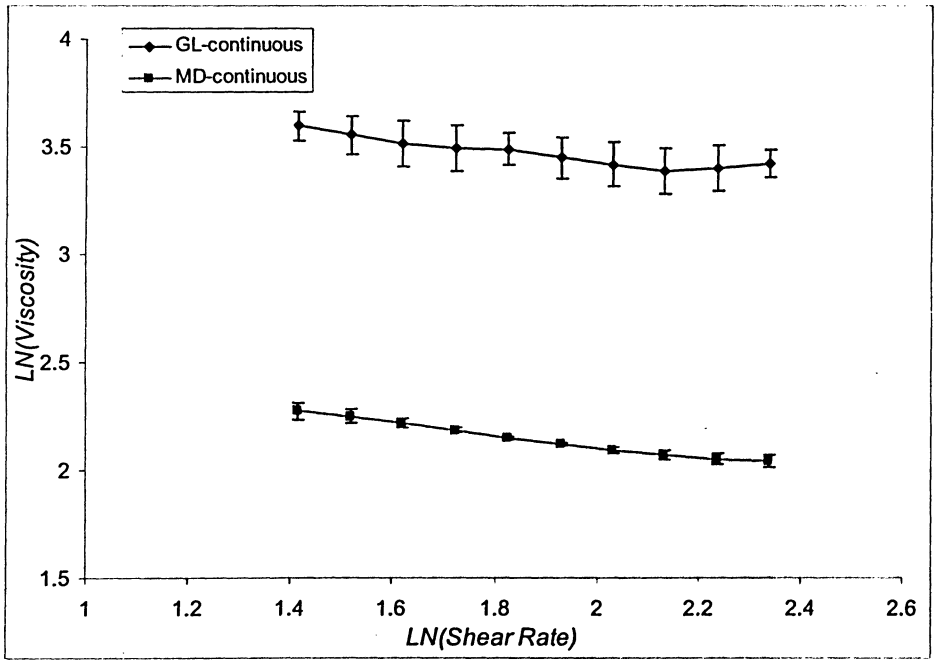

Appendix C-3: Power law plot of cone and plate viscometer results for analysis of shear-dependent viscosity of GL-rich and MD-rich phases at 50°C.

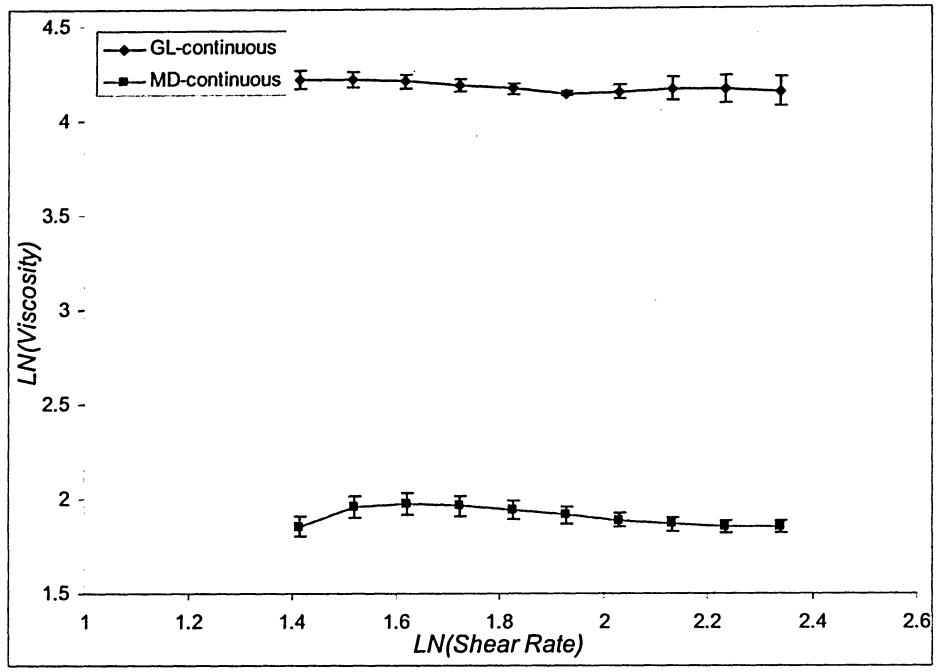

Appendix C-4: Power law plot of cone and plate viscometer results for analysis of shear-dependent viscosity of GL-rich and MD-rich phases at 40°C.

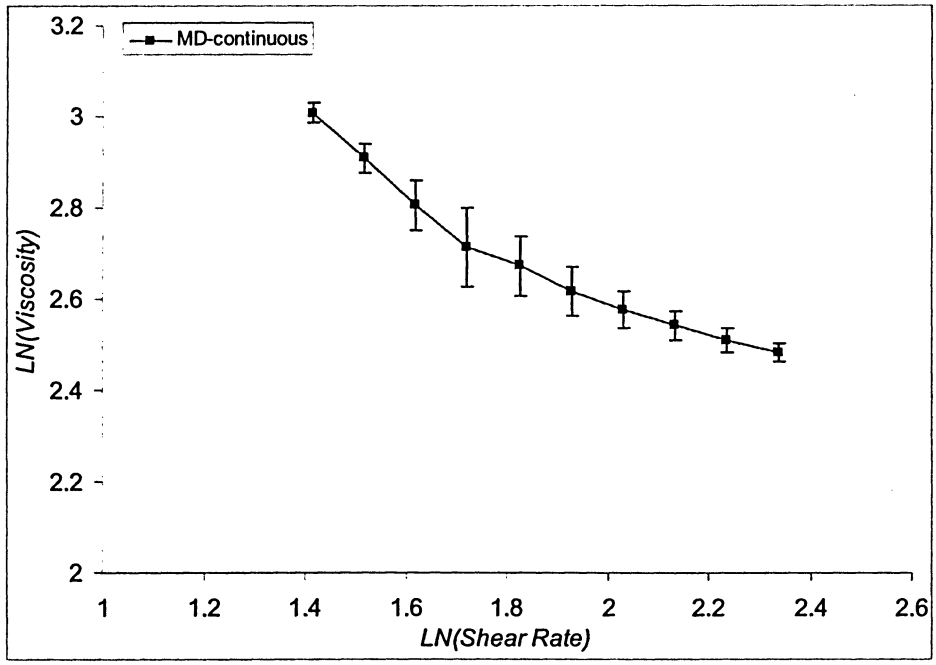

Appendix C-5: Power law plot of cone and plate viscometer results for analysis of shear-dependent viscosity of MD-rich phase at 30°C.

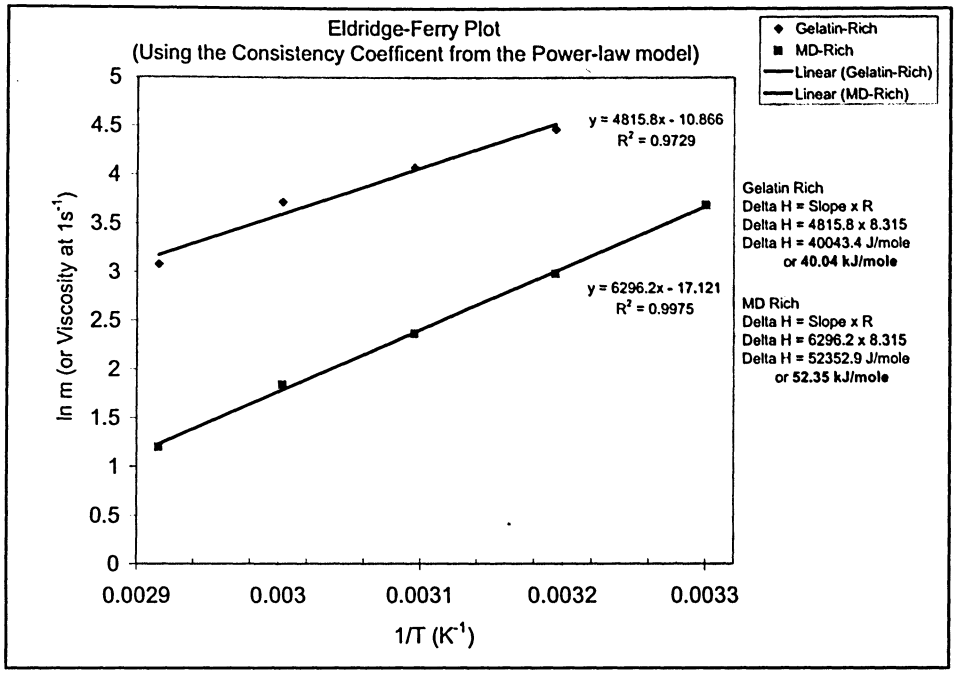

Appendix C-6: Eldridge-Ferry plot of the temperature dependence of the power law consistency coefficient, *m*.

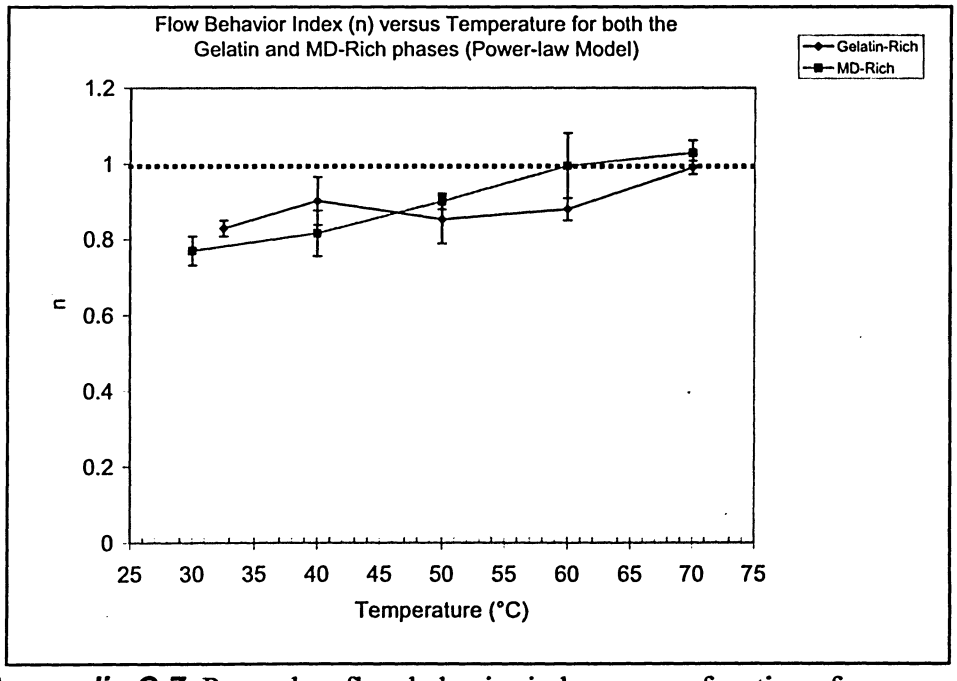

Appendix C-7: Power law flow behavior index, *n*, as a function of temperature for GL-rich and MD-rich phases (proximity to a value of 1 indicates near-Newtonian flow behavior).

Appendix D

Derivation of the McGuire Model of the Coalescence-Induced Coalescence Mechanism of Coarsening

The following is the derivation of the McGuire model of coalescence-induced coalescence, typically undergone by a separated (bio)polymer system during phase coarsening (based on the published work of McGuire *et al.* [20]).

During a coalescence event, the film of continuous-phase fluid between the two active droplets will eventually be expelled. It is with the flow of this fluid that a single coalescence event may induce further coalescence in the system. If another droplet is impinged upon by the expelled fluid, it will travel through the system. It is during this travel that the droplet will likely eventually collide with another droplet, inducing a coalescence event that was brought about, at least in part, by the original coalescence event; hence the moniker *coalescence*-induced coalescence.

The modeling of this behavior is contingent on the elucidation of a number of events, which come together to bring about the series of events discussed above, and they include

- Determination of the ejected fluid velocity profile
- Determination of the post-rupture fluid expulsion time

- Elucidation of the movement of droplets neighboring the coalescence event
- Determination of the number of collisions resulting from ejected fluid
- Determination of the number of collisions, related to size of droplets as a function of time

The actual flow profile of the expelled fluid is simplified and represented by the flow of fluid from a ring of sources (having the same radius as the outer radius of film between deformed droplets, R, and lies on z=0). The momentum-based potential at any point, P, outside the ring due to fluid flow from the ring is given by

$$\Phi = \int_0^{2\pi} \frac{m d\alpha}{l} \tag{D.1}$$

which is related to the radial, axial and angular velocity components:

$$v_r = -\frac{\partial}{\partial r}\Phi \qquad v_z = -\frac{\partial}{\partial z}\Phi \qquad v_\theta = 0 \tag{D.2}$$

If the ring is located on a cylindrical coordinate system, radial and axial velocities of expelled fluid at P are given by

$$v_r = \int_0^{2\pi} \frac{m(r - R\cos(\alpha - \theta))d\alpha}{[R^2 + r^2 + z^2 - 2R\cos(\alpha - \theta)]^{3/2}} \tag{D.3}$$

$$v_z = \int_0^{2\pi} \frac{mzd\alpha}{[R^2 + r^2 + z^2 - 2R\cos(\alpha - \theta)]^{3/2}} \tag{D.4}$$

This set of equations cannot be solved analytically as yet, as functions of r and z must be determined.

The source strength must be specified next. This determination begins by assuming Q is known. The value m is related to Q through conservation of mass based on a volumetric flow rate through a shell enclosing the ring of sources

$$Q = 2\int_0^{2\pi}\int_0^{r_{test}} v_z r dr d\theta + 2\int_0^{2\pi}\int_0^{z_{test}} v_r r_{test} dz d\theta \tag{D.5}$$

Combining equations (D.3), (D.4) and (D.5) integrating yields

$$m = \frac{Q}{8\pi^2} \tag{D.6}$$

The radius of film prior to rupture is taken to be the same as radius of the drops. The velocity of expelled fluid is related to the pressure drop across the interface. Since the pressure outside of the droplets, $P_{outside}$, is constant, the pressure within the droplets, P_{drop}, is related to outside pressure by the Laplace equation

$$P_{drop} = \frac{\gamma}{2R} + P_{outside} \tag{D.7}$$

The pressure in film is related to the neck pressure by the Laplace equation

$$P_{film} = \frac{\gamma}{h_{cr}} + P_{neck} = \frac{\gamma}{h_{cr}} + P_{drop} \tag{D.8}$$

Combining (D.7) and (D.8) yields the change in pressure across the interface

$$\Delta P = P_{film} - P_{outside} = \frac{\gamma}{h_{cr}} + \frac{\gamma}{2R} \tag{D.9}$$

which can be approximated (if the drop radius is much smaller than the critical thickness) as

$$\Delta P = \frac{\gamma}{h_{cr}} \tag{D.10}$$

As the interfacial tension between phases increases, the pressure drop across the interface increases and leads to a higher rate of ejected fluid. Upon rupture of the fluid film, the neck connecting the two droplets propagates outward from $r=r_0$ to $r=R$ over a period of time, t_c. A mass balance on the system during this propagation yields

$$Q = 2\int_0^{h_{cr}/2} 2\pi r_f v_{r,f}\, dz = \frac{d}{dt}(\pi r_0^2 h_{cr}) \tag{D.11}$$

where velocity profile, in this case, is

$$v_{r,f} = \frac{(h_{cr}/2)\Delta P}{2\eta r_f \ln(R/r_0)}\left[1 - \frac{2z_f}{h_{cr}}\right] \tag{D.12}$$

Combining equations (D.10), (D.11) and (D.12) yields the equation for the time required for the neck to propagate outwards

$$t_c = \frac{3\eta R^2}{h_{cr}\gamma}\left[1 - \left(\frac{r_0}{R}\right)^2\left(1 + 2\ln\left(\frac{R}{r_0}\right)\right)\right] \tag{D.13}$$

From this equation, it is apparent that as the viscosity of film increases, the time for required to expel the fluid film contents increases for a constant pressure drop. Similarly, as the interfacial tension increases, the required time decreases.

If the critical wavelength for film rupture is taken to be 1/10 of the film radius (*i.e.*, $r_0=0.1R$), the critical film height required for rupture of the interfacial film is

$$h_{cr} = \left[\frac{9\sqrt{3}(k_B T/\gamma)^{1/2} A_{vw} R^2}{16\gamma} \right]^{1/5} \tag{D.14}$$

Based on the mass balance around the coalescing droplets, the total volume of fluid in the film region is $\pi R^2 h_{cr}$. This fluid is expelled from the interface for a period of time, t_c.

The average volumetric flow rate of fluid out of the film is given by

$$Q = \frac{\pi R^2 h_{cr}}{t_c} \tag{D.15}$$

From this, it is apparent that the methodology for the calculation of r-direction and z-direction velocities of the fluid expelled from the film will be determined systematically by:

- Specifying the value of R
- Determining the critical film thickness/height, h_{cr}
- Determining the coalescence time, t_c, with r_0=0.1R
- Determining the average exiting flow rate, Q
- Determining the source strength of the expelled fluid, m
- Finally, determining the radial, v_r, and axial, v_z, velocities of the expelled fluid

The change in average droplet radius accompanying coalescence-induced coalescence will be dependent on the velocity of the fluid expelled from the interfacial film, but also will depend on the number of coalescence events that occur. The number of droplets whose centers of mass exist in a random differential volume element of the sample is given by

$$n_{v,1} = NdV \tag{D.16}$$

If some droplet, having a radius R, is pushed some distance, y, away from the original coalescence event, the drop sweeps the volume $\pi R^2 y$. The number of droplets whose centers of mass exist in the swept volume is given by

$$n_{v,2} = N(\pi R^2 y) \tag{D.17}$$

The total number of collisions between the moving drop and others in its path is based on

$$\frac{\text{collisions due to drops in dV}}{event} = n_{v,1} \cdot n_{v,2} = N^2 \pi R^2 y dV \tag{D.18}$$

Integrating this value over the entire volume yields

$$\frac{\text{total collisions}}{event} = \int_v \pi y N^2 R^2 dv \tag{D.19}$$

The total number of drops per unit volume is related to the average radii of the droplet population at any time by

$$N = \frac{3v}{4\pi R^3} \tag{D.20}$$

Combining (D.19) and (D.20) yields

$$\frac{\text{total collisions}}{event} = \int_v \frac{9v^2 y}{16\pi R^4} dV \tag{D.21}$$

Here, it is apparent that by knowing y and R the total number of collisions occurring due to one coalescence may be calculated (the distance traveled, y, can be calculated from velocity profiles). Overall, the magnitude of the velocity of expelled fluid is given by

$$(v_r^{\,2} + v_z^{\,2})^{1/2} \tag{D.22}$$

The distance a droplet moves after being exposed to the expelled fluid is

$$y = (v_r^{\,2} + v_z^{\,2})^{1/2} t_c \tag{D.23}$$

Therefore, the total number of subsequent collisions is

$$\frac{\text{total collisions}}{event} = \int_V \frac{9v^2}{16\pi R^4}(v_r^{\,2} + v_z^{\,2})^{1/2} t_c dV \tag{D.24}$$

The change in drop size with time is related to

$$N(t + t_c) - N(t) = -\frac{\text{total collisions}}{event} \tag{D.25}$$

which is simplified by Taylor series expansion

$$N(t + t_c) = N(t) + \left.\frac{dN}{dt}\right|_t t_c \tag{D.26}$$

The change in number of drops per unit volume per time due to one coalescence event is given by

$$\left.\frac{dN}{dt}\right|_t = -\frac{1}{t_c}\frac{\text{total collisions}}{event} \tag{D.27}$$

The change in the number of droplets per unit volume per time is equal to the number of collisions occurring due to one coalescence event divided by time during which the collisions take place. However, many events are taking place in the system at any given time, so the total change in the number of drops per unit time is adjusted to

$$\text{total collisions} = \frac{\text{total collisions}}{\text{event}} \cdot events \tag{D.28}$$

where

$$events = C_1 \frac{v}{(t + t_s)} \tag{D.29}$$

Combining these results gives the operating function of the model, describing the growth rate of drops for a system undergoing coarsening by coalescence-induced coalescence mechanisms:

$$\frac{dR}{dt} = \frac{v^2 C_1}{4(t + t_s)} \int_V (v_r^{\,2} + v_z^{\,2})^{1/2} dV \tag{D.30}$$

Appendix E

Summary of the Concentration-Dependent Extents of GP Crosslinking Recently Reported in Literature

Paper	*GL*	*GP %*	*GP:GL*	*GP:GL*	*X-link Index*
Author, Year	*(w/w)% sample*	*(w/w)% sample*	*(w/w)%*	*(mol/mol)% (x100000)*	*%*
Yao, 2004	25	0.1	0.004	1.20656	55
Yao, 2004	25	0.25	0.01	3.0164	64
Yao, 2004	25	0.5	0.02	6.0328	73
Yao, 2004	25	0.75	0.03	9.0492	73
Yao, 2004	25	1	0.04	12.0656	74
Yao, 2004	25	1.25	0.05	15.082	75
Yao, 2004	25	1.5	0.06	18.0984	75
Yao, 2004	25	1.75	0.07	21.1148	75
Bigia, 2002	5	0.07	0.014	4.22296	13
Bigia, 2002	5	0.15	0.03	9.0492	61
Bigia, 2002	5	0.33	0.066	19.90824	69
Bigia, 2002	5	0.67	0.134	40.41976	80
Bigia, 2002	5	1	0.2	60.328	85
Bigia, 2002	5	1.5	0.3	90.492	83
Bigia, 2002	5	2	0.4	120.656	86
Liang, 2004	8	0.0090492	0.001131	0.341200086	N/A
Nickerson, 2006	10	0	0	0	N/A
Nickerson, 2006	10	0.113115	0.011312	3.41200086	N/A
Nickerson, 2006	10	0.22623	0.022623	6.82400172	N/A
Nickerson, 2006	10	0.339345	0.033935	10.23600258	N/A